Communication Theoretical Modeling and Analysis of Neuronal Communication with Synaptic Plasticity

by

Tooba Khan

A Dissertation Submitted to the
Graduate School of Sciences and Engineering
in Partial Fulfillment of the Requirements for
the Degree of

Doctor of Philosophy

in

Electrical and Electronics Engineering

KOÇ ÜNİVERSİTESİ

April 06, 2022

Communication Theoretical Modeling and Analysis of Neuronal Communication with Synaptic Plasticity

Koç University

Graduate School of Sciences and Engineering

This is to certify that I have examined this copy of a doctoral dissertation by

Tooba Khan

and have found that it is complete and satisfactory in all respects,
and that any and all revisions required by the final
examining committee have been made.

Committee Members:

_____

Prof. Özgür Barış Akan

_____

Prof. Fatih Alagöz

_____

Prof. Alper Tunga Erdoğan

_____

Prof. Hale Saybaşılı

_____

Prof. Beren Semiz

Date: _____

To my loving Family.

ABSTRACT

Communication Theoretical Modeling and Analysis of Neuronal Communication with Synaptic Plasticity
Tooba Khan
Doctor of Philosophy in Electrical and Electronics Engineering
April 06, 2022

Emergence of nanoscale devices and their applications mandates the facilitation of communication between these devices, and hence, the development of nanonetworks, to overcome their computational and power limitations owing to their size. The nanonetworks need novel communication paradigms since they are fundamentally different from the traditional communication networks. The human body is a large-scale network of molecular nanonetworks composed of billions of nanomachines, i.e., cells, where molecules are used to encode, transmit and receive information. The largest and the most vital intra-body nanonetwork is the nervous nanonetwork. Thus, the aim of this thesis is to investigate the nervous nanonetwork from information and communication theoretical perspective, to lay down the foundations of a novel bio-inspired communication paradigm for nanonetworks. We focus on the communication theoretical analysis of single-input-single-output (SISO) as well as multiple-input-single-output (MISO) neuro-spike communication channels, considering memory and metabolic energy constraints. Synaptic plasticity is a ubiquitous phenomenon in central as well as peripheral nervous systems and is associated with memory and learning new behaviors and skills. Thus, we further aim to analyze the neuro-spike communication incorporating the plasticity. The results obtained from this study would allow us to select optimal parameters to realize efficient bio-inspired nanonetworks. Moreover, since neurodegenerative diseases such as Alzheimer's Disease, Parkinson's Disease and Multiple Sclerosis are caused by the malfunction of the sub-processes of the neuro-spike communication, these results can be compared with the results obtained from diseased synapses to develop the future ICT-inspired diagnostic and treatment techniques for neural disorders.

ÖZETÇE

Sinaptik Plastisite ile Nöronal İletişimin İletişim Teorik Modellemesi ve Analizi

Tooba Khan

Elektrik ve Elektronik Mühendisliği, Doktora

06 Nisan 2022

Nano ölçekli cihazların ve uygulamalarının ortaya çıkması, bu cihazlar arasındaki iletişimin kolaylaştırılmasını ve dolayısıyla boyutları nedeniyle hesaplama ve güç sınırlamalarının üstesinden gelmek için nano ağların geliştirilmesini zorunlu kılmaktadır. Nanoağlar, geleneksel iletişim ağlarından temelde farklı oldukları için yeni iletişim paradigmalarına ihtiyaç duyarlar. İnsan vücudu, moleküllerin bilgiyi kodlamak, iletmek ve almak için kullanıldığı milyarlarca nanomakineden, yani hücrelerden oluşan büyük ölçekli bir moleküler nanoağlar ağıdır. En büyük ve en hayati vücut içi nano ağ sinirsel nano ağdır. Bu nedenle, bu tezin amacı, sinirsel nano ağını bilgi ve iletişim teorik perspektifinden araştırmak, nanoağlar için yeni bir biyo-ilhamlı iletişim paradigmasının temellerini oluşturmaktır. Bellek ve metabolik enerji kısıtlamalarını göz önünde bulundurarak, tek girişli tek çıkışlı (SISO) ve çoklu girişli tek çıkışlı (MISO) nöro-spike iletişim kanallarının iletişim teorik analizine odaklanıyoruz. Sinaptik plastisite, merkezi ve periferik sinir sistemlerinde her yerde bulunan bir fenomendir ve hafıza ve yeni davranış ve becerilerin öğrenilmesi ile ilişkilidir. Böylece, plastisiteyi içeren nöro-spike iletişimi analiz etmeyi amaçlıyoruz. Bu çalışmadan elde edilen sonuçlar, verimli biyo-ilhamlı nanoağları gerçekleştirmek için en uygun parametreleri seçmemize izin verecektir. Ayrıca, Alzheimer Hastalığı, Parkinson Hastalığı ve Multipl Skleroz gibi nörodejeneratif hastalıklar, nöro-spike iletişiminin alt süreçlerinin arızalanmasından kaynaklandığından, bu sonuçlar, gelecekteki BİT-ilhamlı teşhis ve tedavi tekniklerini geliştirmek için hastalıklı sinapslardan elde edilen sonuçlarla karşılaştırılabilir.

ACKNOWLEDGMENTS

I would like to express my deep and sincere gratitude to my advisor, Prof. Özgür Barış Akan, who led me into this exciting area of Neuro-spike communications. I am indebted to Prof. Akan for his invaluable mentorship, encouragement to conduct quality research and his confidence in me and my work throughout my time at Koç University. I would have never achieved this success without his utmost support and guidance.

I would also like to express my sincere thanks to Prof. Fatih Alagöz and Prof. Alper Tunga Erdoğan for accepting to supervise this thesis and to drive it further with their valuable comments throughout the process. I am also immensely thankful for the time and contribution of jury members Prof. Hale Saybaşılı and Prof. Beren Semiz.

I am extremely grateful to my colleagues in the Next-generation and Wireless Communications Laboratory (NWCL) for their unconditional emotional and professionl support through out my studies.

Finally, I want to thank my dearest family and friends for their continued love and support.

TABLE OF CONTENTS

LIST OF TABLES

LIST OF FIGURES

ABBREVIATIONS

AD	Alzheimer's Disease
AMPA	α-Amino-3-hydroxy-5-Methyl-4-isoxazolepropionic Acid
ANN	Artificial Neural Network
AP	Action Potential
ATP	Adenosine Triphosphate
BAN	Body Area Network
BBB	Blood Brain Barrier
BER	Bit Error Rate
CA	Cornu Ammonis
CNS	Central Nervous System
EPSP	Excitatory Post-Synaptic Potential
FRET	Fŏorster resonance energy transfer
FS	Fast Spiking
GJ	Gap Junction
H-H	Hodgkin-Huxley
IB	Intrinsic Bursting
ICT	Information and Communication Technology
IoBNT	Internet of Bio-Nano Things
IoT	Internet of Things
IP3	Inositol Triphosphate
LNP	Linear-Nonlinear-Poisson
LTD	Long Term Depression
LTP	Long Term Potentiation

MAT	Multi-timescale Adaptive Threshold
MC	Molecular Communications
MISO	Multiple-Input and Single-Output
NMDA	N-methyl-D-aspartate
NN	Neural Network
PSD	Postsynaptic Density
RP	Ready Pool
RRP	Readily Releasable Pool
RRV	Readily Releasable Vesicle
RS	Regular Spiking
SISO	Single-Input Single-Output
STD	Short Term Depression
STDP	Spike Timing Dependent Plasticity
VDCC	Voltage-Dependent Calcium Channel

Chapter 1

INTRODUCTION

Nanotechnology is one of the frontiers of the scientific research in the current age having a huge set of applications that are being realized in a variety of environments. Some of these include bio-hybrid systems [He et al., 2015], nanoscale sensing [Kagan et al., 2009], intelligent drug delivery [Nakano et al., 2012a] and body area networks (BAN) [Seyedi et al., 2013]. Although nanotechnology promises a big revolution in the future, the implementation challenges are also huge. Due to the limited dimensions of nanomachines, they have scarce processing, memory and networking capabilities. These limitations can be overcome by dense deployment of nanomachines in networked environments, termed as *nanonetworks* [Akyildiz et al., 2008].

Different communication paradigms are suggested for the realization of nanonetworks in physical environment such as nanomechanical, acoustic, electromagnetic, chemical and molecular communications. However, the most promising one is molecular communication [Giné and Akyildiz, 2009], where molecules are used to encode, transmit and receive information.

Molecular communication systems exist in nature and have evolved over billions of years. These systems can be found all around and within us. Understanding this molecular signaling among living cells from information and communication theoretical (ICT) perspective provides novel nanonetworking paradigms and a deep insight into the ICT-based fundamentals of biological systems.

Molecular communication is different from traditional communication paradigms in various aspects such as the sizes of network entities, information transmission mechanisms, noise sources and fundamental performance limits including trans-

mission delay, achievable data rates, range and power. This calls for laying down the foundation of the emerging field of molecular information and communication science. Therefore, the aim of this thesis is to analyze the existing literature on intra-body nanonetworks and molecular communication paradigms, to establish the fundamentals limits of molecular communication and information science.

Nervous system is one the most studied intra-body nanonetwork from communication theoretical perspective to understand fundamentals of molecular communication. However, to realize the bio-inspired and bio-compatible communication paradigm for nanonetworks, more comprehensive understanding of neuro-spike communication is required. Thus, in this thesis, we aim to cover the unexplored areas of neuro-spike communication by analyzing hippocampal pyramidal neurons. Neuro-spike communication, one of the most evolved and investigated form of molecular communication [Balevi and Akan, 2013, Malak and Akan, 2013a, Abbasi and Akan, 2015, Malak and Akan, 2014, Ramezani and Akan, 2015b], is where electrochemical impulses and neurotransmitters are used for information transfer. Within neuron, information is transferred by electrochemical impulses called *action potential (AP) or spike* that travel along an axon that branches out at the end and form connections with other neurons. Most of the neurons are physically disconnected from each other having a small gap called *synaptic cleft*. This connection is commonly known as synapse [Kandel et al., 2000]. The two ends of the synapse are pre- and postsynaptic terminals corresponding to transmitter and receiver neurons, respectively as shown in Fig. 1.1. Spike traveling through axon of transmitter neuron arrives at pre-synaptic terminal and releases neurotransmitters into the synaptic cleft. The major type of neurotransmitter in central excitatory synapses is known as Glutamate. Once released into the cleft, these glutamate molecules are captured by receptors present on postsynaptic terminal generating Excitatory Postsynaptic Potential (EPSP). For successive transmissions, neurotransmitters need to be removed from synaptic cleft before next vesicle release. In Central Nervous System, clearance of these neurotransmitters is achieved through diffusion of molecules out of the cleft as well as by *re-uptake* phenomenon [Danbolt, 2001], where a fraction of

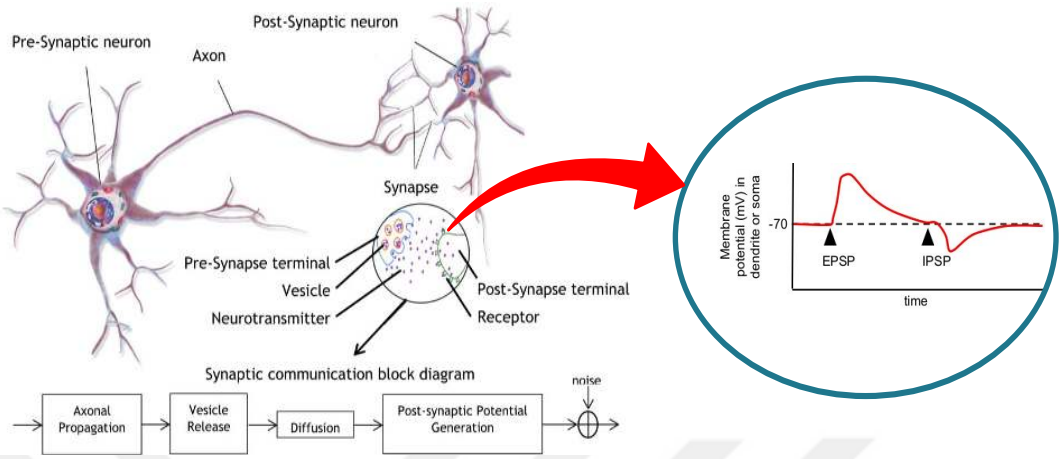

Figure 1.1: Single-input Single-output (SISO) Neuro-spike Communication.

neurotransmitters are re-absorbed by pre-synaptic terminal for re-cycling.

Moreover, in central nervous system, multiple pre-synaptic neurons converge and make individual synapses to a single post-synaptic neuron. The monosynaptic EPSPs generated at each synapse are then integrated at SOMA and spike is generated when this cumulative EPSP reaches a threshold. Thus, in chapter 5 and 6, we focus our analysis on multiple-input multiple-output (MISO) neuro-spike communication channel.

Synaptic plasticity is one of the most crucial phenomena associated with our brains. It is the ability of the brain to reorganize neural pathways based on new experiences. It has been shown through experimental evidence that the amplitude of postsynaptic potential is not fixed but can change over time, either facilitating or inhibiting the information transmission. Different factors can either increase or decrease the transmission efficacy of the synapse and this change can last for minutes, hours or days. Synaptic plasticity has been observed in brain as well as in spinal cord [Cooke and Bliss, 2006, Tahayori and Koceja, 2012]. There are two types of plasticity; *short-term* and *long-term plasticity*. Short-term plasticity leads to short-term changes in synaptic strength, lasts from milliseconds to minutes and regulate the moment-to-moment information flow through a neural circuit. On the other

hand, long-term plasticity leads to persistent changes in synaptic strength, persists for hours to the lifetime of synapse and alters microcircuit function in response to an activity indicating change in computational demands.

In this thesis, we aim to analyze neuro-spike communication in more detail. However, before diving into neuro-spike communication, we study the fundamentals of molecular information and communication science in chapter 2. In chapter 3, we highlighted the research gap in modeling of SISO neuro-spike communication channel and provide a realistic model of diffusion of neurotransmitters in the synapse. In chapter 4, information theoretical analysis of realistic SISO communication channel is achieved and closed-form equation for the capacity of the SISO channel is provided. Moreover, short-term plasticity caused by depletion of readily releasable vesicles is also considered. In chapter 5, we model spike generation in MISO neuro-spike communication channel and analyze the maximum achievable sum rate. Moreover, we consider metabolic energy constraints on information transmission in brain to avoid over estimation of its performance. In chapter 6, we again analyze MISO channel, however, this time we consider the effect of short-term plasticity caused by the dynamic nature of spiking threshold and also evaluated the responses of different types of neurons in terms of firing pattern. In chapter 7, we analyze the effects of long term plasticity on information flow in MISO channel. In chapter 8, we analyze the tripartite synapse, i.e. a synapse enwrapped by an astrocyte that regulate the vesicle release probability of pre-synaptic neuron through a feedback channel. Finally, we conclude our work in chapter 9.

1.1 Fundamental Contributions

The fundamental contributions of this thesis in analyzing neuro-spike communication and in the realization of bio-inspired communication paradigm for nanonetworks can be listed below:

- Establishing fundamentals of molecular information and communication science

- Realistic model for diffusion of neurotransmitters in synaptic cleft considering synaptic geometry and clearance of neurotransmitters from the cleft
- Deriving closed form expression for the capacity of a realistic SISO channel considering all biophysical parameters and channel memory in vesicle release process
- Modeling the spike generation in MISO channel and analyzing maximum achievable sum rate of the channel
- Analyzing MISO neuro-spike communication including the effects of dynamic spiking threshold with different types of neurons
- Enforcing metabolic energy constraints on information transmission in neurons
- Analyzing the effects of synaptic plasticity, short-term as well as long-term, on information flow through neuro-spike communication channel
- Analyzing the effects of synaptic plasticity on information flow, caused by the astrocytes in a tripartite synapse

1.2 Thesis Outline

This thesis is organized into the following chapters:

Chapter 2: In this chapter, we introduce a novel perception of molecular communication paradigm to lay down the foundations of science of molecular information and communication. We review the existing literature on intra-body nanonetworks and molecular communication to highlight the research gap and future directions to resolve open issues. Moreover, we propose a framework to establish the fundamental limits of molecular information and communication science by relating physical and chemical properties of molecular communication channel to its ICT-based characteristics. Finally, we emphasize the significance of molecular communication in biomedical applications.

Chapter 3: In this chapter, we formulate a novel mathematical model for the propagation of neurotransmitters in the synaptic cleft and then binding with the postsynaptic receptors. This model considers three dimensional motion of neurotransmitters in the cleft restricted by the boundaries formed by pre- and postsynaptic terminals as well as the re-uptake of neurotransmitters by pre-synaptic neuron for recycling. Based on this model we develop a fast deterministic algorithm, which calculates expected value of the output of this channel, namely the amplitude of EPSP, for given synaptic parameters. We validate our algorithm by a Monte Carlo simulation, which shows total agreement between the results of two methods. Finally, we utilize our model to quantify effects of variation in synaptic parameters such as position of release site, receptor density, size of postsynaptic density (PSD), diffusion coefficient, uptake probability and number of neurotransmitters in a vesicle, on maximum number of bound receptors that directly affect peak amplitude of EPSP.

Chapter 4: In this chapter, we focus on the fundamental building block of neuro-spike communication, i.e., signal transmission over a synapse, to evaluate its information transfer rate. We aim to analyze a realistic synaptic communication model, which for the first time, encompasses the variation in vesicle release probability with time, synaptic geometry and the re-uptake of neurotransmitters by pre-synaptic terminal. To achieve this objective, we formulate the mutual information between input and output of the synapse. Then, since this communication paradigm has memory, we evaluate the average mutual information over multiple transmissions to find its overall capacity. We derive a closed-form expression for the capacity of the synaptic communication as well as calculate the capacity-achieving input probability distribution. Finally, we find the effects of variation in different synaptic parameters on the information capacity and prove that the diffusion process does not decrease the information a neural response carries about the stimulus in real scenario.

Chapter 5: In this chapter, we quantify the information transmitted through

the multiple-input single-output (MISO) neuro-spike communication channel by taking into account models for axonal propagation, synaptic transmission and spike generation. Moreover, the spike generation and propagation in each neuron requires opening and closing of numerous ionic channels on the cell membrane, which consumes considerable amount of Adenosine Triphosphate (ATP) molecules called metabolic energy. Thus, we evaluate how applying a constraint on available metabolic energy affects the maximum achievable mutual information of this system. To this aim, we derive a closed form equation for the sum rate of the MISO neuro-spike communication channel and analyze it under the metabolic cost constraints. Finally, we discuss the impacts of changes in number of pre-synaptic neurons on the achievable rate and quantify the trade-off between maximum achievable sum rate and the consumed metabolic energy.

Chapter 6: The information from outside world is encoded into spikes by the sensory neurons. These spikes are further propagated to different brain regions through various neural pathways. In the cortical region, each neuron receives inputs from multiple neurons that change its membrane potential. If the accumulated change in the membrane potential is more than a threshold value, a spike is generated. According to various studies in neuroscience, this spiking threshold adapts with time depending on the previous spike. This causes short-term changes in the neural responses giving rise to short-term plasticity. Therefore, in this chapter, we analyze a multiple-input single-output (MISO) neuro-spike communication channel and study the effects of dynamic spiking threshold on mutual information and maximum achievable sum rate of the channel. Since spike generation consumes a generous portion of the metabolic energy provided to the brain, we further put metabolic constraint in calculating the mutual information and find a trade-off between maximum achievable sum rate and metabolic energy consumed. Moreover, we analyze three types of neurons present in the cortical region, i.e., Regular spiking, Intrinsic bursting

and Fast spiking neurons. We aim to characterize these neurons in terms of encoding/transmission rates and energy expenditure. It will provide a guideline for the practical implementation of bio-inspired nanonetworks as well as for the development of ICT-based diagnosis and treatment techniques for neural diseases.

Chapter 7: The information flow in neuro-spike communication channel is regulated by the ability of neurons to change synaptic strengths over time, i.e. synaptic plasticity. Thus, the performance evaluation of the nervous nanonetwork is incomplete without considering the influence of synaptic plasticity. In this chapter, we focus on information transmission among hippocampal pyramidal neurons and provide a comprehensive channel model for MISO neuro-spike communication, which includes axonal transmission, vesicle release process, synaptic communication and spike generation. In this channel, the spike timing dependent plasticity (STDP) model is used to cover both synaptic depression and potentiation depending on the temporal correlation between spikes generated by input and output neurons. Since synaptic strength changes depending on different physiological factors such as spiking rate of presynaptic neurons, number of correlated presynaptic neurons and the correlation factor among them, we simulate this model with correlated inputs and analyze the evolution of synaptic weights with time. Moreover, we calculate average mutual information between input and output of the channel and find the impact of plasticity and correlation among inputs on the information transmission. The simulation results reveal the impact of different physiological factors related to either presynaptic or postsynaptic neurons on the performance of MISO neuro-spike communication. Moreover, they provide guidelines for selecting the system parameters in a bio-inspired neuronal network according to the requirements of different applications.

Chapter 8: In this chapter, we study plasticity effect on vesicle release process in a tripartite synapse. Astrocytes, the most abundant glia cells in brain,

being in physical proximity of pre- and postsynaptic terminals of the chemical synapse, form tripartite synapses. The feedback from astrocytes introduces synaptic plasticity, which modulates information transmission through neurons. Various other synaptic events also cause plasticity, hence combining them in a single model is quite challenging. In this chapter, we study the combined effect of short-term depression (STD) and long-term potentiation (LTP) on vesicle release process in a tripartite synapse. STD decreases the release probability due to slower replenishment rates of releasable vesicles, whereas LTP is due to the positive feedback from astrocytes that increases release probability. Thus, we evaluate vesicle release probability and mutual information between input spikes and vesicle release to quantify the effect of STD and LTP on information transmission. Moreover, the effect of different synaptic parameters such as number of releasable vesicles, input spike rate and replenishment rate of the vesicles, is analyzed on information transmission. It is observed that release probability is predominantly affected by LTP, however, presence of STD decreases the achievable average mutual information over time. Furthermore, the synapses with higher number of releasable vesicles are observed to become stronger with time.

- **Chapter 9:** In this chapter, we conclude the thesis while discussing the key results of this work.

Chapter 2

FUNDAMENTALS OF MOLECULAR INFORMATION AND COMMUNICATION SCIENCE

2.1 Introduction

Information science is an interdisciplinary field that deals with collection, analysis, storage, transmission, and dissemination of information, while the communication theory is a subset of information science that deals with the principles and methods of information transfer between two entities. This fundamental field has shaped the current communication networks over decades. With the recent advancements in nanotechnology, things are quickly moving from traditional communication architecture to micro and nano scales.

Although nanotechnology has enabled the realization of nano devices, they are limited in processing power, storage etc. Thus, dense deployment of these devices in the form of a network can overcome their limitations. However, these networks require novel communication paradigm to cope with their nontraditional methods of information exchange. Molecular communication, a ubiquitous natural phenomenon, is considered as the one of the most promising method of communication for nanonetworks.

Molecular communication is different from traditional communication paradigms in various aspects such as the sizes of network entities, information transmission mechanisms, noise sources and fundamental performance limits including transmission delay, achievable data rates, range and power. This calls for laying down the foundation of the emerging field of molecular information and communication science. Therefore, the aim of this work is to analyze the existing literature on intrabody nanonetworks and molecular communication paradigms, to establish and in-

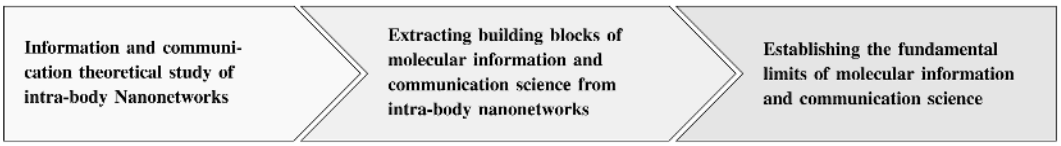

Figure 2.1: Framework to formalize the *science of molecular information and communication.*

troduce the fundamentals of molecular information and communication science and propose future directions towards establishing the fundamental limits of these sciences.

At the same time, this chapter emphasizes the significance of molecular information and communication science in life sciences. This enables the development of ICT-based models of disease affected intra-body nanonetworks which can be used to get deeper insight into the disease and develop novel ICT-based diagnosis and treatment techniques.

Fundamental steps to thoroughly investigate and formalize the science of molecular information and communication are given in Fig. 2.1. In this work, we analyze the literature for existing contributions in each of these steps to propose future directions. Therefore, the rest of the chapter is organized as follows. In Section 2.2, we present the state-of-the-art research and open challenges to model intra-body nanonetworks to extract possible molecular communication paradigms. Then, in Section 2.3, we define and evaluate different molecular communication paradigms on the basis of ICT-based characteristics in the light of existing research. In Section 2.4, we propose potential applications of ICT-based bio-inspired nanonetworks in life sciences for diagnosis and treatment of diseases. Finally, we summarize the main aspects of this chapter in Section 2.5.

2.2 Intra-body Nanonetworks

In order to accomplish novel molecular communication paradigms for nanonetworks, the existing molecular communication systems in nature should be studied. Hence, we first review the previous work that proposes ICT-based models of the molecular communication in intra-body nanonetworks such as nervous, cardiovascular and endocrine systems. Moreover, open issues in modeling and analyzing these nanonetworks with respect to ICT-based parameters are highlighted.

2.2.1 Nervous Nanonetwork

Nervous nanonetwork is an ultra large-scale network of neurons gathering and transmitting information between different parts of the body. The communication between neurons takes place through chemical as well as electrical signaling referred to as neuro-spike communication [Balevi and Akan, 2013].

As depicted in Fig. 2.2(a), a general neural signaling pathway consists of three basic structures; pre-synaptic neuron, post-synaptic neuron and a synaptic gap between the two neurons [Balevi and Akan, 2013]. The information encoded in electrical impulses passes through the axon of a pre-synaptic neuron that conveys this information by releasing neurotransmitters, special types of chemical substances, into the synapse. These neurotransmitters are then received by the post-synaptic neuron. The physical channel model of this single-input single-output (SISO) neuro-spike communication is given in [Balevi and Akan, 2013]. The effect of inter-symbol interference on the achievable information rate of the SISO channel is studied in [Liu et al., 2014]. Since multiple pre-synaptic neurons are needed to transfer information in reality, multiple-input single-output (MISO) communication paradigm is modeled in [Malak and Akan, 2013a]. Moreover, SISO and MISO synaptic interference channels are investigated in [Malak and Akan, 2013b].

Although complete neuro-spike communication channel is considered in [Balevi and Akan, 2013] and [Malak and Akan, 2013a], there are other studies that analyze subparts of this channel. For instance, a trade-off between information rate and

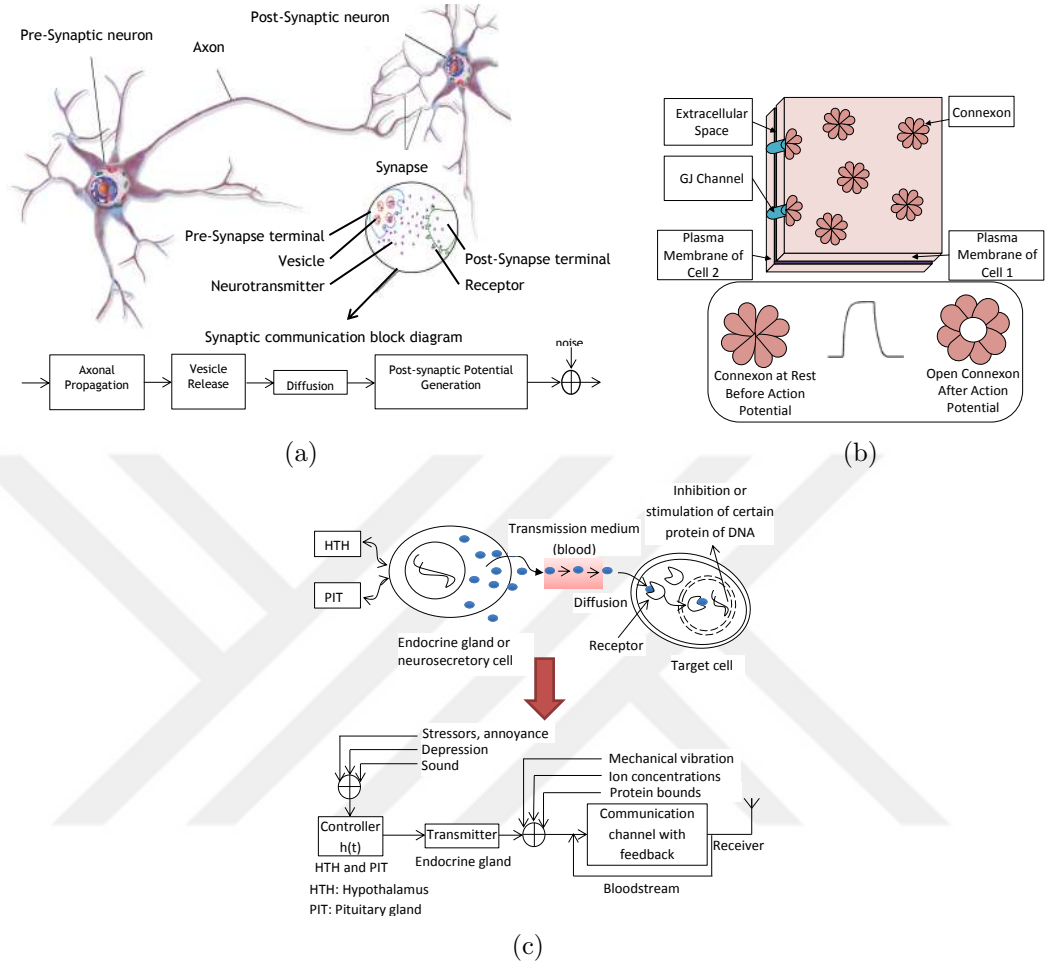

Figure 2.2: Intra-body molecular communications (a) Neuro-spike communication, (b) Gap-junction communication, The AP causes the connexon channels to open, starting diffusion between the cells, (c) The endocrine nanonetwork [Malak and Akan, 2012].

energy efficient transmission is examined within the axonal channel in [Goldberg et al., 2003] and a realistic model for vesicle release, which involves the effects of AP width variation is proposed in [Ramezani and Akan, 2015a]. Moreover, a receiver design in nervous network considering the variability in the anatomy of dendrites on post-synaptic neuron is given in [Cacciapuoti and Caleffi, 2015].

Neuro-spike communication has also been analyzed in the networked environment. An optimization problem for neuronal TDMA is formulated in [Suzuki et al., 2014], in order to find optimum TDMA scheduling. A queueing model for nervous

nanonetwork is also proposed in literature, which identifies the delay of the entire network of neurons [Abbasi and Akan, 2015].

The nervous nanonetwork is an optimum information processing system with respect to energy efficiency rather than the information capacity alone [Levy and Baxter, 1996, Mlynarski, 2014]. The information collected from environment by intra-body nanosensor networks is encoded, processed and transmitted by nervous system to corresponding organs. Several studies have been published to estimate these encoding mechanisms, such as, considering the discrete binary and frequency coding scheme [Levy and Baxter, 1996],interspike interval codes [Crotty and Levy, 2005], and rate and interspike interval decoders [Goldberg and Andreou, 2004]. On the other hand, in studies such as [Moujahid et al., 2011], stimulus response curves are fitted to input-output relationship of neuron with respect to information theoretical parameters. However, more efforts are required to reach the efficiency of neural encoding and decoding mechanism.

Moreover, information capacity of nervous nanonetwork needs to be quantified in order to implement ICT-based solutions of critical diseases of nervous system. A simple synaptic channel is proposed and analyzed from information theory perspective in [Manwani and Koch, 1998] to derive the lower bound on capacity. In another work, the correlation among pre-synaptic terminals is suggested to improve information rate [Malak and Akan, 2013a].

All of the existing ICT-based analysis of nervous nanonetwork use oversimplifying assumptions, hence, more comprehensive studies and experimental work are needed to understand ICT-based functionality of this network as listed bellow.

- ***Realistic models with experimental verification:*** More accurate ICT-based models including effects of AP shape variation, reuptake phenomenon in synapse modeling, and synaptic plasticity are required. Moreover, comprehensive experimental studies are needed to validate the models.

- ***Identifying fundamental characteristics of the model:*** After proposing a comprehensive model, information theoretical studies are needed to ex-

tract and quantify the fundamental characteristics.

- ***Networking paradigms:*** More comprehensive investigation of networking parameters is required to extract efficient routing algorithms, addressing mechanisms and medium access techniques from nervous nanonetwork.

- ***Energy efficient coding:*** Extracting energy efficient encoding and decoding techniques from these nanonetworks would be a milestone in building the foundations of molecular information and communication science.

2.2.2 Cardiovascular Nanonetwork

Two most important types of cells within the heart are the *cardiomyocytes* and the *cardiac pacemaker cells* [Severs, 2000]. Cardiac pacemaker cells are distributed throughout the heart and are responsible to spontaneously generate and propagate APs to cardiomyocytes, which, in turn, create the beating motion of the heart [Severs, 2000]. Cellular bridges form porous gap-junctions (GJs) between the various types of heart cells providing a medium for AP transfer [Jongsma and Wilders, 2000, Rohr, 2004]. Two cells connected in the GJ by means of channels called connexons are shown in Fig. 2.2(b). Connexons remain closed in the rest state, however, when an AP arrives, they open and yield an ion diffusion to occur towards the receiver cell, thus causing the AP to be carried forward to the next cell. Generic GJ communication is studied in [Kumar and Gilula, 1996] and [Nakano et al., 2007].

GJ channel is modeled from the information theoretical perspective by [Kilinc and Akan, 2013a], where a probabilistic physical channel model is provided with a probability mass function for GJ conductance considering the possibility of AP propagation failure. A closed-form expression for channel capacity and correlation between the decrease in capacity and several heart diseases is studied.

More studies are needed to provide foundations for an ICT-based model of cardiovascular molecular nanonetwork. Some open directions are listed bellow.

- ***Experimental verification:*** Assumptions about the independence between

calcium release units and membrane potentials require verification by experimental studies that can shed light on the actual capacity of the cardiovascular system, determining limits of capacity and rate functions for the healthy system.

- ***Large-scale model:*** Physiological studies to find the range and reliability of propagation as well as investigation of networking and routing mechanisms of APs through the heart is needed to consider the contribution of individual cells towards the whole organ.

2.2.3 Endocrine Nanonetwork

The endocrine system comprises a set of glands that secrete different hormones through the circulatory system to their recipient cells [Tepperman et al., 1968]. Transmission of hormones depends on concentrations of various materials sensed in tissues. The required amount of hormones are then added to the blood stream by the endocrine system to maintain homeostasis in body [McGregor, 2005]. The propagation of hormones depends on blood circulation as well as their Brownian motion within the blood stream [Giné and Akyildiz, 2009]. Reception of the hormones is selective because only the target cell can respond to a hormone.

Modeling of entire endocrine system from an ICT perspective is an open research area with huge implications, however, very few studies are present in this field to date. Hormones are considered as modulated molecular information carriers in the model of endocrine nanonetwork in [Malak and Akan, 2012]. The suggested framework is shown in Fig. 2.2(c), where various stimuli cause the Hypothalamus to signal the release of hormones to blood. A similar system is proposed in [Giné and Akyildiz, 2009]. A queueing theory-based insulin mediated GLUT 4 translocation model is present in [Jezewski et al., 2014]. Bidirectional communication between neuroendocrine and immune systems is discussed in [Weigent et al., 1990] and [Blalock, 1994]. In [Sperandio et al., 2003], bacteria-to-host communication via hormones is shown. Communication by means of milk borne hormones between the mother and

the suckling is proposed in [Koldovskỳ et al., 1994].

Further studies are needed to explore the modeling of endocrine nanonetwork in the following directions:

- ***ICT-based parameters:*** Key ICT-based parameters such as channel capacity, end-to-end delay, feedback weights, noise sources, synchronization, networking of subsystems are yet to be modeled for endocrine nanonetwork.

- ***Intra and inter-body networks:*** Potential of the endocrine nanonetwork as a connection between separate intra or inter-body networks also needs to be explored.

2.3 Science of Molecular information and Communication

Nanonetworks are being proposed to utilize different communication paradigms, however, molecular communication is found to be the most suitable method due to its compatibility with both biological and non-biological systems. Molecular communication paradigm is significantly different from traditional communication systems as it uses particles to carry information instead of electromagnetic carriers. Therefore, the ICT-based parameters of molecular communication paradigm are affected by physical and chemical properties of network entities such as diffusion coefficient of the channel, structure and type of molecules used as information carriers. Hence, the classical information science does not suffice to define the fundamentals of molecular communication. Thus, in this section, we outline the framework to establish the fundamental limits of molecular communication and information science. Moreover, we review the recent literature on different propagation mechanisms with the objective of their performance evaluation on the basis of ICT-based characteristics. Furthermore, future work is proposed for better performance analysis of each molecular communication technique.

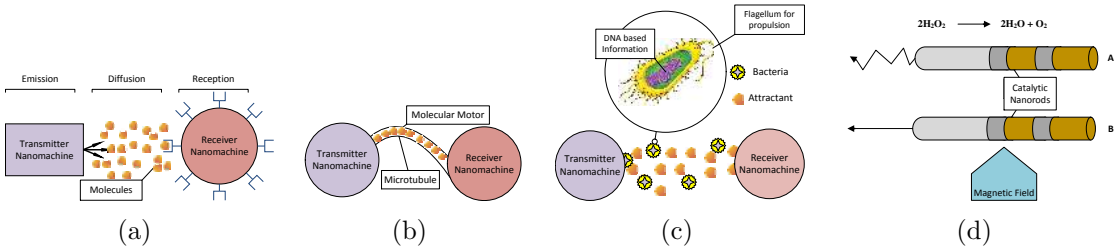

Figure 2.3: Molecular communication paradigms. (a) Diffusion-based molecular communication (b) Wired active molecular communication using a microtubule. (c) Bacteria-based wireless molecular communication. (d) Catalytic nanorods in hydrogen peroxide solution without and with applying a magnetic field applied (A) and (B), respectively.

2.3.1 Diffusion-based Molecular Communication

Most of the communication inside human body is achieved by diffusion of molecules, for example, calcium signaling among living cells, synaptic communication in neurons through neurotransmitters, and intra-cellular communication between different cell organelles. A general physical model of diffusion-based molecular communication is depicted in Fig. 2.3(a). Diffusion-based molecular communication is considered as the most promising paradigm for the applications of nanoscale networks inside human body. It can be categorized into analog and digital communication similar to conventional communication networks [Meng et al., 2014]. A fundamental analog communication model is proposed in [Pierobon and Akyildiz, 2010], where information is encoded by continuously emitting molecules with varying concentration. In digital diffusion-based communication, information is encoded into either types of molecules [Kuran et al., 2011], time of release of molecules [Kadloor et al., 2012] or the intensity of concentration of molecules [Mahfuz et al., 2010].

To develop a communication network, it is necessary to develop a physical model and analyze its ICT-based parameters aiming to achieve reliable and efficient communication. We can find various models of diffusion-based molecular communication in the literature. One such model is proposed in [Meng et al., 2014]. Another model, where particles are released into fluid medium with drift is studied and analyzed in [Kadloor et al., 2012].

One of the most important issues in developing diffusion-based molecular communication is residual molecules from previous transmission which are considered as noise and various approaches are suggested to maximize the rate of information by reducing this noise in [Moore et al., 2009]. Moreover, the information capacity of the channel with residual molecules is studied in [Pierobon and Akyildiz, 2013] by modeling it as *channel with memory*. Other external noise sources and ISI are modeled in [Noel et al., 2014].

Different digital modulation techniques for diffusion-based molecular communication are proposed in [Kuran et al., 2011]. Some of them are compared with respect to their susceptibility to interference in [Kuran et al., 2012]. Some receiver designs are presented in [Meng et al., 2014,ShahMohammadian et al., 2012], and [Kilinc and Akan, 2013b].

Although a significant body of research exists on diffusion-based molecular communication, much work remains to understand this unconventional communication paradigm as follows.

- ***Shadowing effect:*** Existing models should consider more complex situations such as inter and intracellular environment, where shadowing effect needs to be addressed as it can become dominant due to the presence of obstacles.

- ***Effects of asynchronism:*** More realistic assumptions should be considered about the structure and function of transmitter and receiver and effects of asynchronization between them, as asynchronism causes large delays and reduces the information transmission rate.

- ***Amplification:*** A concept of amplifier nanomachine should also be introduced to cater the problem of attenuation in concentration of molecules due to diffusion.

2.3.2 Wired Active Molecular Communication

Wired active molecular communication between a transmitter and a receiver nanomachine is illustrated in Fig. 2.3(b). Information molecules in this communication

paradigm move along preset paths of microtubules to deliver information from the transmitter to the receiver [Moritani et al., 2006]. The flow of information can be self-propelled by molecular nanomotors as in Fig. 2.3(b) or based on the flow generated by another system such as a blood circulatory system. Based on the assumptions of independence between particles, a simple mathematical model for analyzing information rate is derived in [Farsad et al., 2011]. A Markov channel model with a mathematical formula for calculating transition probability matrix of the model is proposed in [Farsad et al., 2014]. Design and optimization of the shape of a rectangular channel in [Farsad et al., 2012] shows that channel capacity is proportional to the perimeter. A secure wired active channel is proposed in [Moritani et al., 2007], where information molecules are encapsulated inside vesicles while transporting the information. Various approaches for self-organizing microtubule networks such as polymerization/depolymerization and molecular motors are investigated in [Enomoto et al., 2011]. Some directions for further studies are mentioned below:

- ***Particle interactions:*** Interactions between various particles traveling together in a microtubule and their effects on the overall ICT-based models need to be identified.

- ***Channel characteristics:*** Effect of channel characteristics such as width, shape and length on the model require further investigation.

2.3.3 Wireless Active Molecular Communication

Bacteria-based Wireless Active Molecular Communication

A typical system of wireless active molecular communication paradigm based on bacteria is shown in Fig. 2.3(c). In this type of communication, first, a bacteria that only responds to a set of specific attractants is chosen as a communication vessel. A DNA-based message is then introduced in the cytoplasm of the bacteria and it is released in the environment. The bacteria propels itself towards the receiver using its flagellum in response to the release of attractant particles by the receiver as shown in

Fig. 2.3(c) [Gregori and Akyildiz, 2010]. Communication range, channel capacity, throughput and end-to-end delay analysis is done in [Cobo and Akyildiz, 2010] shows that bacteria-based communication has huge potential. A physical channel characterization and simulation tool are provided in [Gregori et al., 2011]. Multi-hop communication based on conjugation and the use of antibiotics as message filters is proposed in [Balasubramaniam and Lio, 2013]. Wet lab validations for bacterial conjugation for multi-hop communication are further provided in [Balasubramaniam et al., 2014]. The problem of attractant scheduling for multiple transmitter-receiver pairs in close proximity is analyzed in [Gao et al., 2011]. A simulation tool for bacteria-based communication, BNSim, is introduced in [Wei et al., 2013].

Catalytic Nanomotor Based Wireless Active Molecular Communication

Catalytic nanomotors are usually platinum or gold nanorod particles that are able to propel themselves and small information containing objects, by catalyzing the free chemical energy present in the environment [Gregori and Akyildiz, 2010] as shown in Fig. 2.3(d). Without a controlling magnetic field, the nanorods move in arbitrary directions, however, once under the influence of a magnetic field, they can be forced to travel in specific directions. The speed of these particles depends on their dimensions as well as the atmospheric conditions [Paxton et al., 2004]. Physical channel characterization and parameters such as packet delay and loss probability are presented in [Gregori et al., 2010]. Methods for controlling catalytic nanomotor direction are presented in [Kline et al., 2005].

Open directions for future investigation of wireless active molecular communication include the following:

- ***Bacteria-type independent modeling:*** A definitive general model that can apply to a variety of bacteria-based communication scenarios as opposed to existing models for specific scenarios is required.

- ***Medium sharing:*** Scheduling and channel sharing in a multiple bacteria environment needs to be investigated.

- ***Information encoding:*** Methods for encoding information into DNA also are an open research direction.

- ***ICT-based parameters:*** Research on source coding techniques, channel capacity as well as networking capabilities of the systems will help improve the current models of wireless active transport.

- ***Bio-compatibility:*** Further research is required in the bio-compatibility of catalytic nanomotors.

2.3.4 Physical Contact-based Molecular Communication

Nanocommunication via gap-junctions and synapses are two possible kinds of molecular communication via physical contact. In [Guney et al., 2012], a collision-based mobile ad hoc molecular nanonetwork (MAMNET) is proposed, which uses neuro-spike communication for transmitting information between two nanomachines. It is shown that the size and speed of nanomachines have a direct relation with the average throughput and a reverse relation with the average message delivery delay. Neurons are used as molecular communication medium in [Balasubramaniam et al., 2011]. A microplatform is designed in [Nakano et al., 2008], which is able to pattern the mammalian cells into a predefined network connecting them trough gap-junctions. These preliminary studies are samples of achieving the bio-inspired molecular communication networks.

The open challenges in modeling bio-inspired physical contact-based molecular communication paradigms coincide with the challenges in modeling of neuro-spike communication and GJ as stated in Section II.

2.3.5 FRET-based Molecular Communication

One particular example of molecular devices is the class of fluorophores, e.g., fluorescent proteins, which can be excited by optical and chemical stimuli, and relax to ground-state by releasing photons at visible wavelengths [Lakowicz, 2013]. An excited-state fluorophore non-radiatively transfers its electronic energy state to a

nearby ground-state fluorophore, if their optical spectra overlap. This nanoscale phenomenon is defined as the Förster resonance energy transfer (FRET). As proposed in [Kuscu and Akan, 2012], FRET can be exploited as a wireless molecular communication method between functional fluorophores if the information is encoded into their electronic states. It is shown to enable reliable information transfer at exceptionally high rates, on the order of Mbps. A model for FRET-based MAMNET is provided in [Kuscu and Akan, 2014] consisting of sensor and actor fluorophores, which are promising for cancer diagnosis and treatment with single molecule precision.

Although FRET is extensively studied from communication theoretical perspective, some new directions for further studies are provided below:

- ***Comprehensive analytical models:*** Literature mostly consists of numerical simulation results and lacks comprehensive analytical models that can fully capture the underlying quantum-mechanical processes and provide the fundamental limits such as channel capacity.

- ***Validation:*** Experimental work is currently conducted with ensemble of molecules, and thus, the validation of FRET-based communication between a single-pair of fluorophores is still an open issue.

2.3.6 Fundamental Limits of Molecular Information Science

Fundamental limits of information theory are imposed by nature in order to provide answers to the following questions:

- Minimum number of bits necessary to represent an information signal

- Maximum transmission rate to achieve a reliable communication over a noisy channel

These fundamental limits are established for conventional communication networks through meticulous research that sprang from the classical paper of Shannon on

Table 2.1: The categorization of evaluation parameters.

Infrastructure and Physical Characteristics
Biocompatibility, Molecular dynamics, Molecular physics, Electrical properties, Type of medium, Size of network nodes, Duplexing, Packet type/size, Complexity, Information sources, Noise sources, Modulation types, Feasibility, Power consumption, Synchronization, Security, Type of network nodes
Communication Performance Characteristics
Molecules per bit, Energy per bit, Range, Capacity, Transmission rate, Signal attenuation, Security measures, Reliability, Error rate, Delay
Networking Functionalities
Routing, Medium sharing, Addressing, Broadcast, Medium access, Macro-nano interface

Table 2.2: Qualitative and comparative evaluation of different molecular communication paradigms.

	Diffusion-based MC	**Microtubule-based MC**	**Bacteria-based MC**	**Catalytic Nanomotor based MC**	**Physical Contact-based MC**	**FRET-based MC**
Carrier	*Molecules*	*Molecules*	*Bacteria*	*Nanorods*	*Molecules*	*Proteins*
Duplexing	*Half-duplex*	*Half-duplex*	*Half-duplex*	*Half-duplex*	*Half-duplex*	*Half-duplex*
Biocompatible	*Yes*	*Yes*	*Yes*	*No*	*Yes*	*Yes*
Broadcast	*Yes*	*No*	*Yes*	*No*	*No*	*Yes*
Routing	*No*	*No*	*Yes*	*Yes*	*No*	*No*
Medium Sharing	*Yes*	*Yes*	*Yes*	*No*	*No*	*No*

information theory [Shannon, 1948]. Since molecular communication deals with the particles instead of waves, these fundamental limits need to be re-established after taking into account certain physical and chemical characteristics of information carrier as well as transmission medium that are enlisted as follows.

- Size, type, structure and diffusibility of molecules
- Viscosity, heat capacity, thermal conductivity and electrical conductivity of medium

- Degree of chemical affinity among network entities

Analysis of the effects of these properties on ICT-based characteristics of molecular communication channels, which are listed below, helps reveal the fundamental limits of molecular communication paradigm.

- ***Minimum Molecules per bit:*** This fundamental limit can be affected by viscosity of the medium that affects the diffusion of molecules through the channel as well as binding rate of information carriers with the receiver. Moreover, clearance rate is another limiting factor that prevents ISI by controlling the concentration of residual molecules in the channel.

- ***Minimum Energy per bit:*** Energy per bit is limited by distance between sender and receiver, chemical affinity among network entities as well as electrical properties of the medium and information carriers. Moreover, sending more molecules increases the lower bound of this limit, hence, factors governing limits of number of molecules per bit are also important here.

- ***Channel capacity:*** All the physical and chemical properties of the molecular medium and receiver affect maximum achievable information rate. Moreover, presence of multiple path, for instance, in diffusion-based molecular communication, will also improve the information capacity of the channel.

- ***Bit error rate:*** There are certain phenomenon that causes error in molecular communication such as wandering of molecules away from the receiver, channel delay caused by multiple factors and noise due the presence of molecules released by other sources. Moreover, malfunctioning of the receiver, which can be a result of reaction of residual molecules with the receptors rendering them deactivated, can prevent binding of information carries causing transmission failure.

After defining these limits, optimum source and channel coding techniques are needed to be designed utilizing different ways of encoding information such as type,

concentration and release time of molecules.

2.3.7 Performance Evaluation of Molecular Communication Paradigms

Although focus of this study is mostly on biological applications of the molecular communication architectures described in this section, they also find wide range of applications in non-biological systems [Akyildiz et al., 2008] such as military, Industrial, and environmental applications.

To select the most suitable architecture for a particular application, biological/non-biological, the molecular communication architectures described here, should be evaluated based on the physical and information theoretical characteristics as categorized in Table 2.1. Based on the review of previous work on different molecular communication paradigms, we conclude that there are many open issues in each of these paradigms that remain to be investigated in order to quantify different ICT-based parameters that will, in turn, enable us to quantitatively evaluate these techniques. However, based on the existing literature, a fundamental qualitative evaluation using some basic physical characteristics and networking parameters of various molecular communication paradigms is given in Table 2.2.

2.4 Science of Molecular Information and Communication for Life Sciences

Understanding the fundamentals of molecular nanonetworks finds its major applications in life science. These bio-inspired nanonetworks are expected to pave the

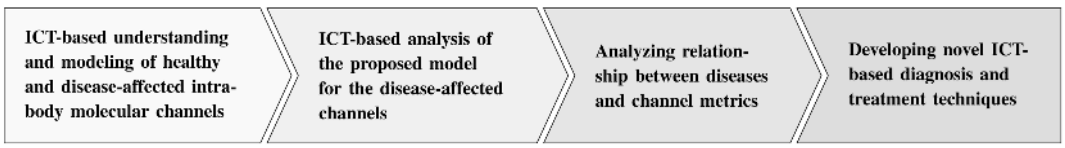

Figure 2.4: Framework for developing ICT-based diagnosis and treatment techniques.

way for novel and effective ICT-based diagnosis and treatment techniques for different diseases related to the natural intra-body nanonetworks. In this section, we emphasize the importance of science of molecular communication and information in developing these ICT-based diagnosis and treatment techniques.

2.4.1 ICT-based Understanding of Intra-body Molecular Communication diseases

A framework for developing ICT-based diagnosis and treatment techniques for intra-body molecular communication diseases is outlined in Fig. 2.4. Based on this framework and current research literature on molecular communication and intra-body nanonetworks, we propose several fundamental approaches to realize these ICT-based techniques.

- *Revealing the ICT-based characteristics of the disease-affected intra-body nanonetworks*: By detecting the fundamental differences between the ICT-based characteristics of healthy and disease-affected networks and their entities, ICT-based metrics may be explored to diagnose diseases. These studies may also enable the development of new treatment techniques inspired by the existing or upcoming theories and tools in the information science.

- *Developing biocompatible nanomachines*: These nanomachines can be used to monitor a certain mechanism inside the body, deliver drug to a specific part of the body or connect to intra-body nanonetwork and act as a part of that network to fix the effects of different diseases.

- *Cancer detection*: Not all of the existing intra-body molecular communications are in accordance with our health. For instance, the cancer cells that grow out of control and can spread to other parts of body need to communicate with and receive support from cells named stromal cells [Leef and Thomas, 2013]. If one can isolate the malignant cells from stromal cell, they would not grow anymore. Hence, understanding the mechanisms of these molecular communications provides a unique opportunity to use communication theoretical tools to interrupt these kind of communications and stop the spread of cancer.

In the following parts, we propose potential of utilizing of aforementioned ICT-based approaches in different intra-body molecular communication diseases.

Nervous System Diseases

Nervous system may face a wide variety of diseases as a result of dysfunction of single neuron or their network. Here, we relate some of the diseases of nervous system to ICT-based parameters of nervous nanonetworks.

- Alzheimer's disease, which degrades the capacity of the brain to encode and retrieve memories, is a result of dysfunction and loss of synaptic communication [Sheng et al., 2012].

- Multiple sclerosis (MS), which decreases the information transmission rate, is resulted from destruction of myelin over axon of neurons [Steinman, 1996].

- Parkinson's disease results from the death of dopamine producing neurons, which control the release of vesicle, an information carrier, in another set of neurons [Harnois and Di Paolo, 1990].

- Amyotrophic lateral sclerosis (ALS), progressive bulbar palsy, and primary lateral sclerosis are common motor neuron diseases that result from degeneration or death of the upper and/or the lower motor neurons. These diseases cause communication link failure in nervous nanonetwork, which affects the ability of the brain to control essential muscle activity such as walking, speaking, swallowing, and breathing [Filippi and Agosta, 2015].

Moreover, the ICT-based models of nervous nanonetworks can be used in building neural implants which can connect to the neural pathway in case of communication failure between brain and a certain part of the body. For instance, currently researchers are able to control the movements of legs of a completely paralyzed rat, by externally stimulating the spinal cord [Wenger et al., 2014]. ICT-based understanding of nervous nanonetwork can enable us to receive and encode the signals from motor cortex to stimulate the spinal cord in the aforementioned scenario.

Another important application is detecting the diseases related to blood brain barrier (BBB), which involves one of the most important and complex intra-body molecular communication channels and tightly protects the entry and exit of molecules to and from the central nervous system (CNS) [Rosenberg, 2012]. The dysfunction of the BBB causes critical cellular damages that may lead to different types of neural diseases. Moreover, existence of these BBB prevents the entrance of drugs to the CNS, which makes the treatment of neural diseases difficult. Hence, in addition to providing diagnosis and treatment techniques for the resulted diseases from dysfunction of BBB, understanding the ICT-based fundamentals of these channels may help to develop effective drug delivery mechanisms for the treatment of diseases in CNS.

Cardiovascular System Diseases

Cardiac arrhythmia forms one of the most prevalent group of heart conditions that cause irregular heartbeat patterns in patients [Jongsma and Wilders, 2000]. The detection of this whole set of diseases is based on standard electrocardiographic techniques that are manually operated by a practitioner, and thus, prone to human error [Opie, 2004]. Therefore, modeling of these diseases may find ICT-based identification and treatment of these conditions.

Endocrine System Diseases

To date, the literature for endocrine system is still in its infancy. Several studies on biochemical processes of different hormones exist in literature, however, the largest body of literature exists on the insulin signaling within the body. Several mathematical models for insulin-sugar cycle are presented in [Unger and Betz, 1998]. Meal simulation model of insulin-sugar cycle and the prevalent intercellular communication is discussed in [Man et al., 2007,Gerozissis, 2004]. Insulin communication within the pancreatic islets is further explored by [Bavamian et al., 2007]. GJ communication for insulin release within pancreatic islets is presented in [Benninger et al., 2011]. In a recent work, a novel method of insulin mediated GLUT 4 translocation

is provided based on queueing theory [Jezewski et al., 2014]. The method provides a unique perspective of the disease and the simulation results are comparable to existing experimental data.

2.4.2 Macro-Nano Scale Molecular Communication

Connecting the nano-devices to internet, termed as internet of nano-things (IoNT) [Akyildiz and Jornet, 2010], would show new horizons of applications. Along with other major applications, IoNT would play a vital role in healthcare by connecting nanonetworks of bio-sensors and actuators operating inside or near human body, which is called BAN [Seyedi et al., 2013], to healthcare provider for remotely monitoring patients' health through internet and administering drugs to patients requiring frequent or periodic dosages.

In the remaining part of this section, we briefly overview how molecular communication based BANs can be used for management of various medical conditions and applications.

Cardiovascular Disease Monitoring

Nanosensors may be used to measure and report critical parameters for cardiovascular diseases such as heart rate and report them to a hub. These readings may then be communicated to actuate automatic drug delivery or request further medical assistance.

Artificial Vision and Artificial Hearing

Artificial vision and hearing by means of stimulation of related brain regions with electrical signals is already a reality [Dobelle, 2000, Eddington et al., 1977]. Further researches in these directions may contribute towards the development of artificial organs.

Hormonal Therapy Management

Hormonal therapies find a variety of applications such as cancer treatment [Locker, 1998] and hormone replacement therapies in sex change [Murad et al., 2010]. By making use of BANs to provide the precise amounts of hormones required by the body, the treatments can become effective, speedy and the considerable side effects of hormone therapy [Dennerstein et al., 1978, Collaborators et al., 2003] may be reduced as well.

Drug Delivery

Targeted drug delivery is the process that aims to deliver medicine to the targeted region in human body saving other areas of the body from its side-effects. In the existing literature, two different approaches for drug delivery are being investigated;

- Encapsulating drug molecules in active bio-nanomachines that are capable of releasing them after reaching their target [Nakano et al., 2012a, Nakano et al., 2014, Chude-Okonkwo et al., 2014]. These machines can be realized by reengineering natural cells [Yoo et al., 2011] or synthetic nano-devices.

- Passive propagation of micro or nano particles of drug, called particulates, in blood stream to reach their target area [Chahibi et al., 2015, Chahibi et al., 2013]. It is proposed to overcome the limitations of pharmacokinetics-based methods of targeted drug delivery [Willmann et al., 2007].

2.5 Conclusion

This study introduced an entirely novel perception of molecular communication paradigms to lay down the foundations of science of molecular information and communication. Human body is an epitome of molecular signaling that is being investigated to design and optimize nanonetworks. Therefore, we seized this opportunity to analyze recent literature on intra-body nanonetworks and molecular communication and present open issues that need to be addressed in order to define

and extract the fundamentals of molecular information and communication science. Based on this investigation we proposed a framework to unveil fundamental limits of molecular information science by relating ICT-based characteristics of molecular communication channel to its physical and chemical properties. Finally, we highlighted the significance of molecular information and communication science in life sciences focusing on its applications in developing ICT-based diagnosis and treatment techniques for the diseases caused by malfunction of intra-body nanonetworks.

Chapter 3

DIFFUSION-BASED MODEL FOR SYNAPTIC MOLECULAR COMMUNICATION CHANNEL

3.1 Introduction

Computational methods have been extensively used to understand underlying dynamics of molecular communication methods employed by nature. One very effective and popular approach is to utilize a Monte Carlo simulation. Although it is very reliable, this method can have a very high computational cost, which in some cases renders the simulation impractical. Therefore, in [Khan et al., 2017], we presented a novel mathematical model for the diffusion and binding of neurotransmitters that takes into account the effects of synaptic geometry in three-dimensional space and re-absorption of neurotransmitters by the transmitting neuron. Based on this model we developed a fast deterministic algorithm, which calculates expected value of the output of this channel, namely the amplitude of EPSP (Excitatory Postsynaptic Potential), for given synaptic parameters. We validated our algorithm by a Monte Carlo simulation, which showed total agreement between the results of two methods. Finally, we used our model to quantify effects of variation in synaptic parameters such as position of release site, receptor density, size of postsynaptic density (PSD), diffusion coefficient, uptake probability and number of neurotransmitters in a vesicle, on maximum number of bound receptors that directly affect peak amplitude of EPSP.

There are number of models available for neuronal communication encompassing its biological functionality at various levels of complexity. Integrate-and-fire model [Dayan and Abbott, 2003] is the simplest spiking model that ignores biophysical mechanisms involved in generating spikes. On the other hand, Hodgkin-

Huxley model [Hodgkin and Huxley, 1952] includes channel conductances, responsible for triggering AP. While addressing the transmission of electrochemical impulses within neuron, these models do not consider biophysical mechanisms involved in inter-neuronal communication such as vesicle release, diffusion of neurotransmitters, receptor-ligand binding and re-uptake of neurotransmitters. In [Balevi and Akan, 2013] and [Veletić et al., 2016a], physical channel models for neuro-spike communication are proposed that encompasses all of these mechanisms to some extent. The information theoretical analysis of synaptic channel model with trial-to-trial variability in EPSP is given in [Malak and Akan, 2013a] and [Manwani and Koch, 2001].

All the given models are only close approximations of synaptic channel since capturing complex dynamics of neural signaling into a single model is quite challenging. Therefore, addressing this problem in modular fashion is a feasible solution. Thus, our focus is to model diffusion of neurotransmitters in synaptic cleft and their binding with postsynaptic receptors including the effects of their reflection from pre- and postsynaptic terminals of synaptic channel.

The existing models of synaptic channel deal with diffusion of neurotransmitters unrealistically without taking into account all geometrical and statistical determinants. In [Balevi and Akan, 2013], authors consider diffusion of neurotransmitters in one-dimension, however, authors of [Veletić et al., 2016a] consider three-dimensional diffusion model without taking into account their reflections from pre- and postsynaptic terminals. In [Malak and Akan, 2013a] and [Manwani and Koch, 2001], the effect of diffusion is combined with other factors into a single parameter that models trial-to-trial variability in EPSP. In [Agmon and Edelstein, 1997, Ventriglia and Di Maio, 2000, Franks et al., 2002], extensive simulation algorithms are used to determine the position of neurotransmitters within the cleft by drawing trajectories of their motion, however, these models are expensive in terms of time and energy. Therefore, a realistic mathematical model for diffusion and binding of neurotransmitters was required to analyze the effects of different statistical and geometrical parameters on synaptic communication at molecular level.

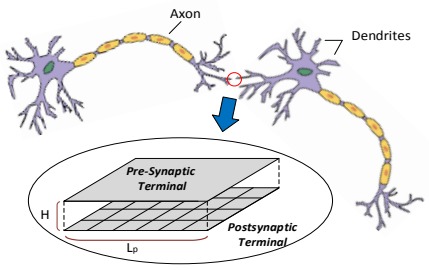

Figure 3.1: Geometry of a synaptic channel.

Thus, for a synapse in hippocampal region of brain, we proposed novel mathematical formulation that realistically models diffusion of neurotransmitters and their binding with postsynaptic receptors, incorporating the effects of synaptic geometry in three-dimensional space. Furthermore, we incorporate the effects of pre-synaptic re-uptake of neurotransmitters in our model and validate it through extensive Monte Carlo simulation and existing experimental work. We consider a Single-Input-Single-Output (SISO) synaptic channel as shown in Fig. 3.1 and, analyze the effects of variation in different synaptic components, namely, vesicle release site, receptor density, PSD size, number of neurotransmitters per vesicle, diffusion coefficient of glutamate and re-uptake probability, on EPSP. Consequently, major sources of trial-to-trial variability [Franks et al., 2003] in single postsynaptic response are discussed. Eventually, this analysis will lead us to understand the mechanism of *synaptic plasticity*. Finally, we analyzed our model of synaptic communication channel by determining error probability in received signal using optimum receiver.

The rest of this chapter is organized as follows. In Section 3.2, we give details of physiological assumptions and Monte Carlo simulation, and formulate a mathematical model for diffusion of neurotransmitters and their binding with postsynaptic receptors. Communication theoretical analysis of derived model is performed in Section 3.3. The results are discussed in Section 3.4. Finally, we conclude this chapter in Section 3.5.

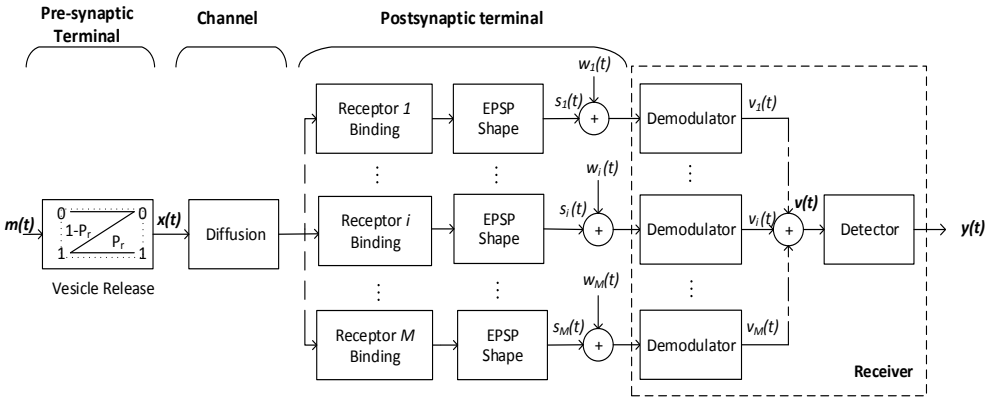

Figure 3.2: Block diagram of a synaptic channel.

3.2 SISO Synaptic Communication Channel Model

In this section, we propose our model for information transfer across synaptic channel, as shown in Fig. 2. We first describe physiological structure of our channel and make certain realistic assumptions to simplify our analysis. Then, we give mathematical description of molecular processes involved, namely diffusion and ligand-receptor binding, to establish an expected input-output relation for synaptic communication channel. The derived relation forms the basis for a deterministic code, which calculates expected behavior of output of the channel. Later, we briefly present the algorithm of a Monte Carlo simulation that corresponds to mathematical description of the channel previously developed. Both of these descriptions carry out the discussion up to receptor binding process. Afterwards, we give a brief discussion on the time-step, which, as an intrinsic property of the model, is related to the reaction rate constant of ligand-receptor pair. This discussion is an integral part of the descriptions of both the deterministic code and the simulation, as it relates experimentally determined parameter, namely the reaction rate constant, to simulation parameters. Finally, we describe EPSP generation following a given profile of ligand-receptor binding.

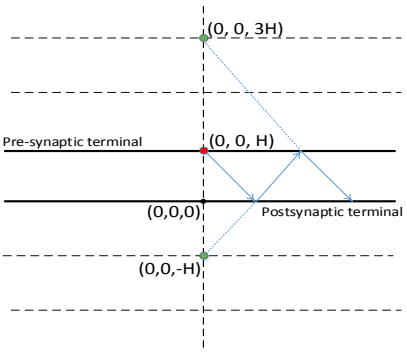

Figure 3.3: Diffusion of neurotransmitters in synaptic cleft

3.2.1 Physiological Assumptions

We model synaptic cleft as a rectangular box with height H, where top and bottom planes correspond to the pre-synaptic and postsynaptic membranes, respectively, both extending to infinity as in Fig. 1. This assumption does not affect the results since vesicles on pre-synaptic terminal and receptors on PSD are restricted to the limited region on both planes. Moreover, we assume that the movements of neurotransmitters are independent of each other. These assumptions allow us to derive exact analytical solution of diffusion process in the cleft under no-flux boundary conditions, i.e., when there is no neurotransmitter flow across both pre- and postsynaptic membranes. Furthermore, the diffusion model with pre-synaptic re-uptake is derived from the former model, i.e., with no-flux boundary conditions, via heuristic arguments.

After vesicle release, diffusion carries neurotransmitters from pre-synaptic end of the cleft to postsynaptic end containing PSD that consists of receptors waiting to capture incoming neurotransmitters to form a ligand-receptor complex. We assume that the receptors are uniformly distributed on PSD, a square-shaped region on the postsynaptic membrane with side length L_p. PSD has two major kinds of receptors, i.e., *AMPA (α-Amino-3-hydroxy-5-methyl-4-isoxazolepropionic acid)* and *NMDA (N-methyl-D-aspartate)* receptors. We suppose that we have only *AMPA* receptors on PSD since they mediate fast synaptic transmission and contribute in the fast

rise in EPSP. NMDA receptors contribute in synaptic plasticity, which is out of the scope of this work.

3.2.2 Mathematical Formulation

Vesicle Release

Vesicles are groups of neurotransmitters enclosed in a thin membrane, which are located right behind the pre-synaptic membrane of the transmitting neuron. Upon the arrival of the AP, depending on the shape of the signal, a number of these vesicles fuse with the pre-synaptic membrane to create a tunnel, through which the transmitters in the vesicles diffuse into the cleft. The region on the pre-synaptic membrane, where this fusion occurs is referred to as the Active Zone (AZ). Since we are considering a central synapse where synaptic boutons contain only one or a few active release zones [Manwani and Koch, 2001,Stevens and Wang, 1995], we can simplify our model by considering that only one vesicle is released in response to an AP.

The arrival of AP at pre-synaptic terminal is a random process owing to the axonal noise. Thus, the channel input $m(t)$ is modeled as an impulse train where probability of receiving an impulse is $P(m = 1) = p$. Impulse allows calcium influx into the cell, which triggers vesicle release with probability P_r. The value of P_r depends on the available vesicle pool size and the feedback from postsynaptic terminal signifying receptor saturation [Malak and Akan, 2013a]. As shown in Fig. 2, vesicle release is represented as a Z-channel, where $1 - P_r$ is probability of no release even if AP arrives at pre-synaptic terminal.

Once vesicle release starts, it takes very short time for all of the transmitters to enter the cleft, as compared to the total duration of diffusion process in the cleft. Thus, we assume that the contents of the vesicle are released instantaneously and the output of this channel is represented as,

$$x(t) = N_0\delta(t), \tag{3.1}$$

where N_0 is a constant and represents the number of neurotransmitters in one vesicle and Dirac delta represents instantaneous release of the vesicle.

Diffusion

Neurotransmitters diffuse into the cleft with a random Brownian motion. The resulting neurotransmitter concentration $C(x, y, z, t)$ is random, and its expected value can be well approximated by Fick's equation:

$$\frac{\partial C(x, y, z, t)}{\partial t} = D\nabla^2 C(x, y, z, t) \tag{3.2}$$

where D is diffusion coefficient, $t \geq 0$ and $(x, y, z) \in \mathbb{R}^2 \times [0, H]$. (3.2) is supplemented with initial distribution provided from the vesicle release module. Assuming that the release occurs at the origin of our xy-plane, due to (3.1) we have

$$C(x, y, z, 0) = N_0 \delta(x, y, z - H). \tag{3.3}$$

As for boundary conditions, we first assume that there is no flux of transmitters through pre- and postsynaptic membranes, which corresponds to the Neuman boundary conditions, i.e.,

$$\frac{\partial}{\partial z} C(x, y, 0, t) = \frac{\partial}{\partial z} C(x, y, H, t) = 0. \tag{3.4}$$

Upon integrating (3.2) over the cleft , one finds that with these boundary conditions, integral of concentration remains constant throughout time, i.e., the expected number of transmitters in the cleft do not change with time.

To find the solution of Fick's equation with initial data as in (3.3) under the boundary conditions given by (3.4), we may use symmetry of both the equation and the domain together with the fundamental solution of Fick's equation [Cussler, 2009], $c_\delta(x, y, z, t)$, in the whole domain $\mathbb{R}^3$ given by

$$c_\delta(x, y, z, t) = \frac{N_0}{(\sqrt{4\pi Dt})^3} e^{\frac{(-x^2-y^2-z^2)}{4Dt}}.$$

If there were no boundaries, then solution of (3.2) with the initial distribution given in (3.3) would be $c_\delta(x, y, z - H, t)$. The no-flux boundary conditions (3.4) intuitively imply that instead of diffusing freely across boundary, transmitters are reflected back into the cleft. The extra transmitters that will stay in cleft because of this reflection can be accounted for by reflecting the initial distribution across boundaries as in Fig. 3. Then, the distribution of transmitters at any given time is represented by free diffusion with initial distribution taken as sum of all reflections plus original source. As Fick's equation is linear, the corresponding solution will be

$$\begin{aligned} C(x,y,z,t) &= 2N_0 \sum_{k=-\infty}^{\infty} c_\delta\Big(x, y, z - (2k+1)H\Big) \\ &= \frac{N_0}{(\sqrt{4\pi Dt})^3} e^{\frac{(-x^2-y^2)}{4Dt}} \left\{ 2 \sum_{k=-\infty}^{\infty} e^{\frac{-(z-(2k+1)H)^2}{4Dt}} \right\} \end{aligned} \tag{3.5}$$

Observe that the coefficient 2 in (3.5) is due to the fact that the source sits right at pre-synaptic boundary, which causes the first reflection from the pre-synaptic side to coincide with the original source. By the symmetries of the equation and the domain, one can easily verify that this solution, restricted to the domain at hand, in fact solves Fick's equation and validates both the initial conditions (3.3) and the boundary conditions (3.4).

To model expected concentration of transmitters in presence of pre-synaptic re-uptake, we follow same arguments as in no-flux case with sole difference that we modify reflection coefficient of pre-synaptic boundary ($z = H$) according to the uptake probability, denoted by P_u in units uptake per hit. This means if $P_u = 0$, no transmitter that reaches the pre-synaptic membrane is absorbed, while $P_u = 1$ means that all particles that reach pre-synaptic terminal in the course of time, are absorbed. After making the corresponding modification to include P_u in (3.5), the new solution is obtained as

$$C_u(R,t) = \frac{N_0}{(\sqrt{4\pi Dt})^3} e^{\frac{(-x^2-y^2)}{4Dt}} \Bigg\{ \sum_{k=-\infty}^{-1} (2-P_u)(1-P_u)^{-(k+1)} e^{\frac{-(z-(2k+1)H)^2}{4Dt}} + \sum_{k=0}^{\infty} (2-P_u)(1-P_u)^{k} e^{\frac{-(z-(2k+1)H)^2}{4Dt}} \Bigg\}. \tag{3.6}$$

Ligand-Receptor Binding

The transmitters, that reach postsynaptic membrane, either get reflected from membrane, or they bind to the receptors in PSD to form a ligand-receptor complex. This binding process is modeled by assuming that AMPA receptors regularly sample a small effective volume V_e around them. The receptors are assumed to have only two configurations, i.e., bound state and unbound state. If a receptor is in unbound state and samples at least one transmitter in its V_e, then it binds to this transmitter.

Glutamate-receptor binding is a reversible process. Glutamate molecules dissociate from receptors and may rebind several times. The effects of rebinding can be observed from the prolonged decaying phase of EPSP, however, in rising phase of EPSP, the effect of unbinding is negligible. Thus, since we are interested in determining the peak of EPSP, we ignore the effects of unbinding process.

We calculate binding probability by first considering that we have only one neurotransmitter in the cleft, the probability of finding that particle inside the effective volume V_e around a receptor at time t is given by the integral

$$P_e(t) = \iiint_{V_e} C(x,y,z,t)dxdydz, \tag{3.7}$$

where depending on whether we model diffusion without or with pre-synaptic uptake, the function C is given by (3.5) or (3.6) with $N_0 = 1$. Note that, as

$$\iiint_{\mathbb{R}^2 \times H} C(x,y,z,t)dxdydz \leq 1, \quad \forall t \geq 0,$$

with equality holding for all times in case of no uptake, and only at $t = 0$ with

uptake, we always have that $P_e(t) \in [0, 1]$.

Owing to the assumption that all particle motions are independent of each other, the random variable $N_e(t)$ representing the number of neurotransmitters found inside V_e at time t has a binomial distribution with the expected value

$$E\left[N_e(t)\right] = N(t)P_e(t), \tag{3.8}$$

where $N(t)$ is the expected total number of unbound neurotransmitters in the cleft at time t. Now, according to our assumption it is sufficient to have a single neurotransmitter inside V_e for a receptor to be in bound state. It follows that the probability that the receptor will remain unbound after a sampling at time t is $(1 - P_e(t))^{N(t)}$, which simply says that the receptor remains unbound if and only if none of the neurotransmitters are inside V_e. Thus, the binding probability P_b for an unoccupied receptor after a sampling at time t is

$$P_b(t) = 1 - (1 - P_e(t))^{N(t)}. \tag{3.9}$$

Observe that, by (3.8) we have following approximation of P_b valid for large N, i.e., large number of transmitters in the cleft,

$$P_b(t) = 1 - (1 - \frac{E\left[N_e(t)\right]}{N(t)})^{N(t)} \approx 1 - e^{-E[N_e(t)]}. \tag{3.10}$$

This binding probability can also be thought of as expected neurotransmitter flux through an unoccupied receptor during the instantaneous sampling process at time t. As a consequence, the expected availability of the receptor decreases, which can be interpreted as that for the next sampling process we will have a less number of receptors at the same spot, a 'fractional receptor' so to speak. Due to this decrease in expected availability of receptor, binding probability, at the next time-step, also decreases by the same amount; after all binding probability given by (3.9) was for a 'whole' receptor. Thus, at the k^{th} sampling process, $k \geq 1$, the binding probability

is found by

$$P_b(k\Delta t) = a(k\Delta t)\left[1 - (1 - P_e(k\Delta t))^{N(k\Delta t)}\right], \tag{3.11}$$

where Δt is the duration of each sampling process or simply a *time-step* and $a \in [0, 1]$ is the expected availability of receptor, which, itself, is then adjusted for the next step by

$$a((k+1)\Delta t) = a(k\Delta t) - P_b(k\Delta t). \tag{3.12}$$

For each receptor, the initial condition that accompanies the iterative scheme (3.11)-(3.12) is

$$a(\Delta t) = 1,$$

which corresponds to the assumption that, before the first sampling all the receptors are unoccupied. The total expected number of bindings at each step, N_b, can be found by adding the binding probabilities of all the receptors

$$N_b(k\Delta t) = \sum_{j=1}^{M_0} P_{b,j}(k\Delta t),$$

where M_0 is the number of receptors in the PSD. Finally, at each time-step, we update the number of unbound neurotransmitters left in the cleft by the formula

$$N((k+1)\Delta t) = \left[N_0 - \sum_{i=1}^{k} N_b(i\Delta t))\right] \iiint_{\mathbb{R}^2 \times H} C(x, y, z, t)dxdydz,$$

where C is given by (3.5) or (3.6) with $N_0 = 1$. The integral term is the contribution of uptake, and the sum that is subtracted is due to receptor binding. The fact that we subtract the transmitters that are bound before applying the effect of uptake is justified by the assumed mutually independent motions of transmitters and the fact

that the bound transmitters cannot be taken up (since we ignore the dissociation), and neither can the transmitters that are taken up bind a receptor.

3.2.3 Monte Carlo Simulation

In this subsection we briefly present the details of a Monte Carlo simulation for the synaptic communication channel, the mathematical model of which we have given above.

Algorithm

A full simulation of a synaptic channel requires simulation of both diffusion and ligand-receptor binding processes simultaneously. As in our model the latter depends only on the existence of a neurotransmitter inside an effective volume V_e, the only thing to simulate in our case is the location of neurotransmitters in a regular grid. This is done by taking random seeds as input in each time-step for each of the three coordinates of neurotransmitters, using the distribution given in (3.6) after normalization. The x and y-coordinates have Gaussian distribution with $mean = 0$ and $variance = 2Dt$. However, z-coordinate follows the distribution derived after considering synaptic geometry given by (3.6).

Similarly, we calculate the position of M_0 receptors uniformly distributed on PSD that is kept fixed during entire simulation for a particular value of receptor density. We consider effective volume V_e around each receptor, where a neurotransmitter-receptor are most likely to bind. In each time-step, we simulate the position of N_0 neurotransmitters, and all unbound receptors having at least one neurotransmitter inside its V_e are considered bound. In next time-step, we subtract number of bound receptors and neurotransmitters from the pool of unbound receptors and neurotransmitters, respectively.

3.2.4 Time-step

The 100% binding probability that we assume at each sampling makes the output of our simulation sensitive to the changes in the time-step Δt. The decrease in the time-

step corresponds to the increase of the sampling rate of the receptors, which yields a rise in the binding rate. Thus, the output of our simulation is highly dependent on the time-step Δt. In what follows, we derive how to choose the correct time step for given effective volume V_e and binding rate constant for glutamate-AMPA pair utilized in literature, see Table I.

In our model we assume only two possible states of the receptors, either bound or unbound. They start in an unbound state, and when they bind to a transmitter, they stay bound forever since we are only analyzing the rising phase of the EPSP. This implies that they are memoryless, i.e., given that the receptor is unbound at time 0, for a fixed concentration of transmitters and any $t, t_0 \geq 0$ the probability of binding in the time interval $[0, t]$ is the same as a binding happening inside the interval $[t_0, t_0 + t]$ provided that the receptor is unbound at time t_0. It follows that the binding probability $\widetilde{P}_b$ of the receptor is exponentially distributed in time with some expected binding time, τ_b, where τ_b depends on the concentration near the receptor. Consequently, the probability that the receptor binds in the time interval $(t, t + \Delta t)$ provided that it remains unbound until time t is given by

$$\widetilde{P}_b((t, t + \Delta t)) = \frac{1}{\tau_b} \int_0^{\Delta t} e^{-\frac{\tau}{\tau_b}} d\tau \approx 1 - e^{-\frac{\Delta t}{\tau_b}}, \tag{3.13}$$

where the approximation is due to the assumption that for small Δt the transmitter concentration near the receptor is constant and consequently τ_b is constant. From this we deduce that, for a given concentration C_t of neurotransmitters near an unbound receptor, on average the receptor captures a neurotransmitter every $\tau_b = \tau_b(C_t)$ seconds. This corresponds to a binding rate constant of

$$\kappa_r = \frac{1}{C_t \tau_b}$$

in units $M^{-1}s^{-1}$. The expected concentration near the receptor C_t can be approxi-

mated as

$$C_t \approx \frac{E\left[N_e(k\Delta t)\right]}{|V_e|},$$

where $|V_e|$ is the size of the effective volume. Thus, the binding rate constant of the memoryless model reads

$$\kappa_r = \frac{|V_e|}{E\left[N_e(k\Delta t)\right]\tau_b} \tag{3.14}$$

Comparing (3.13) with (3.10) we see that the binding probability we have derived in Section 3.2.2 is approximately same as that of a memoryless receptor model provided that one has the identity

$$E\left[N_e(k\Delta t)\right] = \frac{\Delta t}{\tau_b}.$$

Plugging this identity into (3.14) and rearranging we find the desired relation

$$\Delta t \approx \frac{|V_e|}{\kappa_r}.$$

The value of Δt in Table 1 is calculated from this relation.

3.2.5 Postsynaptic Response

When a neurotransmitter is bound to a receptor, a channel opens. This allows ionic flux into the cell, changing its membrane potential called postsynaptic potential. The postsynaptic potential of each receptor is modeled as alpha function [Dayan and Abbott, 2001]

$$s_i(t) = h_i\alpha(t), \tag{3.15}$$

where $\alpha(t) = \frac{t}{t_p}exp(1 - \frac{t}{t_p})$ with h_i as the peak amplitude and t_p as time to peak of the response of each receptor.

3.3 Communication Theoretical Analysis

We use optimum receiver for our model as designed in [Balevi and Akan, 2013] that has following two hypothesis for packet detection:

$$H_1 : v = \sum_i c_i h_i + n_i \tag{3.16}$$

$$H_0 : v = \sum_i n_i \tag{3.17}$$

where v is the input to the detector as shown in Fig. 2, h_i is a random variable due to the randomness in opening of ionic channel once the receptor is bound as well as in the amount of ions that flow into the channel once it is opened. c_i and n_i for each receptor i are

$$c_i = \int_{T_n}^{T_{n+1}} \alpha^2(t)dt \tag{3.18}$$

$$n_i = \int_{T_n}^{T_{n+1}} w_i(t)\alpha(t)dt \tag{3.19}$$

where $w_i(t)$ is a synaptic noise that is considered as additive white Gaussian noise and $[T_n, T_{n+1}]$ is the time interval for receiving one packet of data.

The likelihood ratio for optimum detection is,

$$\Omega = \frac{P(v|H_1)}{P(v|H_0)} = \frac{\frac{1}{\sqrt{2\pi\sigma_1^2}} exp(-\frac{(v-\mu_1)^2}{2\sigma_1^2})}{\frac{1}{\sqrt{2\pi\sigma_0^2}} exp(\frac{-v^2}{2\sigma_0^2})} \tag{3.20}$$

where v/H_1 is also a Gaussian random variable according to the central limit theorem since v is the sum of many independent and identically distributed (i.i.d) random

variables. The threshold value for detection criterion is

$$th = ln\Omega - ln\frac{\sigma_0}{\sigma_1} + \frac{\mu_1^2}{2\sigma_1^2}, \tag{3.21}$$

where

$$\mu_1 = E[v|H_1] = \sum_i c_i E[h_i] \tag{3.22}$$

$$\sigma_1^2 = Var[v|H_1] = \sum_i c_i Var[h_i] + Var[n_i] \tag{3.23}$$

$$\mu_0 = E[v|H_0] = 0 \tag{3.24}$$

$$\sigma_0^2 = Var[v|H_0] = \sum_i Var[n_i] \tag{3.25}$$

and the probability of error in the output is given as,

$$\begin{aligned} P_e =& [P(y < th|x = 0)(1 - P_r) + P(y < th|x = 1)P_r] \\ & P(m = 1) + P(y > th|x = 0)P(m = 0) \end{aligned} \tag{3.26}$$

3.4 Results and Discussion

3.4.1 Determination of EPSP Peak

The peak of EPSP, as described in Section 3.2.5, directly corresponds to the maximum number of bound receptors, $M_{b,max}$. Since we neglect the effects of dissociation of transmitters from AMPA receptors, the number of bound receptors, $M_b(t)$, obtained from our simulation is a monotonically increasing function of time. Consequently, finding peak time, T_p and the peak value, $M_{b,max}$, seems out of reach. However, we may define these quantities by utilizing dissociation rate constant κ_d,

Table 3.1: Simulation Parameters for Diffusion Model

Synaptic cleft height	H	$20nm$ [Savtchenko and Rusakov, 2007]
Neurotransmitters/Vesicle	N_0	3000 [Rusakov et al., 2011]
Diffusion coefficient	D	$0.33\mu m^2/ms$ [Nielsen et al., 2004]
Side length of PSD	L_p	$0.4\mu m$
Receptor Density	$[AMPA]$	$500 - 3000/\mu m^2$ [Montes et al., 2015]
Number of receptors	M_0	$[AMPA] \times L_p^2$
Pre-synaptic Re-uptake	P_u	10%
Binding Rate of AMPA	κ_r	$78 \times 10^6 M^{-1}s^{-1}$
AMPA Dissociation Rate	κ_d	$750s^{-1}$ [Agmon and Edelstein, 1997]
Mean of h_i	$E[h_i]$	1
Variance of h_i	$Var[h_i]$	0.6^2
Variance of noise	$Var[n_i]$	0.01
Effective Volume	V_e	$1nm \times 1nm \times 0.5nm$
Time step	Δt	$3.85ns$
Simulation time	T_p	$100.9\mu s$

which we have ignored so far. We choose T_p such that at $t = T_p$ the total binding and dissociation rates are equal, where the total binding rate, $r_b(t)$, at a given time t is the rate of change of $M_b(t)$ with respect to time, and the total dissociation rate $r_d(t)$ is found by multiplying κ_d and $M_b(t)$ at time t. We choose $M_{b,max}$ as the value of $M_b(t)$ at $t = T_p$. This method of choosing T_p and $M_{b,max}$ exactly corresponds to the assumption that total amount of dissociation from the receptors up until the peak time is negligible.

3.4.2 Comparison of two methods

We perform Monte Carlo simulation described in Section 3.2.3 with parameters given in Table I. A square PSD of side length L_p is modeled by a 21×21 grid of small squares with a single receptor in the center of each, i.e. $M_0 = 441$. This corresponds to a receptor density of approximately 2750 $receptors/\mu m^2$ falling into the range given in Table I. The time course of glutamate-receptor binding is depicted in Fig. 4. To represent the simulation results, i.e., $M_b(t)$ after each time-step, the squares containing bound receptors are highlighted.

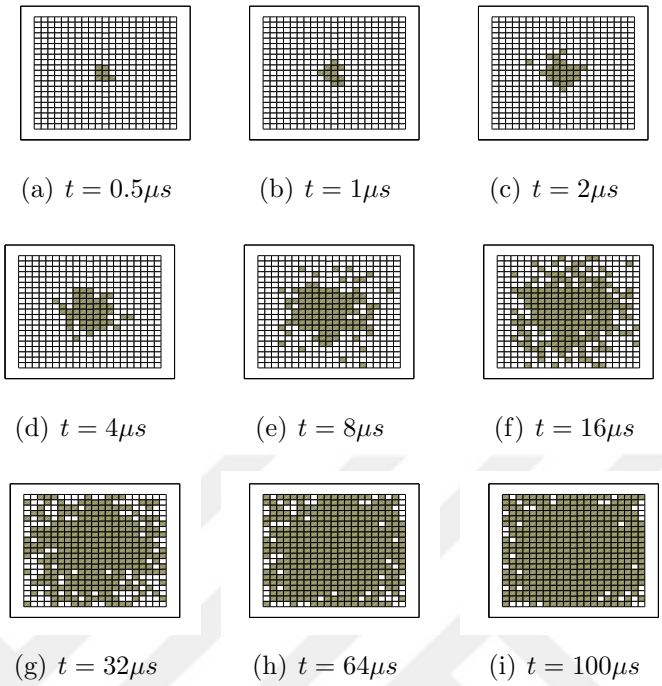

(a) $t = 0.5\mu s$ (b) $t = 1\mu s$ (c) $t = 2\mu s$

(d) $t = 4\mu s$ (e) $t = 8\mu s$ (f) $t = 16\mu s$

(g) $t = 32\mu s$ (h) $t = 64\mu s$ (i) $t = 100\mu s$

Figure 3.4: Time-course of glutamate-receptor binding on 21×21 grid of receptors with vesicle release site in the center.

It can be observed that the receptors exactly opposite to the vesicle release site are the first to bind due to maximum concentration of neurotransmitters at this point. We see that with these parameters the receptor grid is almost saturated in response to single vesicle release as in Fig. 4. Interestingly, this result is in agreement with the other existing experimental work [Clements, 1996, Tong and Jahr, 1994, Tang et al., 1994] as well as the simulation model developed in [Agmon and Edelstein, 1997]. The significant difference between the number of neurotransmitters in a vesicle and the receptors present on the PSD assures saturation with single vesicle release.

The results obtained by theoretical model of Section 3.2.2 and by simulation algorithm described in Section 3.2.3, are compared in Fig. 5(a) and (b) for different sets of parameters. In Fig. 5(a), the theoretical model is validated for different values of N_0 and in Fig. 5(b), the theoretical model is validated for different values of uptake probability P_u. It is observed that the time-course of glutamate-receptor

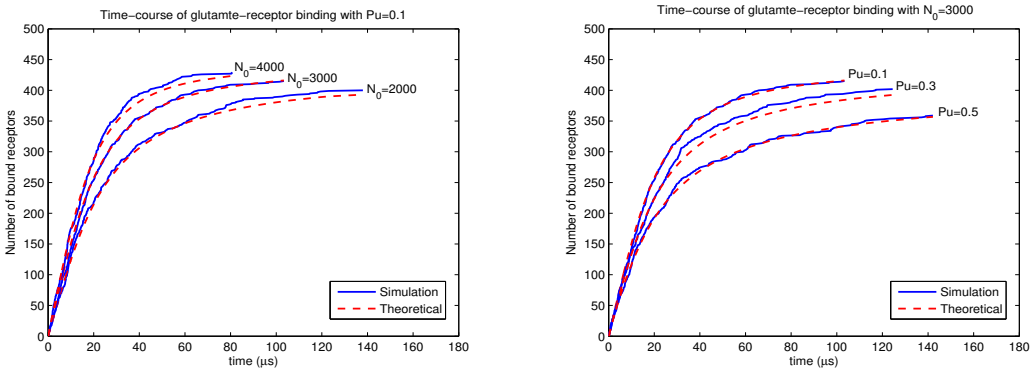

(a) (b)

Figure 3.5: Time-course of glutamate-receptor binding (a) with $P_u = 0.1$ (b) with $N_0 = 3000$.

binding from both the methods are similar. This observation signifies the importance of the theoretical model for diffusion and binding of the neurotransmitters developed in this work, as it is *much faster* than the simulation algorithm requiring position of neurotransmitters as random seeds in each time step. For comparison, the calculation of data with $N_0 = 3000$ and $Pu = 0.1$ plotted in both Fig. 5(a) and 5(b), took approximately 3 minutes on a PC for the deterministic code, while it took 1.5 hours on the same PC for each experiment of the simulation.

This significant improvement in speed allows us to analyze in greater detail the factors affecting peak amplitude of EPSP, which are directly related to $M_{b,max}$. Therefore, in the following, we observe the effects of variations in different synaptic parameters such as the uptake probability, the number of neurotransmitters in a vesicle, the diffusion coefficient, the receptor density and the size of PSD, on $M_{b,max}$ and T_p.

3.4.3 Factors Affecting Maximum Bound Receptors

Number of neurotransmitters per vesicle and pre-synaptic re-uptake

The variations in these quantities have direct effect on neurotransmitter concentration near PSD, and therefore, alter receptor binding dynamics significantly. High number of neurotransmitters N_0 per vesicle, or a low uptake probability P_u results

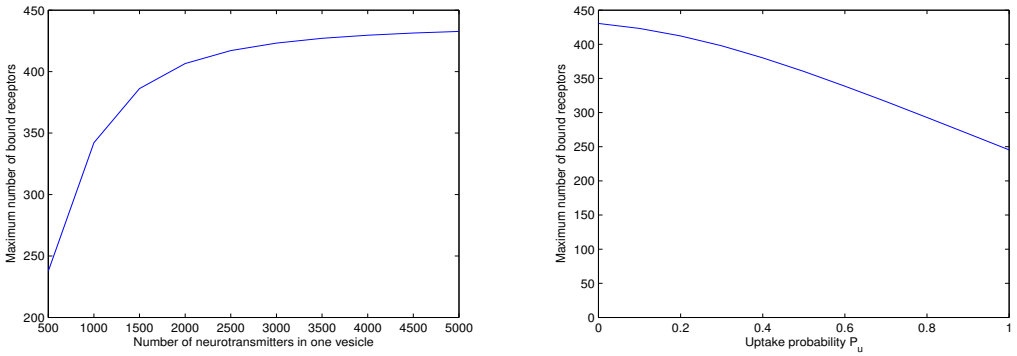

(a) (b)

Figure 3.6: Variation in Maximum Number of bound receptors with (a) Number of Neurotransmitters per vesicle (b) Uptake Rate.

in a higher concentration of transmitters in the cleft, which, in turn, yields a faster binding rate and a higher value of $M_{b,max}$ as shown in Fig. 6.

We see in Fig. 6(a) that PSD almost saturates for N_0 larger than 2000 transmitters per vesicle, but for lower quantities the variation in $M_{b,max}$ becomes significant. Thus, a possible explanation for trial-to-trial variability of EPSP amplitude is that N_0 varies in the range $500 - 2000$. The large variance of $M_{b,max}$ over this range also increases the neurons ability to encode and decode information.

Fig. 6(b) shows that even in case of no reflections from pre-synaptic boundary, i.e., $P_u = 1$, the value of $M_{b,max}$ is significantly high, at around 250, which is more than half of the available receptors. This number is much higher for plausible values of P_u. This observation is in correspondence with the previous results of [Franks et al., 2002] that the pre-synaptic re-uptake has small effect on the peak amplitude of EPSP.

Time to reach maximum bound receptors T_p, somewhat counter-intuitively, is inversely related to $M_{b,max}$, as seen in Fig. 7. After all, binding more receptors takes more time as expected. However, this is an observed phenomenon [Sayer et al., 1990], and it is a recurring theme, in that, for any variation of a physiological parameter, which increases the transmitter concentration in the cleft, $M_{b,max}$ increases, whereas T_p decreases.

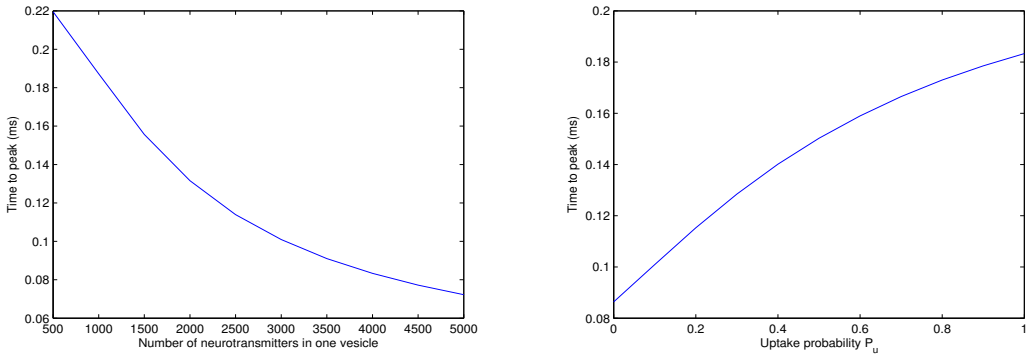

(a) (b)

Figure 3.7: Variation in time to peak with (a) Number of Neurotransmitters per vesicle (b) Uptake Rate.

Vesicle release site

We first observe the effect of changing location of vesicle release site on $M_{b,max}$. We add an offset of $200nm$ in x-direction in the original position of release site and obtain corresponding time-course of glutamate-receptor binding from Monte Carlo simulation as shown in Fig. 8. It is apparent that change in release site changes distribution and number of bound receptors reinforcing the argument that relocation of release site is one of the factors that change synaptic efficacy in subsequent trials.

For larger values of offset in vesicle release position the binding process takes significantly more time to reach its peak as shown in Fig. 9. As expected, moving release site away from receptor grid reduces the value of $M_{b,max}$ and increases the time to peak. This can be explained by the same reasoning given for the changes caused by varying vesicle size and uptake probability, and the fact that, the further away from the PSD the transmitter release occurs, the lower will be the transmitter concentration near the PSD.

An important feature to observe from Fig. 9(a) is how the reducing effect of the uptake on $M_{b,max}$ grows with the offset in the transmitter release location. This follows from the fact that, on a longer journey to the PSD the uptake mechanism captures more transmitters. This fact supports the notion that the synaptic channel noise due to contamination by transmitters from surrounding AZ-PSD pairs is small,

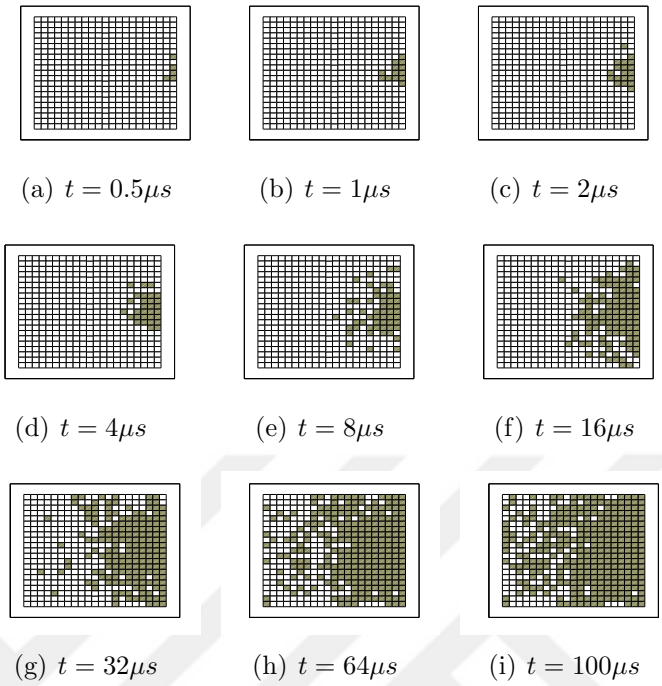

(a) $t = 0.5\mu s$ (b) $t = 1\mu s$ (c) $t = 2\mu s$

(d) $t = 4\mu s$ (e) $t = 8\mu s$ (f) $t = 16\mu s$

(g) $t = 32\mu s$ (h) $t = 64\mu s$ (i) $t = 100\mu s$

Figure 3.8: Time-course of glutamate-receptor binding on 21×21 grid of receptors with vesicle release site on the right edge.

which is in accordance with the findings of [Franks et al., 2002] that signaling at different glutamatergic synapses are independent of each other.

Receptor density and the size of the PSD

We simulate our model for different receptor densities keeping PSD area and other variables constant as mentioned in Table I such that number of unbound receptors in the given area increases. We observe in the Fig. 4 that a significant difference in N_0 and M_0 achieved high level of saturation of PSD, i.e., approximately 96%. Therefore, we can intuitively predict that decreasing the difference in N_0 and M_0, obtains lower level of saturation. Thus, it is shown in Fig. 10(a) that the percentage of PSD saturation decreases with the increase in receptor density, however, the level of saturation does not fall significantly since the largest value for concentration in our simulation gives value of M_0 that is still quite lower than N_0. Therefore, we may observe drastic fall in saturation level for much higher values of receptor densities.

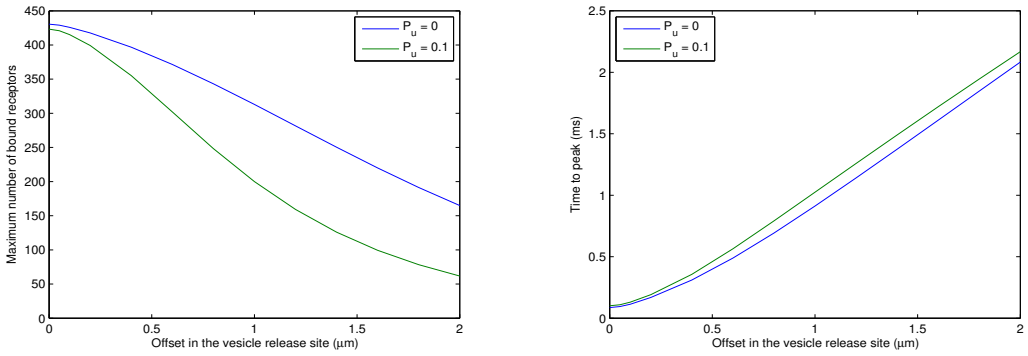

(a) (b)

Figure 3.9: Effect of offset in vesicle release site on (a) Maximum number of bound receptors (b) Time to peak.

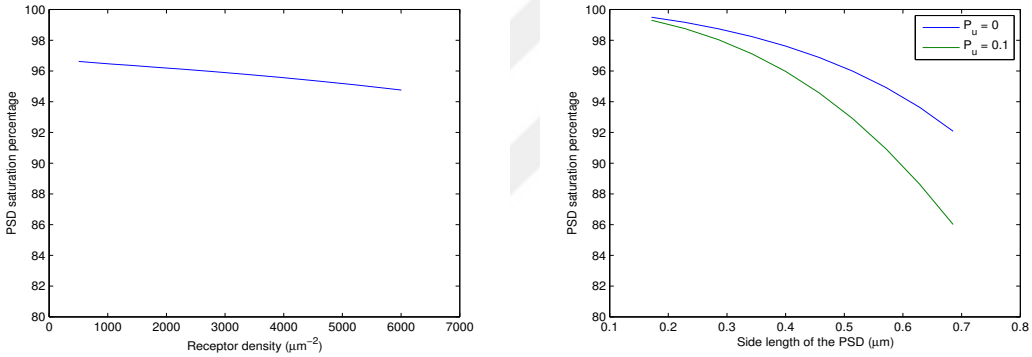

(a) (b)

Figure 3.10: PSD saturation with (a) receptor density (b) PSD size.

Furthermore, we just vary the PSD area with a fixed receptor density at 2750 receptors/μm^2, the reduction in saturation level is quite significant as shown in Fig.10(b). The reason for this effect is similar as for the effect caused by increasing off-set in vesicle release site. In both cases, distance between vesicle release site and a certain set of receptors is increased resulting in lower concentration of neurotransmitters around the receptors away from the release site, decreasing their binding probability, hence, we obtain lower level of saturation. This rate of reduction in saturation level is increased by increasing the uptake rate that further reduces number of neurotransmitters.

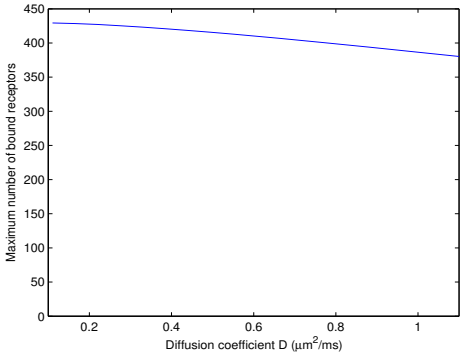

Figure 3.11: $M_{b,max}$ Vs D

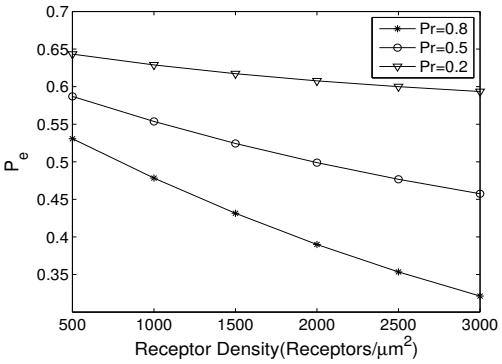

Figure 3.12: P_e Vs [AMPA].

Diffusion coefficient

The diffusion coefficient D encapsulates the rate of spread of glutamate molecules inside extracellular fluid medium of synaptic cleft, a higher value corresponding to faster spread. In literature, different values of D has been used by different authors, all falling in the range $0.1 - 1\ \mu m^2/ms$ [Agmon and Edelstein, 1997, Franks et al., 2002, Ventriglia and Di Maio, 2000]. As seen in Fig. 11, $M_{b,max}$ decreases with increasing D since with a larger D the transmitters spread and leave the volume above the PSD faster.

3.4.4 Error Probability

Probability of error P_e is a major performance measure of a communication channel. We simulate our model using parameters listed in Table 3.1 and determine $M_{b,max}$ for different values of receptor density keeping PSD size constant. The response generated by bound receptors is detected by optimum receiver described in Section 3.3.

Using (18), we evaluate P_e as a function of postsynaptic receptor density for different values of vesicle release probabilities, as shown in Fig. 12. We keep incoming spike probability constant at $P(m = 1) = 0.7$. It can be observed that for a certain value of P_r, P_e always reduces with the increase in receptor density. This result complies with the fact that given high probability of vesicle release, higher number of receptors on PSD would obtain higher value of $M_{b,max}$ ensuring accurate detection, thus, reducing probability of error.

The advantage of the proposed model is that it enables us to analyze synaptic parameters on molecular level producing faster results than the conventional simulation models, as shown by the above discussion. Thus, we dedicated a subsection to analyze each important factor affecting the dynamics of the synaptic communication. Moreover, this study leads to the analysis of important parameters such as variation in vesicle size or receptor density that are responsible for synaptic plasticity in neurons and therefore, memory formation.

3.5 Conclusion

In this chapter, we investigated one of the most advanced mechanism of molecular communication that exists in nature. We focused on the point-to-point synaptic channel in hippocampal neuron and introduced a novel mathematical formulation of neurotransmitters' diffusion in synaptic cleft that encompasses the effects of geometrical structure of synapse and re-uptake phenomenon. As a result of this mathematical achievement we have developed a deterministic code, which calculates the expected behavior of synaptic molecular communication channel. The predictions of

this code are successfully verified by a corresponding Monte Carlo simulation. This is one of the main contributions of this work, as the code developed takes much less time for the same task compared to the Monte Carlo approach.

Moreover, we observed the effects of variations in various synaptic parameters on number of maximum bound receptors and time to reach this maximum, which together determine EPSP profile. The results obtained in this analysis comply with the outcomes of existing physiological studies and simulations in literature. We also discussed the possible causes of trial-to-trial variability in peak amplitude of EPSP. Eventually, we performed communication theoretical analysis of our model by evaluating error probability in output detection.

Chapter 4

INFORMATION THEORETICAL ANALYSIS OF SISO SYNAPTIC COMMUNICATION

4.1 Introduction

In nervous system, sensory information from outside world as well as signals from other organs are encoded into AP's, which are transmitted through a neuronal network to be processed by brain. Information theory provides a mean to estimate the transmission capacity of this complex communication network along with quantifying the reliability of the synaptic communication model [Borst and Theunissen, 1999] .

Neuro-spike communication has been studied from information theoretical perspective at different levels of complexities and for various network topologies [Kostal and Kobayashi, 2015,Manwani and Koch, 2001,Malak and Akan, 2013a,Veletić et al., 2016b]. The capacity of neuro-spike communication is evaluated in [Kostal and Kobayashi, 2015, Galluccio et al., 2013] using Hodgkin-Huxley (HH) model through numerical simulations. In [Manwani and Koch, 2001], the information transfer rate for single-input single-output (SISO) system has been calculated under signal detection and signal estimation paradigms. Moreover, the closed-form expression for the capacity of SISO and multiple-input single-output (MISO) neuro-spike communication is derived in [Malak and Akan, 2013a] using probabilistic model. This work is further extended in [Ramezani et al., 2017] to find the information rate in a SISO model with multiple synaptic terminals between two neurons. In [Veletić et al., 2016b], the upper bound of the capacity for a SISO synaptic communication is derived using Bernoulli distribution to model diffusion of neurotransmitters through the cleft, which ignores the synaptic geometry and the removal of residual neuro-

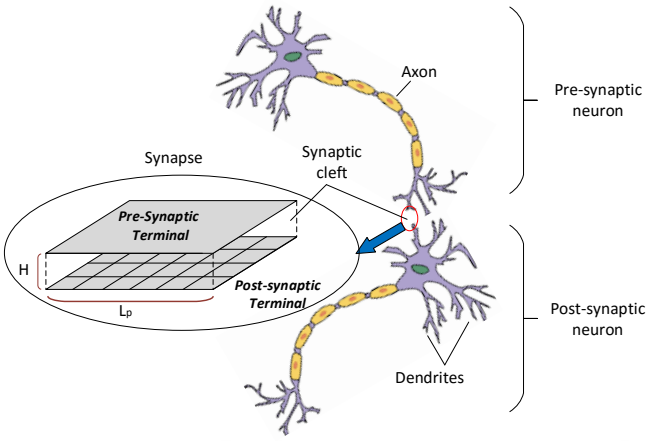

Figure 4.1: Synaptic communication model.

transmitters from the cleft. All the above cited studies have ignored the variability in the response due to (i) variations in vesicle release probability with time as explained in [Matveev and Wang, 2000] and (ii) effect of synaptic geometry, diffusion of neurotransmitters and their clearance from the synaptic cleft, which would affect the mutual information, thus, capacity of the synaptic transmission. Recently, the variation in vesicle release probability is considered in [Ramezani and Akan, 2017d], where it is shown that ignoring this variation causes overestimation of capacity of vesicle release process. Since, according to the data processing inequality, further processing does not increase the information, all of the above stated studies overestimated the capacity of the synaptic communication. Moreover, the capacity is only evaluated for the vesicle release process in [Ramezani and Akan, 2017d], thus, there is a need to evaluate the capacity of complete synaptic model.

The main contribution of this chapter is to derive analytical closed-form expressions for the information capacity of SISO synaptic transmission using realistic communication model for hippocampal pyramidal neurons. In our model, variation in vesicle release probability due to memory of neuron from previously released vesicles is taken into account. Moreover, the diffusion model that considers the synaptic geometry and clearance of neurotransmitters from the cleft between successive transmissions is used. Since the arrival of spike initiates the vesicle release process, the

input of the system is considered as spike train. Moreover, the maximum number of bound receptors in response to each incoming spike is assumed as output since it contributes to generating the post-synaptic potential. We derive the information capacity and evaluate capacity-achieving input distribution for this SISO communication system for each incoming spike, i.e. for a single transmission. Then, to derive the overall capacity for multiple transmissions, we evaluate average mutual information using the steady-state release probability.

This whole chapter would serve as the basis for evaluating the capabilities of bio-inspired nanonetworks that utilize neuro-spike communication paradigm. Moreover, understanding of intra-body nervous nanonetworks from information theoretical perspective, would aid in designing ICT-inspired diagnostic and treatment techniques for neurodegenerative diseases that alter the typical ranges of the synaptic parameters. For instance, Alzheimer's disease (AD) reduces the available neurotransmitters [Mann and Yates, 1986], thus, decreasing the overall capacity of the synaptic transmission. Therefore, the calculation done in this chapter would serve as the basis for the diagnosis of AD by comparing the capacity of healthy and diseased synapses.

The remainder of this chapter is organized as follows. The synaptic communication model including vesicle release process, diffusion and receptor binding is presented in Section 4.2. The overall capacity for multiple transmissions is derived in Section 4.3, and numerical results are provided and analyzed in Section 4.4. Finally, this chapter is concluded in Section 4.5.

4.2 Communication Theoretical Modeling of Synaptic Transmission

Spike arrival initiates the synaptic communication by changing the membrane potential of the pre-synaptic terminal, which is followed by the release of neurotransmitters to the synaptic cleft, their diffusion inside the cleft and binding with the receptors located on post-synaptic terminal. To analyze this communication system, we consider the synapse in the shape of a box with height H as shown in Fig. 4.1. The top and bottom surfaces of the box correspond to the pre- and post-synaptic

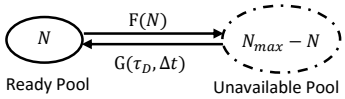

Figure 4.2: Pool-based model for neurotransmitter release and replenishment.

membranes, respectively, and are considered to be infinite in dimensions. This assumption is in accordance with the diffusion model provided in [Khan et al., 2017]. After vesicle is released from pre-synaptic terminal, neurotransmitters are diffused through the cleft and captured by post-synaptic receptors present on post-synaptic density (PSD). PSD occupies a limited square shaped region on the post-synaptic terminal with side length L_p as shown in Fig. 4.1.

In this section, we present the communication model for three processes involved in synaptic transmission known as vesicle release, diffusion and neurotransmitter-receptor binding. This communication model will later be used to derive the maximum mutual information between the input and output of the system.

4.2.1 Vesicle Release Process

Synaptic transmission is initiated with the arrival of spikes to the axonal terminal of the pre-synaptic neuron, which allows the influx of calcium ions by opening the voltage dependent calcium channels (VDCCs). After entering into the pre-synaptic terminal, calcium ions diffuse inside it, where they can bind to calcium buffers or sensors. Binding of enough calcium ions with a calcium sensor, which is located near the available vesicles for release, initiates the fusion of these vesicles with membrane. This causes the release of the content of vesicle, i.e., neurotransmitters, to the synaptic cleft [Bear et al., 2007].

In this work, we consider existence of two distinct pools of vesicles in the pre-synaptic terminal as suggested in [Matveev and Wang, 2000] and utilize the pool-based vesicle release and replenishment model shown in Fig. 4.2. In this model, the ready pool (RP) contains the vesicles ready for release, called readily releasable vesicles (RRVs), and the unavailable pool contains the released vesicles showing the

capacity for replenishment of RP. In Fig. 4.2, the capacity of RP, i.e., the number of RRVs when no vesicle is released, is called N_{max}. $F(N)$ is the vesicle release probability when N, $N \leq N_{max}$, vesicles are available in RP. The mean recovery time for replenishment of one vesicle vacancy is τ_D and $G(\tau_D, \Delta t)$ is the probability of refilling one vesicle after Δt seconds.

As it is mentioned in [Matveev and Wang, 2000], the number of vesicles that are available to refill RP is much more than N_{max}, hence, the replenishment of one released vesicle can be modeled by the first event of a Poisson process [De La Rocha and Parga, 2005]. Thus, the probability of one vacancy replenishment is derived as

$$G(\tau_D, \Delta t) = 1 - \exp\big(-\tau_D^{-1}\ \Delta t\big) \tag{4.1}$$

and the number of recovered vesicles after Δt seconds is derived based on Binomial distribution given by $B(N_{\max} - N, G(\tau_D, \Delta t))$.

Vesicles can release spontaneously or upon arrival of a spike. Hence, we consider both of these scenarios while deriving the vesicle release probability.

Evoked Release

After arrival of a spike to the pre-synaptic terminal until release of a vesicle, the release of every RRV is independent from others. However, after release of one vesicle, the others are temporarily prevented from release in hippocampal pyramidal neurons [Matveev and Wang, 2000]. Hence, we utilize the uni-vesicular release model as given below.

The release probability for each of the existing vesicles in RP is governed by a Poisson process with rate $\lambda_v(t)$, which is a function of (i) opening of VDCCs and their distance from calcium sensors, (ii) binding of calcium ions to buffers, calcium sensors and pumps, and (iii) diffusion of calcium ions and buffers [Ramezani and Akan, 2017c]. If a spike with duration equal to Δt_s arrives at the pre-synaptic terminal at time t_0, the vesicle release happens in the time interval given by $[t_0, t_0 + \Delta t_s]$. Thus,

the fusion rate for each vesicle during a period of Δt is defined as

$$\alpha_v(\Delta t) = \int_{t_0}^{t_0+\Delta t} \lambda_v(t)dt,$$

where $\Delta t \leq \Delta t_s$. Then, as a result of using the univesicular release model, the probability of evoked release in the time interval $[t_0, t_0 + \Delta t]$ is given as [Malak and Akan, 2013a],

$$P\{Release|Spike\ arrival\} = \begin{cases} 1 - \exp(-N\alpha_v(\Delta t)), & \Delta t \leq \Delta t_s \\ 1 - \exp(-N\alpha_v(\Delta t_s)), & \Delta t > \Delta t_s \end{cases} \tag{4.2}$$

where N is the number of RRVs.

Spontaneous Release

The spontaneous vesicle release is independent from evoked release. Since, the average waiting time for spontaneous release of each RRV is eight minutes, 480 [s] [Murthy and Stevens, 1999], the spontaneous release probability from a synapse with N vesicles during Δt seconds is derived as follows.

$$P\{Release|No\ spike\} = 1 - \exp(-\frac{N\Delta t}{480}) \tag{4.3}$$

4.2.2 Diffusion Process

After a vesicle release, neurotransmitters follow Brownian motion to diffuse across the synaptic cleft. The concentration of neurotransmitters in three-dimension at any time t, denoted as $C(x, y, z, t)$, is random and its expected value can be calculated from Fick's equation given below,

$$\frac{\partial C(x, y, z, t)}{\partial t} = D_c \nabla^2 C(x, y, z, t), \tag{4.4}$$

where D_c is diffusion coefficient, $t \geq 0$ and $(x, y, z) \in \mathbb{R}^2 \times [0, H]$. While considering the reflections of neurotransmitters from pre- and post-synaptic membranes, the

solution of Fick's equation is given in [Khan et al., 2017]. This gives the expected concentration of neurotransmitters in the cleft as follows,

$$C(x,y,z,t) = \frac{N_0}{(\sqrt{4\pi D_c t})^3} e^{\frac{(-x^2-y^2)}{4D_c t}} \left\{ 2 \sum_{k=-\infty}^{\infty} e^{\frac{-(z-(2k+1)H)^2}{4D_c t}} \right\}, \tag{4.5}$$

where N_0 is the number of neurotransmitters in a vesicle. Moreover, in presence of pre-synaptic re-uptake of neurotransmitters, (4.5) is modified as,

$$\begin{aligned} C(x,y,z,t) = & \frac{N_0}{(\sqrt{4\pi D_c t})^3} e^{\frac{(-x^2-y^2)}{4D_c t}} \left\{ \sum_{k=-\infty}^{-1} (2-P_u)(1-P_u)^{-(k+1)} e^{\frac{-(z-(2k+1)H)^2}{4D_c t}} \right. \\ & \left. + \sum_{k=0}^{\infty} (2-P_u)(1-P_u)^{k} e^{\frac{-(z-(2k+1)H)^2}{4D_c t}} \right\}, \end{aligned} \tag{4.6}$$

where P_u [uptake/hit] is the uptake probability [Khan et al., 2017].

On the receiver side, the neurotransmitters hit the receptors and bind to them with some probability. According to [Khan et al., 2017], we consider that receptors are uniformly distributed on the PSD and the only neurotransmitters which are inside a small volume, i.e., V_e, around each receptor are likely to bind.

To calculate the expected concentration of neurotransmitters inside V_e, i.e., C_t, we assume that there is only one neurotransmitter in the cleft. Thus, according to [Khan et al., 2017], the probability of finding that neurotransmitter inside V_e at time t is given by

$$P_e(t) = \iiint_{V_e} C(x,y,z,t) dx dy dz, \tag{4.7}$$

where C is given by (4.6) with $N_0 = 1$.

According to [Khan et al., 2017], all particles move independently from each other. Thus, the number of neurotransmitters found inside V_e at time t can be represented by a binomial random variable, $N_e(t)$, having expected value

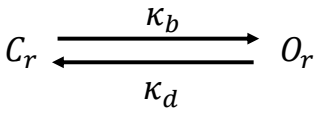

Figure 4.3: Kinetic scheme of AMPA receptors.

$$E\left[N_e(t)\right] = N_t(t)P_e(t), \tag{4.8}$$

where $N_t(t)$ is the expected total number of unbound neurotransmitters in the cleft at time t. Thus,

$$C_t \approx \frac{E\left[N_e(t)\right]}{|V_e|} \tag{4.9}$$

where $|V_e|$ is the size of the effective volume.

4.2.3 Neurotransmitter-Receptor Binding

PSD in hippocampal neurons contains two major kinds of receptors, i.e., *AMPA (α-Amino-3-hydroxy-5-methyl-4-isoxazolepropionic acid)* and *NMDA (N-methyl-D-aspartate)*. However, we only consider AMPA receptors uniformly distributed in PSD, since NMDA receptors contribute in synaptic plasticity, which is not addressed in this study. Binding of neurotransmitters to AMPA receptors increases membrane potential of post-synaptic neuron, i.e., generates excitatory post-synaptic potential (EPSP).

To derive the probability of neurotransmitter binding to an AMPA receptor, we utilize the simplified kinetic model demonstrated in Fig. 4.3. As it is shown in [Destexhe et al., 2002], this simplified model provides fairly good approximations for the time course and the dynamic behavior of synaptic currents compared to the complex multi-state kinetic models.

When receptor r, $r \in [0, M_0]$, is in the closed state, i.e., C_r, it is available for binding to a neurotransmitter. After binding, the receptor moves to the open state, i.e., O_r, and allows the influx of ions that changes the membrane potential of post-synaptic terminal. The probability of being in each of these states changes with time depending on the expected concentration of neurotransmitters near receptor, i.e., C_t, as given in the following equations,

$$\begin{aligned} \frac{dC_r}{dt} &= -\kappa_b C_r C_t + \kappa_d O_r, \\ C_r + O_r &= 1, \end{aligned} \tag{4.10}$$

where κ_b and κ_d are binding and dissociation rates for AMPA receptors, respectively. O_r and C_r also represent the opening and closing probabilities of AMPA receptors, respectively, that depend on both time and the position of the receptors.

4.3 Capacity Analysis of Synaptic Communication

The extensive analysis of synaptic transmission from information theoretical perspective is required to lay down the foundation of bio-inspired nanonetworks. Thus, in this section, we aim to derive the closed-form expression of the capacity of the synaptic transmission that depends on the availability of readily releasable vesicles, which changes with time and depends on the previous vesicle releases. Therefore, we discretize time into windows of equal durations, i.e., Δt, and select Δt sufficiently small so that at most one spike can exist at each window [Malak and Akan, 2013a]. Note that by considering the width of spike equal to Δt_s, Δt must be selected greater than or equal to Δt_s to have complete spike duration in one window.

In each time step, we can maximize mutual information over all possible spiking probabilities to estimate capacity of the system. However, since the number of RRVs changes over time, the vesicle release probability also changes. Hence, according to the definition, mutual information would also vary with time. Thus, we need to find average mutual information from 1st to nth time step and derive the spiking probability that maximizes it to reach the overall capacity until time step n. Finally,

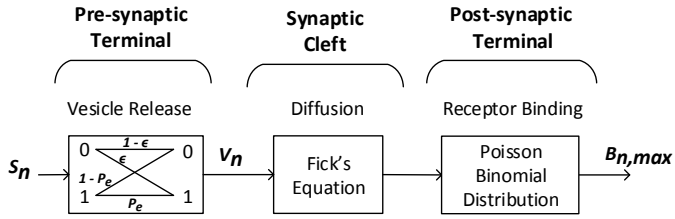

Figure 4.4: Block diagram of the synaptic communication.

we extend this calculation to find the capacity of synaptic transmission when n approaches to infinity.

4.3.1 Mutual Information in Each Time Step

The input and output of the synaptic communication model shown in Fig. 4.4 are S_n and $B_{n,max}$, respectively, in nth time slot. Here, S_n depicts the existence of spike at input and $B_{n,max}$ shows the maximum number of bound receptors at the post-synaptic terminal as a result of vesicle release. Hence, the mutual information of the system at each time step can be defined as follows,

$$I(S_n, B_{n,max}) = \mathcal{H}(B_{n,max}) - \mathcal{H}\Big(B_{n,max}|S_n\Big), \tag{4.11}$$

where the entropies in (4.11) follow the general formula given as $\mathcal{H}(\mathcal{X}_n) = -\sum_i P\{\mathcal{X}_n = i\} \log_2 P\{\mathcal{X}_n = i\}$.

By conditioning over the spike arrival, we can write the probability $P\{B_{n,max} = i\}$ as given below,

$$P\{B_{n,max} = i\} = \sum_{j=0}^{1} P\{B_{n,max} = i|S_n = j\}P\{S_n = j\}, \tag{4.12}$$

where $i \in [0, M_0]$ and M_0 is the total number of receptors on the post-synaptic terminal. Same as [Malak and Akan, 2013a, Manwani and Koch, 2001], we model the spike arrival with a Poisson process. Hence, assuming the rate of this process

as λ, the probability of spike arrival at nth time slot can be calculated as $P\{S_n = 1\} = 1 - exp(-\lambda\Delta t) \triangleq p$.

To derive the probability $P\{B_{n,max} = i|S_n = j\}$, we can condition over the vesicle release process as follows.

$$P\{B_{n,max} = i|S_n = j\} = \sum_{k=0}^{1} P\{B_{n,max} = i|V_n = k\}P\{V_n = k|S_n = j\}, \quad (4.13)$$

where V_n indicates the release of vesicle in nth window. Since, the neurotransmitters are removed from synaptic cleft between successive vesicle releases through re-uptake and diffusion [Khan et al., 2017], the synaptic noise due to residual neurotransmitters is not significant and we consider $P\{B_{n,max} = 0|V_n = 0\} = 1$.

To find the probability $P\{B_{n,max} = i|V_n = 1\}$, we define the opening probability of rth receptor as $O_r(t)$, where $r \in [0, M_0]$ and $0 \leq t \leq \Delta t$. As shown in [Khan et al., 2017], a smaller time step called $\Delta\tau << \Delta t$ can be used to calculate $O_r(t)$ in each Δt. We are interested in the maximum number of bound receptors, $B_{n,max}$, since it contributes to the peak of EPSP. After binding to a neurotransmitter, the receptors stay in open state until EPSP reaches its maximum value. Hence, utilizing the maximum opening probability for rth receptor during nth time step, i.e., $O_{r,n} = \max_{0\leq t\leq\Delta t}\big(O_r(t)\big)$, we can calculate $B_{n,max}$ by defining the variable $x_{r,n}$ as follows.

$$x_{r,n} = \begin{cases} 0, & 1 - O_{r,n} \\ 1, & O_{r,n} \end{cases}. \quad (4.14)$$

The $\sum_{i=1}^{M_0} x_{r,n}$ shows the maximum number of open receptors during time step Δt. Hence, the probability of having i open receptors upon vesicle release, i.e., $P\{B_{n,max} = i|V_n = 1\}$, is equal to $P\{\sum_{r=0}^{M_0} x_{r,n} = i\}$, which can be modeled by Poisson Binomial distribution with mean, μ_n, and variance, σ_n^2, as shown in [Fernandez and Williams,

2010],

$$\mu_n = \sum_{r=0}^{M_0} O_{r,n} \tag{4.15}$$

$$\sigma_n^2 = \sum_{r=1}^{M_0} O_{r,n}(1 - O_{r,n}). \tag{4.16}$$

Thus, the probability $P\{B_{n,max} = i|V_n = 1\}$ is calculated as follows,

$$P\{B_{n,max} = i|V_n = 1\} = \frac{1}{M_0 + 1} \sum_{l=0}^{M_0} E^{-li} \prod_{r=1}^{M_0} \Big[1 + (E^l - 1)O_{r,n}\Big], \tag{4.17}$$

where $E = exp(\frac{2\sqrt{-1}\pi}{M_0+1})$.

Next step is deriving the conditional vesicle release probability given in (4.13), i.e., $P\{V_n = k|S_n = j\}$. As it is shown in Fig. 4.4, a binary channel can be used to model the vesicle release process at each time step. According to (4.2) and (4.3) and the pool-based vesicle release and replenishment model depicted in Fig. 4.2, the probability of release in nth time slot when RP has N vesicles is expressed as follows,

$$P\{V_n = 1|N_n = N, S_n = 1\} = 1 - \exp\big(-N\alpha_v(\Delta t_s)\big) \triangleq P_e, \tag{4.18}$$

$$P\{V_n = 1|N_n = N, S_n = 0\} = 1 - \exp\big(-\frac{N\Delta t}{480}\big) \triangleq \epsilon, \tag{4.19}$$

where (4.18) shows the probability of evoked release, (4.19) depicts the spontaneous release probability and N_n indicates the number of available vesicles in RP at the beginning of nth time slot. Then, the conditional vesicle release probability can be written as follows,

$$P\{V_n = k|S_n = j\} = \sum_{N_n=0}^{N_{max}} P\{V_n = k|N_n = N, S_n = j\}P\{N_n = N\}.$$

In [Ramezani and Akan, 2017d], an array named P_n is defined with dimension $1 \times (N_{\max} + 1)$ having ith element equal to $P\{N_n = i - 1\}$. Then, a recurrence

relation is derived for P_n as follows,

$$P_n = P_{n-1}DR. \tag{4.20}$$

Here, D and R are $(N_{\max}+1)\times(N_{\max}+1)$ matrices indicating the impact of pool depletion and replenishment on the probability of having a given number of RRVs, respectively. To derive the probability of having different number of RRVs in time slot n, (4.20) is simplified to $P_n = P_1(DR)^{n-1}$, where P_1 is equal to $[0, 0, ..., 0, 1]$ indicating that RP is full, i.e., $N = N_{max}$, before the arrival of spikes.

The (i, j)th element of D, i.e., D_{ij}, represents the probability of transition from having $N_{n-1} = i-1$ to $N_n = j-1$ as a result of vesicle release. Since we are using the univesicular release model, at most one vesicle can be released from the pool. Hence, the nonzero elements of matrix D occur only where $j \in \{i, i-1\}$ and can be derived from vesicle release probability shown in Fig. 4.2, $F_n(.)$, as $D_{ii} = 1 - F_n(i-1)$ and $D_{i(i-1)} = F_n(i-1)$. Using the spiking probability, p, and the probabilities given in (4.2) and (4.3), the vesicle release probability in nth slot when RP has i vesicles, i.e., $F_n(i)$, involving both spontaneous and evoked releases, is derived as follows,

$$F_n(i) = 1 - \Big[\exp\big(-i\alpha_v(\Delta t_s)\big)p + \exp\big(-\frac{i\Delta t}{480}\big)(1-p)\Big]. \tag{4.21}$$

The (i, j)th element of R, i.e., R_{ij}, represents the probability of transition from having $N_{n-1} = i-1$ to $N_n = j-1$ as a result of vesicle replenishment process. Since the number of refilled vesicles when the RP has i RRVs can be derived from Binomial distribution given by $B(N_{\max}-i, G(\tau_D, \Delta t))$ as explained in Section 4.2.1, the matrix R is an upper triangular matrix whose (i, j)th element for $\forall j \geq i$ is defined as follows,

$$R_{ij} = \binom{N_{\max}-(i-1)}{j-i} G(\tau_D, \Delta t)^{j-i}\Big(1 - G(\tau_D, \Delta t)\Big)^{N_{\max}-(j-1)}.$$

4.3.2 Information Capacity of synaptic transmission

We define the maximum mutual information achieved during first n time slots as $C_n = max_p \sum_{l=1}^{n} \frac{I(S_l;M_{l,max})}{n}$. Then, the overall capacity of synaptic communication is defined as $C = \lim_{n\to\infty} C_n$, for which we evaluate the convergence of $I(S_n; B_{n,max})$. Based on the recurrent equation given by (4.20), the number of vesicles in RP can be modeled by a finite-state Markov chain. Moreover, the steady state probability of each state in this Markov chain, i.e., $\pi = [\pi_0, \pi_1, \ldots, \pi_{N_{\max}}]$, can be derived by solving the linear equations $\pi = \pi DR$ and $\sum_{i=0}^{N_{\max}} \pi_i = 1$. Then, to find $\lim_{n\to\infty} I(S_n; B_{n,max})$, we calculate the limit of (4.13) when n tends to infinity as follows,

$$\lim_{n\to\infty} P\{B_{n,max} = i|S_n = j\} = \sum_{k=0}^{1} P\{B_{n,max} = i|V_n = k\} \sum_{N=0}^{N_{max}} P\{V_n = k|S_n = j, N_n = N\}\pi_N.$$

Now, the limit of (4.12) as n tends to infinity is found as

$$\lim_{n\to\infty} P\{B_{n,max} = i\} = \sum_{j=0}^{1} P\{S_n = j\} \lim_{n\to\infty} P\{B_{n,max} = i|S_n = j\}.$$

Therefore, the mutual information, $I(S_n; V_n)$, converges as given below.

$$\begin{aligned} \lim_{n\to\infty} I(S_n; B_{n,max}) &= \mathcal{H}(\lim_{n\to\infty} B_{n,max}) - \mathcal{H}(\lim_{n\to\infty} B_{n,max}|S_n) \\ &\triangleq I_\infty, \end{aligned} \tag{4.22}$$

where the entropies in the above equation follow the general formula given as

$$\mathcal{H}(\lim_{n\to\infty} \mathcal{X}_n) = -\sum_i \lim_{n\to\infty} P\{\mathcal{X}_n = i\} \log_2 \Big(\lim_{n\to\infty} P\{\mathcal{X}_n = i\}\Big).$$

Considering the binary channel of vesicle release block in Fig. 4.4, since the crossover probability when there is no spike at input, ϵ, is very small in real scenario, the mutual information at the output of this block decreases if P_e reduces. Since the number of RRVs decreases with time as a result of pool depletion; ac-

cording to (4.18), the evoked release probability, P_e, thus, $I(S_n; V_n)$, also reduces with time. Moreover, according to data processing inequality, further processing does not increase the information. Hence, $I(S_n; B_{n,max})$ also decreases with time. Furthermore, according to (4.22), $I(S_n; B_{n,max})$ converges to I_∞, thus, its average over time also converges to I_∞, i.e.,

$$\lim_{n\to\infty} \sum_{l=1}^{n} \frac{I(S_l; B_{l,max})}{n} = I_\infty, \tag{4.23}$$

and the capacity of synaptic communication can be calculated as follows,

$$C = \max_{p} I_\infty. \tag{4.24}$$

4.4 Evaluation

In this section, we intend to evaluate the capacity of the synaptic communication and find how it is affected by varying different synaptic parameters. Since the output of the system, i.e., the maximum number of bound receptors, depends on spiking probability, p, capacity of RP, N_{max}, and number of neurotransmitters in a vesicle, N_0, we first evaluate the impact of these parameters on the mutual information between input and output. The values of all simulation parameters are selected from the experimental studies as shown in Table 4.1. Furthermore, we highlight how the mutual information changes over the multiple synaptic transmissions. Thus, we calculate the average mutual information over n transmissions and maximize it to find the capacity until nth time slot. Finally, with the use of steady-state probability of number of RRVs, we find the overall mutual information and capacity along with the capacity-achieving input probability distribution.

4.4.1 Mutual Information in Each Time Step

In this section, we calculate the mutual information in each time step for different values of synaptic parameters, i.e., N_{max} and N_0, and spiking probability, p, and discuss the effects of changing these parameters on information transfer rate. Since

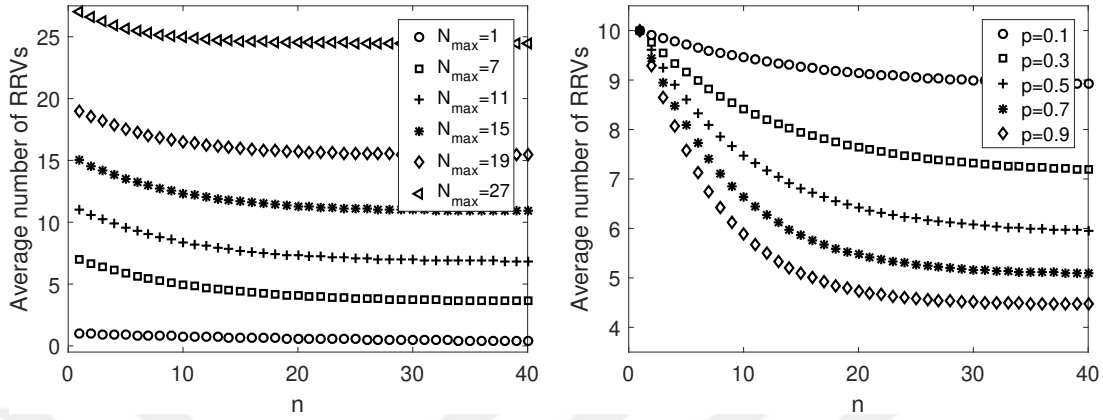

(a) $N_0 = 500, p = 0.5$ (b) $N_{\max} = 10, N_0 = 500$

Figure 4.5: Average number of available vesicle for release for different (a) capacity of ready pool, N_{max} and (b) spiking probabilities, p.

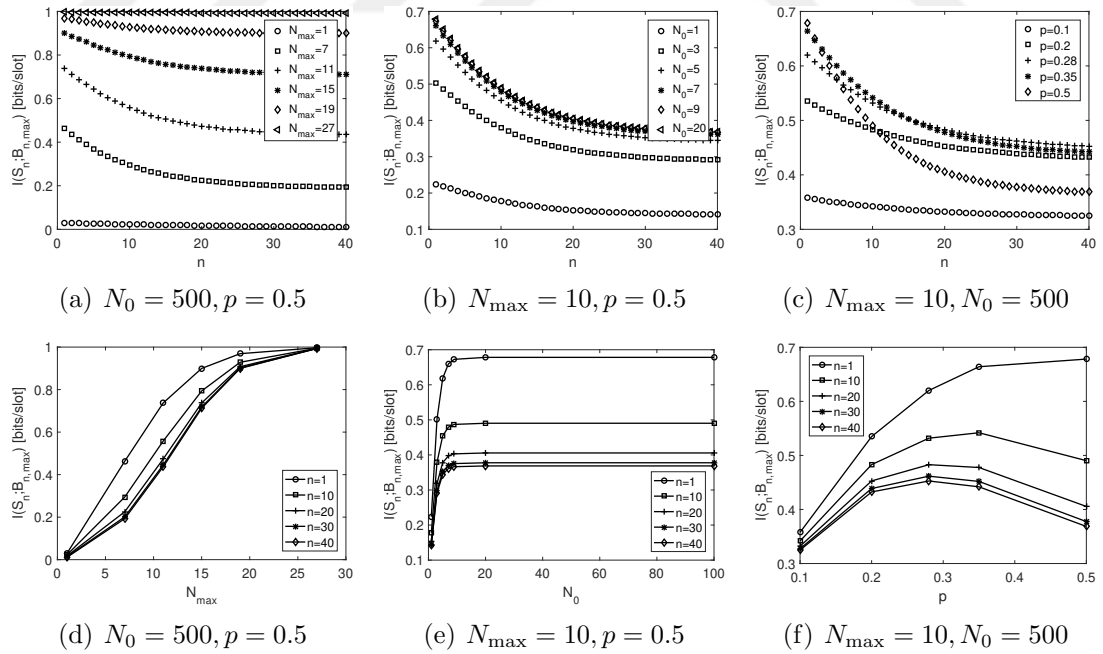

(a) $N_0 = 500, p = 0.5$ (b) $N_{\max} = 10, p = 0.5$ (c) $N_{\max} = 10, N_0 = 500$

(d) $N_0 = 500, p = 0.5$ (e) $N_{\max} = 10, p = 0.5$ (f) $N_{\max} = 10, N_0 = 500$

Figure 4.6: Mutual information between spiking and maximum number of bound receptors for different (a,d) capacity of ready pools, N_{max}, (b,e) number of neurotransmitters in a vesicle, N_0, and (c,f) spiking probabilities, p.

Table 4.1: Simulation Parameters for SISO Channel

Parameters	**Symbols**	**Values**
Synaptic cleft height	H	20 nm [Savtchenko and Rusakov, 2007]
Diffusion coefficient	D_c	0.33 μm^2/ms [Nielsen et al., 2004]
Side length of PSD	L_p	0.4 μm [Khan et al., 2017]
Number of receptors	M_0	441 [Montes et al., 2015]
Pre-synaptic Re-uptake	P_u	10% [Khan et al., 2017]
Binding Rate of AMPA	κ_b	$78 \times 10^6 \frac{1}{\text{Ms}}$ [Agmon and Edelstein, 1997]
Dissociation Rate of AMPA	κ_d	750 s^{-1} [Agmon and Edelstein, 1997]
Effective Volume	V_e	$1 \times 1 \times 0.5$ nm^3
Simulation time step	$\Delta\tau$	3.85 ns [Khan et al., 2017]
Spike width	Δt_s	4 ms [Bear et al., 2007]
Discretization time step	Δt	Δt_s [Ramezani and Akan, 2017d]
Average fusion rate	$\alpha_v(\Delta t_s)$	$0.06\sqrt{N}$ [Dobrunz and Stevens, 1997]
Mean vacancy recovery time	τ_D	$\frac{0.6}{N_{max}}$ [De La Rocha and Parga, 2005]

the vesicle release process is the only part of the system that has memory, i.e., the number of RRVs changes after each transmission, we analyze the impact of variation of number of RRVs with time on mutual information. Among the aforementioned parameters, N_0 is not affecting the number of RRVs, hence the average number of available vesicles for release is plotted for different values of N_{max} and p in Fig. 4.5.

The pool-based vesicle release and refill model shown in Fig. 4.2 is used to derive the statistics of number of RRVs. As it is shown in Fig. 4.5, the number of RRVs reduces with time, thus, we can conclude that the release rate of vesicles is faster than their refill rate, i.e., the neuron does not have enough time between multiple transmissions to refill all of the released vesicles. It can also be observed in Fig. 4.5(a) that increasing N_{max} increases the average number of vesicles available in each time slot. This is due to two reasons, i.e., higher value of N_{max} results in (i) having more number of RRVs in the beginning of simulation, and (ii) faster vacancy replenishment according to the definition of τ_D given in Table 4.1. Moreover, according to Fig. 4.5(b), increasing the spiking probability, p, while keeping N_{max} fixed, decreases the average number of RRVs. Since the evoked release probability,

P_e, is higher than spontaneous release probability, ϵ, increasing spiking probability, p, causes the release of more number of vesicles in multiple transmissions. Moreover, the refill rate is constant, thus, the average number of RRVs decreases with time by increasing spiking probability, p.

The mutual information between input and output of the system is shown in Fig. 4.6 for different values of N_{max}, N_0 and p. It is observed that the mutual information reduces over time. The reason of this reduction can be explained considering the binary channel of vesicle release block in Fig. 4.4. Since the crossover probability when there is no spike at input, ϵ, is very small in real scenario, the mutual information at the output of this block would be maximum if $(1 - P_e)$ tends to zero, i.e., as the evoked release probability, P_e, increases. On the other hand, the diffusion and binding processes cannot increase the information about input according to the data processing inequality. Thus, the overall mutual information of the system is directly related to the evoked release probability. According to (4.18), this release probability decreases with reduction in the number of RRVs and the average number of RRVs reduces with time as shown in Fig. 4.5. Therefore, mutual information also reduces over time as shown in Fig. 4.6. Moreover, since the number of RRVs, N_n, eventually reaches its steady state value according to the Markov chain model indicated in Section 4.3.2, mutual information also saturates to a constant value.

In Fig. 4.6(a), the mutual information is plotted against time for different values of N_{max}. It can be observed that the reduction rate of mutual information decreases with the increase in the value of N_{max}. This is due the fact that high values of N_{max} leads to higher number of RRVs, N_n, in each time slot as shown in Fig. 4.5(a), which saturates the evoked release probability, P_e, according to (4.18). Therefore, the rate of change of mutual information tends to zero for higher values of N_{max} as shown in Fig. 4.6(a) and Fig. 4.6(d). Furthermore, for very low values of N_{max}, the signal transmission happens rarely, thus, mutual information is close to zero for all time.

It can also be observed in Fig. 4.6(a) and Fig. 4.6(d) that in each time slot we have higher value of mutual information as the value of N_{max} increases. This is due

to having more number of RRVs, thus, higher evoked release probability, as a result of increasing N_{max}.

Next, we evaluate the effect of changing the number of neurotransmitters in a vesicle, N_0, on mutual information. We select N_{max} as 10, which is reported in [Schikorski and Stevens, 1997] for average capacity of RP in hippocampal pyramidal neurons. As can be observed in Fig. 4.6(b) and Fig. 4.6(e), the output has more information about input if there is a higher number of neurotransmitters in a vesicle. Moreover, the mutual information attains saturation after certain value of N_0 as a result of having enough bound receptors to detect the signal transmission in case of spike arrival. Furthermore, for very low values of N_0, the neurotransmitters are lost in the cleft or uptaken by the pre-synaptic terminal before reaching the post-synaptic receptors, thus, resulting in lower value of mutual information.

The change in mutual information of synaptic transmission with respect to spiking probability is shown in Fig. 4.6(c) and Fig. 4.6(f). The mutual information decreases with higher rate with increasing spiking probability as shown in Fig. 4.6(c). This is due to more reduction in the number of RRVs by increasing spiking probability as shown in Fig. 4.5(b). Moreover, since the number of RRVs, N_n, changes with time, the spiking probability that maximizes mutual information also changes in each time slot. This change is apparent in Fig. 4.6(f) as the peak of mutual information is moving towards left.

The mutual information between spiking and output of vesicle release process is reported in [Ramezani and Akan, 2017d]. By comparing the achievable mutual information for the overall synaptic communication shown in Fig. 4.6 and the results of [Ramezani and Akan, 2017d], we can see that the diffusion and binding processes do not decrease the mutual information after certain value of N_0. Thus, we can conclude that if the value of N_0 is very high, which is the case in real scenario [Rusakov et al., 2011], enough amount of the released vesicle are always received by the post-synaptic neuron, which shows the reliability of the synaptic system.

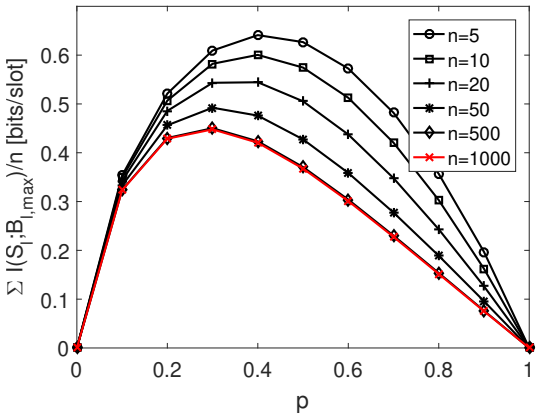

Figure 4.7: Average mutual information for $N_{max} = 10$ and $N_0 = 500$.

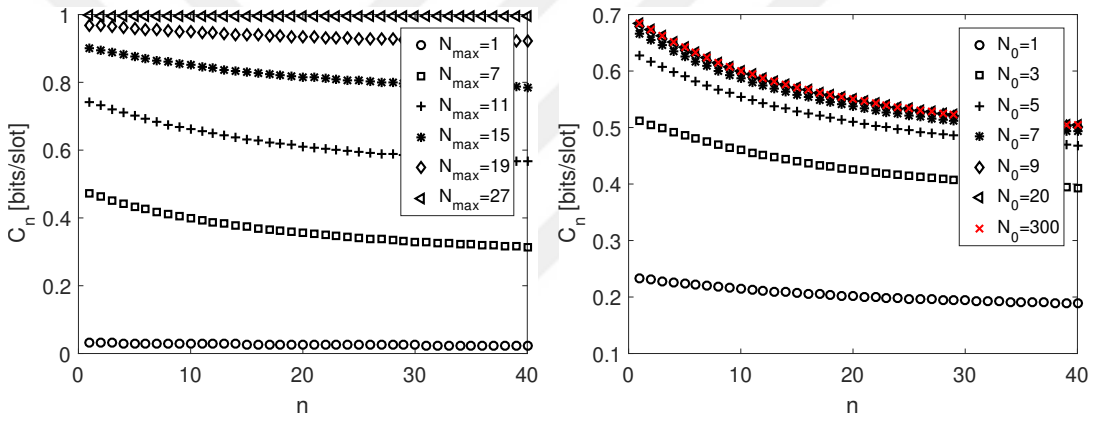

(a) $N_0 = 500$ (b) $N_{max} = 10$

Figure 4.8: Maximum mutual information from 1st to nth slot for different values for (a) capacity of RP, N_{max}, and (b) number of neurotransmitters in a vesicle, N_0.

4.4.2 Average Mutual Information and Capacity for n Synaptic Transmissions

In the previous section, we observed that the mutual information changes with time, hence we need to find average mutual information over several transmissions to evaluate the capacity of synaptic communication. The mutual information averaged over n consecutive time slots, always starting from the first time slot, is shown in Fig. 4.7. It is apparent in the figure that average mutual information reduces as the system use increases, which is a result of the depletion of RP. Moreover, the spiking probability that maximizes the average mutual information is also decreasing with

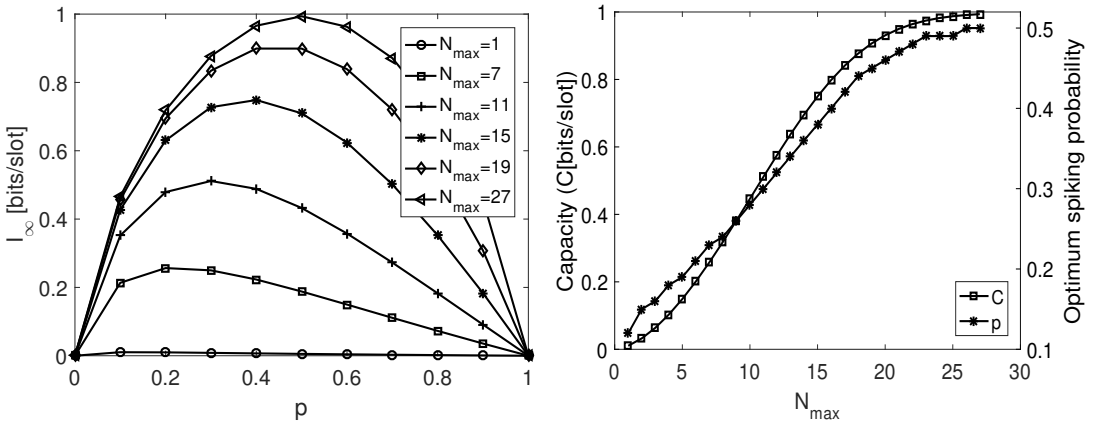

(a) $\lim_{n\to\infty} \sum_{l=1}^{n} \frac{I(S_l;V_l)}{n} = I_\infty$

(b) Channel capacity and optimum spiking probability

Figure 4.9: Average mutual information of the system, system capacity and capacity-achieving spiking probability in steady state for $N_0 = 500$ and different values of N_{max}.

time as indicated by the peak of the curve that moves towards left.

The average mutual information is maximized over spiking probability, p, to calculate the capacity over multiple transmissions, for different values of N_{max} and N_0 as shown in Fig. 4.8(a) and Fig. 4.8(b), respectively. In both cases, the capacity reduces with time as a result of reduction in mutual information over multiple transmissions as observed in Fig. 4.6. Moreover, increase in both N_{max} and N_0 increases the capacity as a result of higher vesicle release probability and increased chances of neurotransmitters to reach the receptors, respectively. Furthermore, as we have seen in Fig. 4.6(e), the mutual information in each time step saturates with increasing N_0. Hence, it can be observed in Fig. 4.8(b) that the capacity of the system over multiple uses also saturates after a specific value of N_0.

4.4.3 Mutual Information and Capacity at Steady-State

To evaluate the capacity of synaptic communication, we calculated the steady state probabilities of having different number of RRVs and use them to derive the mutual information between input and output of the system as n tends to infinity, I_∞. This also corresponds to the average mutual information evaluated over infinite

consecutive time slots as given by (4.23).

The I_∞ is plotted against spiking probability for different values of N_{max} and N_0 in Fig. 4.9(a) and Fig. 4.10(a), respectively. Similar to the average mutual information, we can observe that I_∞ also increases with N_{max} and N_0. Moreover, I_∞ is maximized over spiking probability, p, to calculate the capacity for different values of N_{max} and N_0 as shown in Fig. 4.9(b) and Fig. 4.10(b), respectively. Since changing the N_{max} affects the number of RRVs, which in turn affects the steady state probabilities of having different number of RRVs, the capacity-achieving spiking probability also changes as shown in Fig. 4.9. However, as it can be seen in Fig. 4.10, changing N_0 does not change capacity-achieving spiking probability since it is not affecting the availability of vesicles.

It can also be observed from Fig. 4.9(b) and Fig. 4.10(b) that capacity improves with increasing N_{max} and N_0, respectively. This is a result of dependence of I_∞ on these factors as explained earlier. As it can be observed in Fig. 4.10(b), the capacity reaches the maximum value for N_0 around 10. However, more number of bound receptors is needed for spike generation, thus, there are more neurotransmitters in a vesicle in real scenarios. Selecting the system parameters as reported in experimental studies for hippocampal pyramidal neurons, i.e., $N_{max} = 10$ [Agmon and Edelstein, 1997] and $500 \leq N_0 \leq 3000$ [Rusakov et al., 2011, Ventriglia and Di Maio, 2000], the capacity of synaptic communication model for information transmission among these neurons is calculated as $C = 0.44$ bits/slot $= 110$ bits/s. These results can be compared with the results obtained from the diseased synapses to have an ICT-inspired diagnosis technique for neurodegenerative diseases. Moreover, for designing a molecular communication based nanonetworks, these results can be used to decide about the optimal parameters to achieve maximum capacity.

4.5 Conclusion

In this chapter, we analyzed a realistic physical reference model as the most basic realization of nanonetworks that utilize neuro-spike communication paradigm from information theoretical perspective. We formulated the mutual information

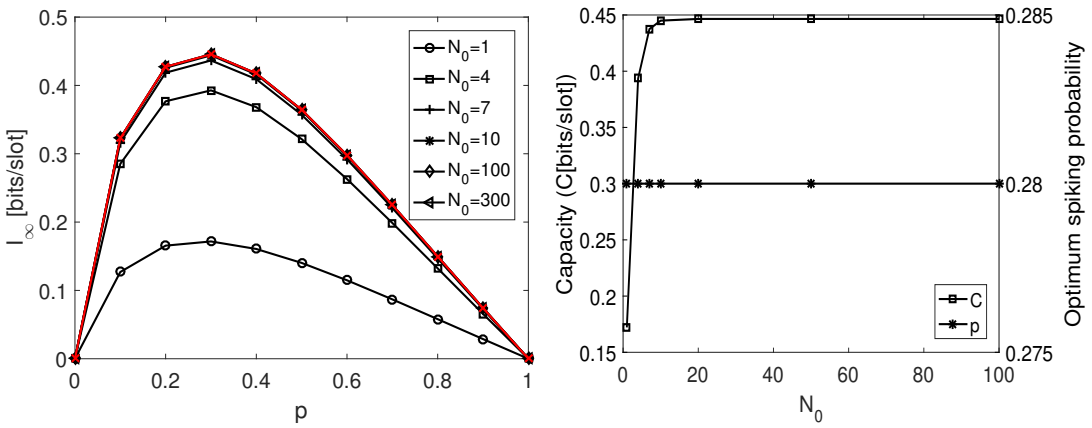

(a) $\lim_{n\to\infty} \sum_{l=1}^{n} \frac{I(S_l;V_l)}{n} = I_\infty$

(b) Channel capacity and optimum spiking probability

Figure 4.10: Average mutual information of the system, system capacity and capacity-achieving spiking probability in steady state for $N_{max} = 10$ and different values of N_0.

between input and output of a SISO synaptic communication for a single transmission. Since this system has memory, we found the average mutual information over multiple transmissions to evaluate its overall capacity. Moreover, we derived a closed-form expression for the capacity of synaptic transmission and calculated the capacity-achieving spiking probability. Finally, we found the effects of change in various synaptic parameters, such as spiking probability, number of readily releasable vesicles (RRVs) and number of neurotransmitters in a vesicle, on the information capacity of the system.

Chapter 5

SUM RATE OF MISO NEURO-SPIKE COMMUNICATION CHANNEL WITH CONSTANT SPIKING THRESHOLD

5.1 Introduction

Information theoretical analysis of neuro-spike communication is done in various studies [Galluccio et al., 2013,Manwani and Koch, 2001,Ramezani et al., 2017,Veletić et al., 2016b, Malak and Akan, 2013a, Ramezani and Akan, 2017e, Ramezani et al., 2018a] using different channel models. In [Galluccio et al., 2013], Hodgkin-Huxley (HH) model is used to calculate information capacity. In [Manwani and Koch, 2001], the information transfer rate for single-input single-output (SISO) system is calculated using a probabilistic model, which is extended in [Ramezani et al., 2017] to find the information rate in a SISO model with multiple synaptic terminals between two neurons. In [Veletić et al., 2016b], the upper bound of the capacity for a SISO synaptic communication is derived using Bernoulli distribution to model diffusion process.

Cortical neurons need to receive stimulation from several input neurons to fire an action potential [Bear et al., 2007]. Moreover, neurospike communication is a communication paradigm for nanonetworks, where nanomachines can receive information from several inputs. Hence, the information transfer rate for MISO neuro-spike communication is derived in [Malak and Akan, 2013a]. However, all these studies ignore the impact of synaptic geometry, diffusion of neurotransmitters, their clearance from the synaptic cleft and the spike generation. The realistic communication models are used in chapter 4 [Ramezani and Akan, 2017e,Ramezani et al., 2018a] to study the capacity of vesicle release process and synaptic transmission, respectively.

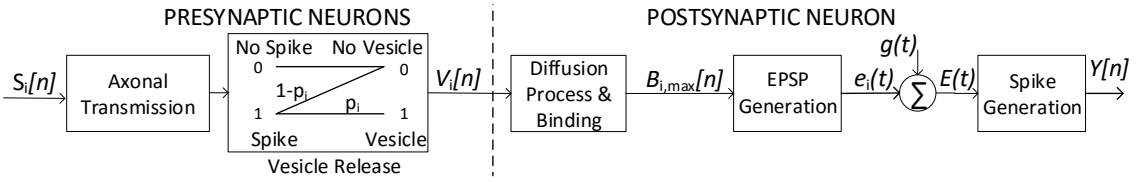

Figure 5.1: Block diagram of the communication channel between ith pre-synaptic neuron and the output neuron.

However, the performance of the overall neuro-spike communication channel with multiple input neurons is not considered in previous chapters.

The brain consumes dramatically lower power compared to man-made computers [Sengupta and Stemmler, 2014]. Moreover, as shown in [Harris et al., 2015], the properties of thalamic relay synapses are set to maximize information transmitted per used ATP molecule instead of information transmitted per second. The information capacity of the H-H model and an empirical neuronal signaling model is investigated under metabolic cost constraint in [Kostal and Kobayashi, 2015] and [Kostal et al., 2013], respectively. It is concluded that the capacity increases as the upper bound on the consumed metabolic energy is relaxed. Therefore, including metabolic constraints in the model is inevitable to accurately evaluate the rate of information transmission over neuro-spike communication channel.

In this chapter, we consider the MISO neuro-spike communication among hippocampal pyramidal neurons. Thus, the input of the communication channel is spike trains of all pre-synaptic terminals and the output is the fired spikes in post-synaptic neuron. We consider realistic communication models for different processes involved in this communication such as synaptic geometry, diffusion of neurotransmitters, and their re-uptake by pre-synaptic terminal. Using this communication model and considering all possible variations in biophysical parameters of pre- and post-synaptic neurons, we analyze the maximum achievable rate of information transmission over our model subject to the metabolic cost constraints and derive a general closed form equation for the sum rate of MISO neuro-spike communication channel. Moreover, to get an insight on the impact of the number of pre-synaptic neurons on the perfor-

mance of MISO channel while reducing the complexity of the system, we consider the same biophysical parameters for all pre-synaptic neurons and derive a closed form equation for the sum rate of the channel, which is later used in simulations. Finally, we study how the performance of MISO channel is influenced by changes in the biophysical parameters of the channel, which can happen as a result of different diseases.

The rest of the chapter is organized as follows. In Section 5.2, we describe the MISO synaptic channel model. In Section 5.3, we formulate the sum rate of MISO neuro-spike communication channel under metabolic cost constraints. In Section 5.4, we present and discuss simulation results. Finally, we conclude the chapter in Section 5.5.

5.2 Model Description

In this section, we define processes included in the MISO neuro-spike communication channel as shown in Fig. 5.1.

5.2.1 Axonal Transmission

Linear-Nonlinear-Poisson (LNP) model is one of the neural coding models used to encode external stimulus into spiking rate [Malak and Akan, 2013a]. According to LNP model, the resulting spike train follows Poisson random distribution. Thus, pre-synaptic neurons generate spike trains, $S_i(t)$, following Poisson processes with rate λ_i [Ramezani and Akan, 2017e], where $i \in [1, M]$ and M is the number of pre-synaptic inputs. After firing a spike in a pre-synaptic neuron, another spike cannot be generated for a short time called refractory period [Bear et al., 2007]. Hence, we can divide time into windows of equal duration Δt, where Δt is small enough to contain only one spike. Thus, a discrete time random variable $S_i[n]$ is defined to indicate the occurrence of a spike in nth time step with the probability $P\{S_i[n] = 1\} = 1 - \exp(-\lambda_i \Delta t)$.

Each spike is then transmitted to pre-synaptic terminals through axon. Although the spike shape may change during axonal transmission [Geiger and Jonas,

2000], more experimental data is needed to accurately model functionality of axon [Ramezani and Akan, 2017b]. Hence, we consider the axon as an ideal filer, which is a fairly accurate model for hippocampal pyramidal neurons since their axonal transmission is highly reliable due to the existence of myelin sheaths and Node of Ranviers [Veletić et al., 2016a]. Thus, the output of axonal transmission in ith pre-synaptic neuron is $S_i[n]$.

5.2.2 Vesicle Release Process

At least two pools of vesicles exist in each pre-synaptic terminal depending on their distance from the membrane and their mobility [Bear et al., 2007]. The pool of vesicles that are ready for release on the arrival of spike is called readily releasable pool (RRP) with size N_i, where $i \in [1, M]$. Similar to [Malak and Akan, 2013a], instantaneous replenishment of RRP after each release is considered, i.e., N_i remains constant over time.

The rate at which vesicles are fused with the membrane of ith pre-synaptic terminal in nth window is $\alpha_i = 0.06\sqrt{N_i}$ [Dobrunz and Stevens, 1997]. Then, the probability of vesicle release during nth window, i.e., $V_i[n] = 1$, given spike arrival is [Malak and Akan, 2013a]

$$P\{V_i[n] = 1 | S_i[n] = 1\} = 1 - exp(-N_i\alpha_i) \triangleq P_i.$$

Since the spontaneous release probability is very low in hippocampal neurons [Murthy and Stevens, 1999], we ignore it in this study, thus, $P\{V_i[n] = 1 | S_i[n] = 0\} = 0$.

5.2.3 Diffusion Process

Once a vesicle is released, neurotransmitters diffuse through the synaptic cleft to reach post-synaptic density (PSD) that contains receptors. As defined in [Khan et al., 2017], we consider a rectangular synaptic cleft for ith synapse with height H_i and a square shaped PSD with side length L_i on post-synaptic membrane. In [Khan et al., 2017], the pre- and post-synaptic membranes are assumed to have infinite

dimension. Then, the expected value of concentration of neurotransmitters in the synaptic cleft from ith pre-synaptic input at time t, $C_i(x, y, z, t)$, is given as,

$$\begin{aligned} C_i(x,y,z,t) = & \frac{T_0}{(\sqrt{4\pi D_c t})^3} e^{\frac{(-x^2-y^2)}{4D_c t}} \\ & \Bigg\{ \sum_{k=-\infty}^{-1} (2-P_{i,u})(1-P_{i,u})^{-(k+1)} e^{\frac{-(z-(2k+1)H_i)^2}{4D_c t}} \\ & + \sum_{k=0}^{\infty} (2-P_{i,u})(1-P_{i,u})^{k} e^{\frac{-(z-(2k+1)H_i)^2}{4D_c t}} \Bigg\}, \end{aligned} \tag{5.1}$$

where T_0 is the number of neurotransmitters in a vesicle, $P_{i,u}$ is the uptake probability in ith synapse and its unit is uptake per hit, D_c is diffusion coefficient, $0 \leq t \leq \Delta t$ and $(x, y, z) \in \mathbb{R}^2 \times [0, H_i]$.

The neurotransmitters that reach post-synaptic terminal bind to the receptors residing on the PSD. These receptors are assumed to be uniformly distributed on the PSD and a small effective volume, i.e., $v_{i,r}$, is considered around rth receptor located in ith synapse such that the neurotransmitters that are inside this volume are likely to bind with the receptor [Khan et al., 2017]. The expected concentration of neurotransmitters inside $v_{i,r}$, i.e., $C_{v_{i,r}}(t)$, is calculated in [Khan et al., 2017] as

$$C_{v_{i,r}}(t) \approx \frac{\overline{T_{i,r}(t)}}{|v_{i,r}|}$$

where $T_{i,r}(t)$ is the number of neurotransmitters found inside $v_{i,r}$ at time t and $|v_{i,r}|$ is the size of the effective volume. As shown in [Khan et al., 2017], $T_{i,r}(t)$ can be modeled by a binomial random variable, having expected value $\overline{T_{i,r}(t)} = T_i(t)P_{i,r}(t)$. Here, $T_i(t) \leq T_0$ is the expected total number of unbound neurotransmitters in the ith synaptic cleft at time t and $P_{i,r}(t)$ is the probability of finding a released neurotransmitter inside $v_{i,r}$ at time t. This probability is calculated in [Khan et al., 2017] as

$$P_{i,r}(t) = \iiint_{v_{i,r}} C_i(x,y,z,t) dx dy dz,$$

where C_i is given by (5.1) with $T_0 = 1$, $i \in [1, M]$, $r \in [1, R_0]$ and R_0 is the total number of receptors on a PSD.

5.2.4 Neurotransmitter-Receptor Binding

Binding of the released neurotransmitters to receptors located on the post-synaptic terminal can either (i) decrease the membrane potential of the output neuron, happening in inhibitory synapses, or (ii) increase it, occurring in excitatory synapses [Bear et al., 2007]. The focus of this study is on hippocampal pyramidal neurons, where excitatory synapses are the most abundant type [Bear et al., 2007] and the major receptors are *AMPA* and *NMDA*. Since NMDA receptors contribute in synaptic plasticity, which is not addressed in this chapter, we only consider the excitatory post-synaptic potential (EPSP) generated by AMPA receptors. Moreover, we utilize the kinetic model demonstrated in Fig. 5.2 for binding of neurotransmitters to AMPA receptors since it provides a good approximation for the time course and the dynamic behavior of synaptic currents [Destexhe et al., 2002].

In the Kinetic model shown in Fig. 5.2, κ_b and κ_d are binding and dissociation rates for AMPA receptors, respectively. Each receptor r, $r \in [1, R_0]$, located in the synaptic terminal made by ith pre-synaptic neuron can have two states, (i) close state, $C_{i,r}$, where the receptor is available to bind to a neurotransmitter, and (ii) open state, $O_{i,r}$, where the receptor is bound to a neurotransmitter and cannot bind to another one before unbinding from the current one. The expected concentration of neurotransmitters near receptor, i.e., $C_{v_{i,r}}(t)$, controls the probability of these states as given below.

$$\begin{aligned}\frac{dC_{i,r}(t)}{dt} &= -\kappa_b C_{i,r}(t) C_{v_{i,r}}(t) + \kappa_d O_{i,r}(t),\\ C_{i,r}(t) + O_{i,r}(t) &= 1,\end{aligned}$$

where $(n-1)\Delta t \leq t \leq n\Delta t$. $O_{i,r}(t)$ and $C_{i,r}(t)$ represent the opening and closing probabilities of a receptor, respectively, that depend on both time and the position of receptors.

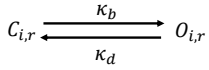

Figure 5.2: Kinetic scheme of AMPA receptors.

5.2.5 Post-synaptic Potential at Each Synapse

The receptors allow the influx of ions to the post-synaptic neuron after entering the open state. This changes the post-synaptic membrane potential, which is modeled as

$$e_i(t) = \begin{cases} h_i \frac{t}{t_p} exp(1 - \frac{t}{t_p}), & t \geq 0 \\ 0, & t < 0 \end{cases} \tag{5.2}$$

where h_i is the peak EPSP amplitude contributed by ith synapse and t_p is time to reach the peak [Malak and Akan, 2013a].

Considering the vesicle release in nth time step, the contribution of ith synapse in the post-synaptic membrane potential can be written as $e_i(t - t_n) = B_{i,max}[n]h_p(t - t_n)$, where $h_p(t) = h_p \frac{t}{t_p} exp(1 - \frac{t}{t_p})$, h_p is the maximum membrane potential contributed by each receptor, $B_{i,max}[n]$ is the maximum number of bound receptors, and t_n is the beginning of nth time step. After binding to a neurotransmitter, receptors stay in open state until EPSP reaches its maximum value [Khan et al., 2017]. Hence, the maximum of $O_{i,r}(t)$ for $(n-1)\Delta t \leq t < n\Delta t$ and all receptors in ith synapse can be used to derive $B_{i,max}[n]$. Consider $O_{i,r}[n] = \max_{(n-1)\Delta t \leq t < n\Delta t} \left(O_{i,r}(t)\right)$ and define the variable $x_{i,r}[n]$ as follows.

$$x_{i,r}[n] = \begin{cases} 0, & 1 - O_{i,r}[n] \\ 1, & O_{i,r}[n] \end{cases}$$

Then, $\sum_{r=1}^{R_0} x_{i,r}[n]$ shows the maximum number of open receptors during nth time step. Hence, the probability of having j open receptors upon vesicle release can be

derived as $P\{B_{i,max}[n] = j|V_i[n] = 1\} = P\{\sum_{r=1}^{R_0} x_{i,r}[n] = j\}$. Thus, this probability can be modeled by Poisson Binomial distribution with mean, $\mu_i[n] = \sum_{r=1}^{R_0} O_{i,r}[n]$, and variance, $\sigma_i[n]^2 = \sum_{r=1}^{R_0} O_{i,r}[n](1 - O_{i,r}[n])$ [Fernandez and Williams, 2010].

5.2.6 Spike Generation

The EPSP generated by each synapse is integrated at soma to derive the membrane potential of post-synaptic neuron as

$$E(t) = e_0 + \sum_{i=1}^{M} \sum_{t_n \leq t, \forall n} V_i[n] e_i(t - t_n) + g(t), \tag{5.3}$$

where e_0 is the resting membrane potential, t_n is the beginning of nth time slot and $g(t)$ is the noise in post-synaptic membrane voltage. Different noise sources such as thermal noise, leakage from ionic channels and synaptic noise can corrupt the membrane voltage of the output neuron. Synaptic noise is due to the multiple access to the synapse, which results in the reception of residual neurotransmitters released at thousands of other synapses in previous time steps. Since signal of different neurons has the same random structure and due to the central limit theorem, the probability density function of the post-synaptic noise converges to a Gaussian process, whose mean and variance are considered as zero and σ_n^2, respectively [Malak and Akan, 2013a].

A spike occurs in the post-synaptic neuron when the changes in the post-synaptic membrane potential is strong enough. To model this process, we consider a fixed spiking threshold, θ_0. When $E(t) \geq \theta_0$ a spike is fired by post-synaptic neuron, i.e., $Y[n] = 1$, and the post-synaptic membrane potential is set to the resting membrane potential, i.e., e_0. While the spike generation threshold can change according to previous stimulations of the post-synaptic neuron [Kobayashi et al., 2009], considering a fix spiking threshold provides the chance to analyze the impact of spike generation on the performance of neuro-spike communication for the first time in the literature.

5.3 Sum Rate Analysis with Metabolic Energy Constraint on Neuronal Signaling

For analyzing the achievable rate of information transmission over our model, we use basic definitions from information theory. The input and output of our model are the spike train, $S_i[n]$ and the generated spikes at output, $Y[n]$, respectively. Thus, the mutual information of the channel is derived as

$$I(S^M[n]; Y[n]) = H(Y[n]) - H(Y[n]|S^M[n]), \tag{5.4}$$

where $S^M[n] = \{S_1[n], S_2[n], ..., S_M[n]\}$. While within each time step the generated EPSP at output neuron, i.e., $E(t)$, changes with time, the channel model shown in Fig. 5.1 does not vary from one time step to another time step. Moreover, the probability distribution of spike generation at inputs does not change with time. Furthermore, we study the situation where the width of $e_i(t)$ given in (7.1) is smaller than discretization time step, Δt. Hence, the channel transmission probability, i.e., $P\{Y[n]|S^M[n]\}$, and the probability of spike generation at the output neuron, i.e., $P\{Y[n] = 1\}$, thus, the mutual information among input and output of the channel, i.e., $I(S^M[n]; Y[n])$, does not depend on the time step.

The capacity region of the multiple-access channel is the maximum mutual information, maximized over all input distribution, $p(S^M[n])$. Since in real scenario, spike trains from different inputs are independently generated by $S_i[n] \sim Poiss(\lambda_i)$, the mutual information can be maximized over λ_i for $\forall i$ to study the maximum achievable rate of information transmission over this channel. Defining R_i as the achievable rate for ith pre-synaptic neuron, the upper bound on the achievable sum rate of the MISO channel is derived as

$$\sum_{i=1}^{M} R_i \leq \max_{\forall i,\ \lambda_i} I(S^M[n]; Y[n]) \triangleq C.$$

Note that C is the maximum rate at which we can send information with a vanishingly low probability of error over this channel using the Poisson distribution for

spike generation at input neurons. However, in physical systems, this sum rate is limited by some physical, chemical or biological factors. In neuronal networks, one of the significant limiting factors is the energy being consumed for neural activities, w, in terms of number of ATP molecules, called metabolic energy. For the MISO channel with M pre-synaptic and one post-synaptic neuron, the metabolic energy associated with each input-output pair in nth time window is calculated as [Attwell and Laughlin, 2001],

$$w(S^M[n], Y[n]) = (M+1)\beta\Delta t + \kappa(Y[n] + \sum_{i=1}^{M} S_i[n]),$$

where $\beta = 0.342 \times 10^9$ ATP molecules per second is required to maintain resting potential and $\kappa = 0.71 \times 10^9$ ATP molecules is required to generate a single spike [Kostal and Kobayashi, 2015]. Thus, the average metabolic energy consumed in nth time step is

$$w_p[n] = \sum_{S^M, Y} w(S^M[n], Y[n]) p(S^M[n], Y[n]). \tag{5.5}$$

Considering that average consumed metabolic energy in nth time step must be bound to W ATP molecules, the maximum achievable transmission rate of the MISO channel under the metabolic cost constraints is given below.

$$C(W) = \max_{\forall i,\ \lambda_i : w_p[n] \leq W} I(S^M[n]; Y[n]). \tag{5.6}$$

To derive the mutual information between input, $S^M[n]$, and output, $Y[n]$, of the MISO neuro-spike communication channel, we calculate $p\{Y[n]\}$ and $p\{Y[n]|S^M[n]\}$ in this section. The membrane potential of the post-synaptic neuron before spike generation is given by (5.3). Since, the time is discretized, we consider that the spikes occur at the beginning of each time slot. Thus, by selecting the Δt greater than or equal to the duration of Action Potential, there is no overlap among the

EPSP in consecutive time-steps. Hence, $P\{Y[n]=1\}$ can be derived as,

$$\begin{aligned} P\{Y[n]=1\} &= P\{E(t)>\theta_0\} \\ &= P\{e_0+\sum_{i=1}^{M} V_i[n]B_{i,\max}[n]h_p(t-t_n)+g(t)>\theta_0\}. \end{aligned}$$

By conditioning over $V^M[n]=\{V_1[n],V_2[n],...,V_M[n]\}$ and $B^M[n]=\{B_{1,\max}[n],B_{2,\max}[n],...,B_{M,\max}$ the $P\{Y[n]=1\}$ can be derived as

$$P\{Y[n]=1\}=\sum_{\underline{v},\underline{b}} P\{B^M=\underline{b},V^M=\underline{v}\}$$
$$P\Big\{g(t)>\theta_0-e_0-\sum_{i=1}^{M} v_i b_i h_p(t-t_n)|B^M=\underline{b},V^M=\underline{v}\Big\},$$

where $\underline{v}$ and $\underline{b}$ are $1\times M$ arrays with ith element $v_i\in\{0,1\}$ and $b_i\in[0,R_0]$, respectively. The Gaussian noise is independent from vesicle release process and the neurotransmitter-receptor binding, thus, we get

$$\begin{aligned} P\{Y[n]=1\} &= \sum_{\underline{v},\underline{b}} P\{B^M=\underline{b},V^M=\underline{v}\} \\ &\quad P\Big\{g(t)>\theta_0-e_0-\sum_{i=1}^{M} v_i b_i h_p(t-t_n)\Big\}. \end{aligned} \tag{5.7}$$

In the spike generation process, $Y[n]=1$ if $g(t)>\theta_0-e_0-\sum_{i=1}^{M} v_i b_i h_p(t-t_n)$ at any instant of time within $t_n<t<t_n+\Delta t$. Moreover, $g(t)$ is Gaussian, thus, $P\{g(t)>g_0\}$ increases as g_0 decreases. Therefore, by achieving the minimum of $\theta_0-e_0-\sum_{i=1}^{M} v_i b_i h_p(t-t_n)$ that happens when $h_p(t-t_n)$ is maximum, (5.7) can be simplified to,

$$\begin{aligned} P\{Y[n]=1\} &= \sum_{\underline{v},\underline{b}} P\{B^M=\underline{b},V^M=\underline{v}\} \\ &\quad P\Big\{g(t_n+t_p)>\theta_0-e_0-\sum_{i=1}^{M} v_i b_i h_p\Big\}, \end{aligned}$$

where

$$P\{B^M = \underline{b}, V^M = \underline{v}\} = P\{B^M = \underline{b}|V^M = \underline{v}\}P\{V^M = \underline{v}\}$$
$$= \left(\prod_{i=1}^{M} P\{B_{i,\max}[n] = b_i|V_i[n] = v_i\}\right)P\{V^M = \underline{v}\}.$$

Here, $P\{B_{i,\max}[n] = 0|V_i[n] = 0\} = 1$ and $P\{B_{i,\max}[n] = b_i|V_i[n] = 1\}$ is given by Poisson Binomial distribution. Moreover,

$$P\{V^M = \underline{v}\} = \sum_{\underline{s}} P\{V^M = \underline{v}|S^M = \underline{s}\}P\{S^M = \underline{s}\}$$
$$= \sum_{\underline{s}} \left(\prod_{i=1}^{M} P\{V_i[n] = v_i|S_i[n] = s_i\}\right)P\{S^M = \underline{s}\}$$

where $\underline{s}$ is a $1 \times M$ array with ith element $s_i \in \{0, 1\}$ and $P\{S^M = \underline{s}\}$ depends on the correlation among the spike trains of different inputs. Whereas, $P\{V_i[n] = v_i|S_i[n] = s_i\}$ is defined in Section 5.2.2. According to the low of total probability $P\{Y[n] = 1\}$ can be written as

$$P\{Y[n] = 1\} = \sum_{s} P\{Y[n] = 1|S^M[n] = \underline{s}\}P\{S^M = \underline{s}\}$$

and the conditional probability $P\{Y[n]|S^M[n]\}$ is derived as

$$P\{Y[n] = 1|S^M[n] = \underline{s}\} =$$
$$\sum_{\underline{b},\underline{v}} \left(P\Big\{g(t_n + t_p) > \theta_0 - e_0 - \sum_{i=1}^{M} v_i b_i h_p\Big\}\right.$$
$$\prod_{i=1}^{M} P\{B_{i,\max}[n] = b_i|V_i[n] = v_i\}$$
$$\left.\prod_{i=1}^{M} P\{V_i[n] = v_i|S_i[n] = s_i\}\right).$$

In this section, we derived the closed form equation for sum rate of MISO neuro-spike communication channel considering a detailed channel model. To simulate

derived equations for $P\{Y[n]=1\}$ and $P\{Y[n]=1|S^M[n]=\underline{s}\}$, all possible combinations of $\underline{b}$, $\underline{v}$ and $\underline{s}$ must be considered. Since $b_i \in [0, R_0]$ and $v_i, s_i \in [0,1]$, the number of these combinations is $R_0^M \times 2^M \times 2^M$. Hence, while derived formulas can be used to study the performance of neuro-spike communication for small values of M, the complexity of simulating this model grows exponentially with the number of pre-synaptic neurons, i.e., M, as a result of complexity of neuro-spike communication. Hence, to provide a framework for analyzing impacts of increasing number of pre-synaptic terminals and variations in biophysical parameters of the channel when M is high, we consider a simplified scenario in next section. We assume that all pre-synaptic neurons have the same biophysical parameters and derive another closed form equation for mutual information among input and output of the channel under this situation. The following analysis also gives insights on the performance of artificial nanonetworks, where identical nanomachines communicate with each other using the communication paradigm inspired from synaptic transmission.

5.3.1 Pre-synaptic Neurons with Same Synaptic Structure

Here, we assume that biophysical parameters of all input neurons and their synapse to the output neuron are the same, i.e., for $\forall i_1, i_2 \in [1, M]$ and $\forall r$ following equations hold.

$$N_{i_1} = N_{i_2} \qquad P_{i_1} = P_{i_2} \qquad H_{i_1} = H_{i_2}$$
$$L_{i_1} = L_{i_2} \qquad P_{i_1,u} = P_{i_2,u} \qquad v_{i_1,r} = v_{i_2,r}$$

Hence, the number of spikes arrive at input determines number of released vesicles. Consequently, the number of bound neurotransmitters to the receptors and the generated post-synaptic potential only depend on the number of arrived spikes at input. In other words, knowing which pre-synaptic neuron is transmitting a spike does not affect the output. Hence, (5.4) can be written as follows.

$$I(S^M[n]; Y[n]) = H(Y[n]) - H(Y[n]|\sum_{i=1}^{M} S_i[n] = s_t). \tag{5.8}$$

In the following, we derive $P\{Y[n]=1\}$ and $P\{Y[n]=1|\sum_{i=1}^{M} S_i[n]=s_t\}$. By conditioning over number of bound neurotransmitter, $P\{Y[n]=1\}$ can be written as

$$P\{Y[n]=1\}=\sum_{b_t} P\Big\{\sum_{i=1}^{M} V_i[n]B_{i,\max}[n]=b_t\Big\} \\ P\Big\{g(t)>\theta_0-e_0-b_t h_p\Big\},$$

where $b_t \in [0, MR_0]$ shows total number of bound receptors in all synapses to the post-synaptic terminal. Since all pre-synaptic neurons and their synapse to the post-synaptic neuron are identical, number of released vesicles is the important parameter in finding b_t and the place of release is not important. Hence, without loss of generality, we assume that in case of j release, the vesicle release is occurred from 1st to jth synapse. Thus, $P\big\{\sum_{i=1}^{M} V_i[n]B_{i,\max}[n]=b_t\big\}$ can be written as

$$P\Big\{\sum_{i=1}^{M} V_i[n]B_{i,\max}[n]=b_t\Big\}= \\ \sum_{j=1}^{M} P\Big\{\sum_{i=1}^{j} B_{i,\max}=b_t|\sum_{i=1}^{M} V_i[n]=j\Big\}P\Big\{\sum_{i=1}^{M} V_i[n]=j\Big\} \\ +P\Big\{\sum_{i=1}^{M} V_i[n]B_{i,\max}[n]=b_t|\sum_{i=1}^{M} V_i[n]=0\Big\}P\Big\{\sum_{i=1}^{M} V_i[n]=0\Big\}$$

where $P\{\sum_{i=1}^{M} V_i[n]B_{i,\max}[n]=0|\sum_{i=1}^{M} V_i[n]=0\}=1$. Considering $j\geq 1$ released vesicles, the total number of bound receptors, b_t, cannot be greater than jR_0. Hence, for $b_t > jR_0$,

$$P\Big\{\sum_{i=1}^{j} B_{i,\max}=b_t|\sum_{i=1}^{M} v_i=j\Big\}=0$$

and for $b_t \leq jR_0$,

$$P\Big\{\sum_{i=1}^{j} B_{i,\max} = b_t | \sum_{i=1}^{M} v_i = j\Big\} = P\Big\{\sum_{i=1}^{j}\sum_{r=1}^{R_0} x_{i,r}[n] = b_t\Big\},$$

which can be modeled by Poisson Binomial distribution with mean, $\mu_t[n]$, and variance, $\sigma_t[n]^2$, as shown in [Fernandez and Williams, 2010],

$$\mu_t[n] = \sum_{i=1}^{j}\sum_{r=1}^{R_0} O_{i,r}[n] \tag{5.9}$$

$$\sigma_t[n]^2 = \sum_{i=1}^{j}\sum_{r=1}^{R_0} O_{i,r}[n](1 - O_{i,r}[n]). \tag{5.10}$$

Next step is deriving $P\{\sum_{i=1}^{M} V_i[n] = j\}$. The number of released vesicles depends on the total number of spikes arrived in different pre-synaptic terminals in nth time window. Thus,

$$P\Big\{\sum_{i=1}^{M} V_i[n] = j\Big\} = \sum_{s_t} P\Big\{\sum_{i=1}^{M} V_i[n] = j | \sum_{i=1}^{M} S_i[n] = s_t\Big\} P\Big\{\sum_{i=1}^{M} S_i[n] = s_t\Big\}.$$

Since we ignore the probability of spontaneous release in this study, number of released vesicles to all synapses, i.e., j, cannot be greater than total number of arrived spikes to all pre-synaptic terminals, i.e., s_t. Hence, for $j > s_t$,

$$P\Big\{\sum_{i=1}^{M} V_i[n] = j | \sum_{i=1}^{M} S_i[n] = s_t\Big\} = 0$$

and for $j \leq s_t$,

$$P\Big\{\sum_{i=1}^{M} V_i[n] = j | \sum_{i=1}^{M} S_i[n] = s_t\Big\} = \binom{s_t}{j} P_i^j (1-P_i)^{s_t - j}.$$

According to the low of total probability $P\{Y[n]=1\}$ can be written as

$$P\{Y[n]=1\} = \sum_{s_t=0}^{M} \Big(P\Big\{Y[n]=1 | \sum_{i=1}^{M} S_i[n] = s_t\Big\} \\ P\Big\{\sum_{i=1}^{M} S_i[n] = s_t\Big\}\Big)$$

and the conditional probability $p\{Y[n] | \sum_{i=1}^{M} S_i[n] = s_t\}$ is derived as

$$P\Big\{Y[n]=1 | \sum_{i=1}^{M} S_i[n] = s_t\Big\} = \\ \sum_{j=1}^{s_t} \sum_{b_t=0}^{jR_0} P\Big\{g(t) > \theta_0 - e_0 - b_t h_p\Big\} \\ P\{\sum_{i=1}^{j} \sum_{r=1}^{R_0} x_{i,r}[n] = b_t\} \binom{s_t}{j} P_i^j (1-P_i)^{s_t - j} \\ + P\Big\{g(t) > \theta_0 - e_0\Big\}(1-P_i)^{s_t}.$$

Note that the second term of this equation is derived for $j=0$ and consequently $b_t = 0$.

Considering spike arrival in different pre-synaptic neurons as independent, the probability of having s_t spikes in all pre-synaptic terminals, i.e., $P\{\sum_{i=1}^{M} S_i[n] = s_t\}$ is derived based on Poisson-Binomial distribution with mean, μ_{st}, and, variance, σ_{st}^2, given below.

$$\mu_{st} = \sum_{i=1}^{M} P\{S_i[n]=1\}, \tag{5.11}$$

$$\sigma_{st}[n]^2 = \sum_{i=1}^{M} P\{S_i[n]=1\}\big(1 - P\{S_i[n]=1\}\big).$$

Table 5.1: Simulation Parameters for MISO Channel

Parameters	**Symbols**	**Values**
Time to peak of EPSP	t_p	220 μs [Khan et al., 2017]
Size of RRP	N_i for $\forall i$	10 [Schikorski and Stevens, 1997]
Resting potential	e_0	-65 mV
Spiking threshold	θ_0	-45 mV [Plonsey and Barr, 2007]
Noise standard deviation	σ_n	0.1 mV [Malak and Akan, 2013a]
Neurotransmitters/vesicle	T_0	300
Synaptic cleft height	H_i for $\forall i$	20 nm [Savtchenko and Rusakov, 2007]
Diffusion coefficient	D_c	0.33 μm^2/ms [Nielsen et al., 2004]
Side length of PSD	L_i for $\forall i$	0.4 μm [Khan et al., 2017]
Receptor density	$[AMPA]$	500/μm^2 [Montes et al., 2015]
Pre-synaptic re-uptake	$P_{i,u}$ for $\forall i$	10% [Khan et al., 2017]
Binding rate of AMPA	κ_b	$78 \times 10^6 \frac{1}{\text{Ms}}$
AMPA Dissociation rate	κ_d	750 s^{-1} [Agmon and Edelstein, 1997]
Effective volume	$\lvert V_{i,r}\rvert$ for $\forall i, r$	$1 \times 1 \times 0.5$ nm^3
Simulation time step	$\Delta\tau$	3.85 ns [Khan et al., 2017]
Time step, spike width	$\Delta t = \Delta t_s$	4 ms [Ramezani and Akan, 2017e]

Note that by using same spike rate for different pre-synaptic terminals, $P\{\sum_{i=1}^{M} S_i[n] = s_t\}$ can be derived based on Binomial distribution with mean, μ_{st}, and, variance, σ_{st}^2.

5.4 Simulation Results and Discussion

In this section, we evaluate the sum rate of MISO neuro-spike communication channel by considering same characteristics for all pre-synaptic inputs given in Table I. Moreover, we consider that all pre-synaptic neurons use same spiking rate, i.e, $\lambda_i = \lambda$. Note that we utilize a smaller simulation time step, called $\Delta\tau$, within Δt to derive $O_{i,r}(t)$ [Khan et al., 2017]. Moreover, the peak EPSP amplitude contributed by ith synapse is calculated as $h_i = h_p B_{i,max}[n]$, where h_p is fixed such that $h_i = 1$ mV for parameters given in Table I [Malak and Akan, 2013a]. Variations in param-

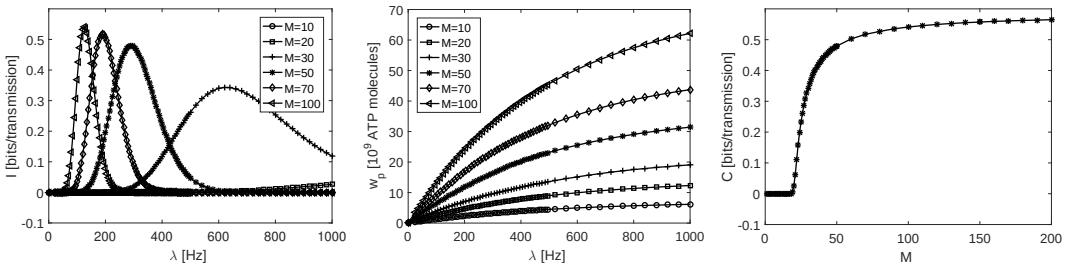

(a) (b) (c)

Figure 5.3: (a) Mutual information, I, (b) average consumed metabolic energy, w_p, and (c) maximum achievable sum rate for different number of neurons, M.

eters may lead to different values of h_i as $B_{i,max}[n]$ may change. Furthermore, t_p depends on synaptic parameters such as number of neurotransmitters in each vesicle, re-uptake probability, synaptic geometries, and offset in vesicle release site [Khan et al., 2017]. If these parameters change in a way that t_p increases, the shape of $e_i(t)$ widens, which can result in $e_i(t)$ that is wider than the discretization time step, Δt. In this case, the probability of spike generation at output, i.e., $P\{Y[n] = 1\}$, depends on released vesicles in previous time steps, thus the mutual information of the channel changes with time, which is not under the focus of this study. The results reported in this section give insight in the way neurons communicate and the performance of nanonetwork designed based on neuro-spike communication paradigm. Further studies are required to investigate impacts of selecting synaptic parameters that lead to bigger values of t_p on the performance of this communication channel.

5.4.1 Mutual Information

In this section, we evaluate impacts of changes in spiking rate, λ, and the number of inputs, M, on the mutual information between input and output of the channel, I.

To generate a spike in post-synaptic terminal, its membrane potential needs to increase from resting potential, i.e., $e_0 = -65$mV, to spiking threshold, i.e., $\theta_0 = -45$mV. Two factors are important in finding the average number of spikes needed at input to cause this required potential change (i) vesicle release probability

after spike arrival to a pre-synaptic terminal, i.e., $P_i = 0.85$, and (ii) the average contribution of each pre-synaptic terminal in post-synaptic membrane potential after vesicle release, which is considered as $\overline{B_{i,max}[n]}h_p = 1\text{mV}$ same as [Malak and Akan, 2013a]. Hence, on average, arrival of more than $\frac{\theta_0 - e_0}{\overline{B_{i,max}[n]}h_p P_i} = 23.52$ spikes in all pre-synaptic terminals is needed to generate a spike in post-synaptic neuron. Moreover, the average number of spikes arrive to all pre-synaptic terminals is $\mu_{st} = M\big(1 - exp(-\lambda\Delta t)\big)$ according to (5.11). Hence, the probability of spike generation in post-synaptic terminal tends to zero for $M \leq 23$ independent from the activation of pre-synaptic terminals, thus, the mutual information between input and output of the channel is negligible as shown in Fig. 5.3. However, the chance of arrival of enough spikes for activating post-synaptic terminal increases for higher values of M.

As it is shown in the Fig. 5.3(a), for $M \in [30, 50, 70, 100]$, increasing λ first improves the mutual information between input and output until reaching its maximum value. Then, further increase in λ decreases the mutual information. The reasons of this trend is investigated in the following.

- For *small values of* λ, the probability of spike arrival in each pre-synaptic terminal during a time step, i.e., $P\{S_i[n] = 1\} = 1 - \exp(-\lambda\Delta t)$, is very small. Thus, the total number of spikes arrived in all pre-synaptic input is insufficient to fire a spike in post-synaptic neuron. Hence, if λ is small, the probability of spike generation in post-synaptic terminal, thus, the mutual information between input and output of the channel, tends to zero.

- For *very big values of* λ, the probability of spike arrival in each pre-synaptic terminal tends to 1. Thus, if the number of input neurons, M, is high enough, there is sufficient number of spikes in all pre-synaptic inputs to generate a spike in post-synaptic terminal during all time steps. Hence, the mutual information between input and output of the channel tends to zero.

- *Increasing spiking rate,* λ, monotonically increases the probability of spike arrival in ith pre-synaptic terminal, which in turn increases the number of all

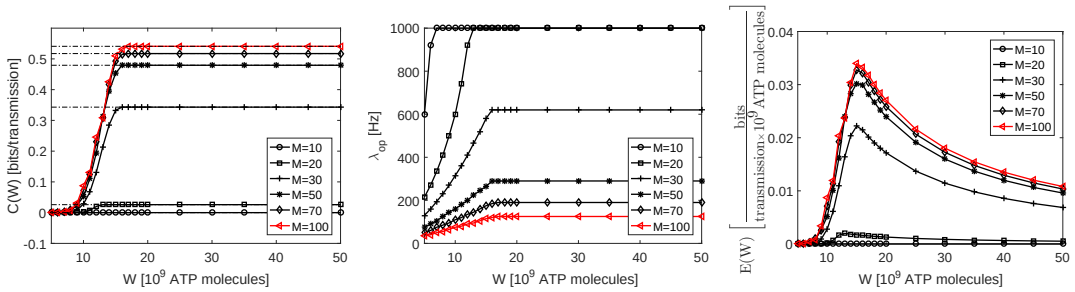

(a) (b) (c)

Figure 5.4: (a) Sum rate of MISO synaptic channel with metabolic cost constraint (b) the spiking rate that maximizes the sum rate, i.e., λ_{op} and (c) the maximum achievable sum rate per unit metabolic energy.

spikes arrived in all pre-synaptic neurons. Hence, the probability of spike generation in post-synaptic terminal, i.e., $P\{Y[n] = 1\}$ monotonically increases from 0 in low values of λ to 1 in higher values of λ. Note that, the maximum mutual information happens when $P\{Y[n] = 1\}$ reaches an optimum value. Moreover, I becomes less than its maximum value for pre-synaptic activities causing higher or lower $P\{Y[n] = 1\}$ compared to its optimum value. Hence, increase in spiking rate, λ, increases the mutual information, I, until reaching its maximum value as shown in Fig. 5.3(a). However, after reaching the maximum mutual information, increasing λ decreases I since it causes more deviation from optimum value of $P\{Y[n] = 1\}$.

Moreover, since the average number of spikes arrive to all pre-synaptic terminals is $\mu_{st} = M(1 - exp(-\lambda\Delta t))$, the maximum mutual information can be achieved with lower value of M if λ is increased.

As it is shown in Fig. 5.3(a), the changes in mutual information with respect to λ is faster for higher values of M. This makes the performance of the system sensitive to jitters in λ for higher values of M, which should be considered in future applications of this communication paradigm.

The average consumed metabolic energy, w_p, for different spiking rates, λ, and number of input neurons, M, is shown in Fig. 5.3(b). Either increasing λ or M increases the number of spikes at the input, which in turn increases the average

required metabolic energy, w_p, based on (5.5). Moreover, the metabolic energy required to maintain resting potential also increases for higher values of M.

5.4.2 Performance for Different Number of Pre-synaptic Inputs

The sum rate of the MISO channel without considering the metabolic cost constraint is calculated by maximizing the mutual information, shown in Fig. 5.3(a), over λ. As depicted in Fig. 5.3(c), higher number of pre-synaptic terminals, M, increases the maximum achievable sum rate, i.e., C, since the average and standard deviation of number of spikes in the input increases. However, the increase rate of C is decreasing by increasing M. This should be considered in design of nanoscale communication systems based on neuro-spike communication since increasing number of inputs does not efficiently improve the achievable sum rate of the system.

5.4.3 Maximum Achievable Sum Rate Versus Metabolic Cost

Limiting the average metabolic energy available for this MISO communication, i.e., W, controls the average number of pre-synaptic terminals that can have a spike in a given time step. Hence, it affects the maximum achievable mutual information. The maximum achievable sum rate of the MISO channel as a function of W is shown in Fig. 5.4(a) for different number of pre-synaptic neurons. The dotted lines in this figure show the sum rate that can be achieved for a particular number of inputs in the absence of metabolic cost constraint.

By increasing W more number of spikes are allowed in the input, which increases the mutual information as observed in Fig. 5.3(a). Hence, relaxing the upper bound on the average consumed metabolic energy increases the maximum achievable sum rate of the channel, $C(W)$, as it is shown in Fig. 5.4(a). Moreover, $C(W)$ increases with almost the same rate for each M since it is a function of average number of spikes allowed at the input, which is not affected by changing M for a constant W. As it is shown in Fig. 5.4(a), $C(W)$ is saturating after reaching the peak of mutual information for each value of M. Furthermore, this peak is occurring at almost the same value of W for all M since it depends on number of pre-synaptic input and

the required metabolic energy for spike generation is very higher than the required energy for achieving resting potential in neurons. However, it can be observed that as number of pre-synaptic inputs increases a slightly higher W is required to achieve the peak of mutual information.

The average number of spikes in the input of the MISO neuro-spike communication is limited by the metabolic cost constraint, i.e., $w_p < W$. Hence, possible values of spiking rate, λ, that can be used to calculate the maximum achievable sum rate in (5.6) is changing for different values of W. Values of spiking threshold that maximizes the the sum rate, i.e., λ_{op}, are shown in Fig. 5.4(b) for different values of W. Since increasing W allows bigger values of λ to be used in (5.6), we can observe that higher λ_{op} is obtained for bigger values of W for each M. It is also shown in Fig. 5.4(b) that λ_{op} saturates at the value corresponding to the peak of mutual information in Fig. 5.3(a). Moreover, the maximum sum rate is achieved at lower λ_{op} for higher values of M since average number of spikes at the input increases with increasing M for a certain value of λ.

5.4.4 Information-Cost Efficiency

The amount of consumed metabolic energy is an important factor in determining the rate of error free information transmission between brain and the outside world. As shown in Fig. 5.4(a), the sum rate of MISO neuro-spike communication increases with increasing W until reaching a saturation point. After this point, providing more metabolic energy does not improve the achievable sum rate. Hence, we find a trade-off in terms of information-cost efficiency, $E(W) = \frac{C(W)}{W}$, as shown in Fig. 5.4(c). The parameter $E(W)$, showing the maximum achievable sum rate per unit metabolic energy, can be used to select the optimum value of W in designing a MISO neuro-spike communication system . It can be observed that if enough metabolic energy is not provided for the system, the number of active inputs are decreased, thus reducing the maximum achievable sum rate. Moreover, increasing the available metabolic energy after reaching the peak of $E(W)$ does not improve the performance of the system.

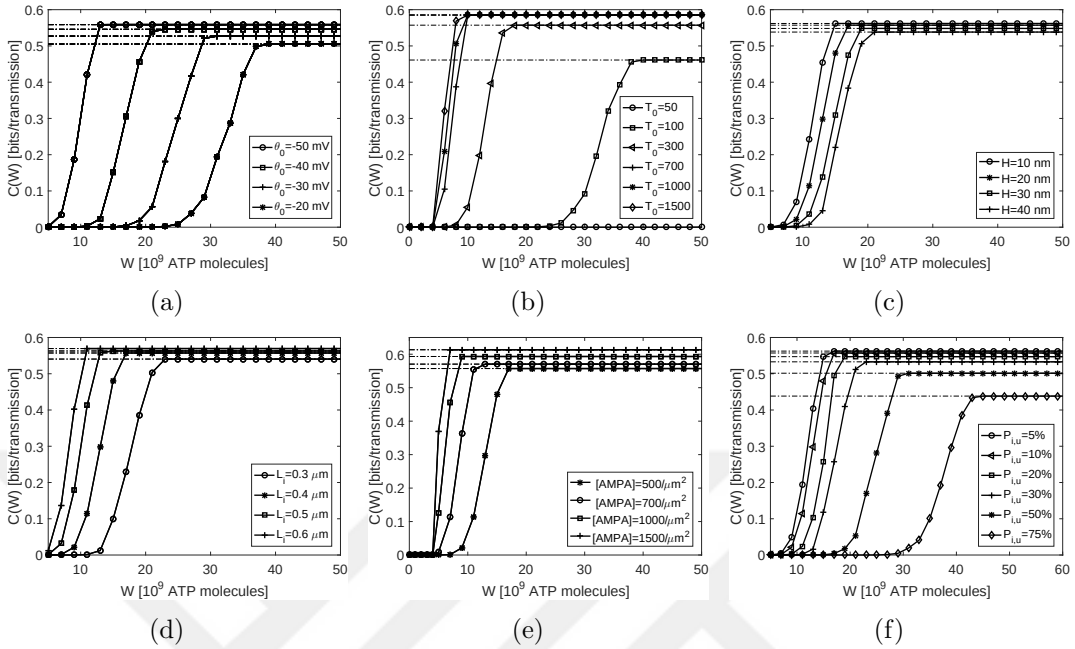

Figure 5.5: Sum rate of MISO synaptic channel with metabolic cost constraint considering $M = 150$ and different (a) spiking thresholds, (b) number of released neurotransmitter, (c) synaptic cleft heights, (d) synaptic cleft side lengths, (e) density of receptors, (f) uptake probabilities.

5.4.5 Impacts of Spike Generation Thresholds on Sum Rate

The spike generation threshold changes according to the memory of postsynaptic neuron [Kobayashi et al., 2009], which can affect the information transmission over the MISO neuro-spike communication channel. Here, we utilize the closed form equation derived for the sum rate of the MISO synaptic channel with constant spiking threshold in Section III, and find the impact of variations in the spiking threshold on the performance of the channel. As depicted in Fig. 5.5(a), more metabolic energy is required to reach the peak of $C(W)$ by increasing the spiking threshold, θ, since more number of spikes are required in the input for spike generation at output neuron. Moreover, the peak of $C(W)$ decreases with increasing spiking threshold, θ_0, when M is constant as shown in Fig. 5.5(a), which is the same as observations in Fig. 5.3(c). The reason is that changes in $\theta_0 - E(t)$, which is important in deriving the probability of spike generation at output neuron, is the same for (i) increasing

spiking threshold θ_0 when number of input neurons is constant, considered in Fig. 5.5(a), and (ii) decreasing number of input neurons M, which leads to smaller $E(t)$, when spiking threshold, θ_0, is constant, studied in Fig. 5.3(c).

5.4.6 Sum Rate vs Number of Released Neurotransmitters

One of the important factors for the performance of neuro-spike communication channel is the number of neuro-transmitters in each vesicle, which can be different from one neuron to another one and can also be affected by different diseases such as Parkinson [Hornykiewicz, 1998]. Here, we analyze how changes in number of neurotransmitters in a vesicle, T_0, affects the performance of MISO neuro-spike communication channel. By increasing T_0, number of bound neurotransmitters per vesicle release increases which results in higher amplitude of EPSP per synapse. This scenario is equivalent with increasing M when T_0 is fix, for which changes in sum rate is shown in Fig. 5.3(c). Hence, the peak of $C(W)$ is higher for bigger values of T_0 as shown in Fig. 5.5(b). Furthermore, bigger values of EPSP per synapse results in need for less number of pre-synaptic spikes to fire a spike at output neuron. Hence, the peak of $C(W)$ is reached with consuming lower metabolic energy. Moreover, changes in $C(W)$ caused by increasing T_0 saturate since the available number of receptors in postsynaptic neuron is limited and almost all of them are bound to a neurotransmitter in the saturation point. Hence, further increase of T_0 does not affect the EPSP generation and the performance of this channel.

5.4.7 Sum Rate for Different Synaptic Geometries

Synaptic geometries strongly affect the number of neurotransmitters that bind to receptors of since by increasing either the height or the length of the synapse, the distance that neurotransmitters need to pave to reach receptors increases. This increases the chance of diffusion of neurotransmitters to outside of synaptic cleft or re-uptake of them by pre-synaptic terminal, which results in reduction of the amplitude of EPSP generated per vesicle release. Hence, more number of pre-synaptic spikes, thus, more metabolic energy, is required for spike generation. As a result,

peak of $C(W)$ occurs at higher values of W as shown in Fig. 5.5(c) and Fig. 5.5(d).

5.4.8 Sum Rate vs Density of Post-synaptic Receptors

Increasing the density of post-synaptic receptors, increases the number of bound neurotransmitters, thus, the peak of EPSP generated, per vesicle release. These consequences are the same with the outcomes of increasing number of neurotransmitters per vesicle when the density of receptors is constant as discussed in Section 5.4.6. Hence, increasing the receptors density results in bigger peak of $C(W)$ and the occurrence of peak at lower W as shown in Fig. 5.5(e). Moreover, the amount of changes in $C(W)$ reduces by increasing density of receptors since after some point the released neurotransmitters are not enough for binding to the newly added receptors.

5.4.9 Sum Rate vs Clearance of Neurotransmitters from Synapse

In this section, we study the impact of changes in the probability of uptake of neuro-transmitters by pre-synaptic neurons, $P_{i,u}$, on the performance of MISO neuro spike communication. Increasing $P_{i,u}$ reduces number of bound neurotransmitters to receptors of post-synaptic neuron, thus, decreases the amplitude of EPSP generated, per vesicle release. These consequences are the same with the outcomes of decreasing number of neurotransmitters per vesicle when $P_{i,u}$ is constant as discussed in Section 5.4.6. Hence, increasing $P_{i,u}$ results in smaller peak of $C(W)$ and the occurrence of peak at higher W as shown in Fig. 5.5(f).

5.5 Conclusion

Certain limitations and constraints exist on the transmission capacity of a MISO neuro-spike communication system as a result of different stochastic processes involved in it and the available metabolic energy for neurons to carry out their routine processing. In this chapter, we derived the closed form equation for the mutual information between input and output of a MISO neuro-spike communication system. Moreover, we quantified the maximum rate of information transmission after tak-

ing into account the consumed metabolic energy in terms of ATP molecules. Furthermore, we have studied impacts of number of pre-synaptic terminals, biological parameters of the channel and available metabolic energy on the maximum achievable sum rate of the MISO neuro-spike communication. The results provided in this chapter gives insights on (i) selecting channel parameters while designing bio-inspired nanonetworks based on neuro-spike communication and (ii) the impact of diseases that change the neuro-spike communication channel characteristics on the performance of nervous nanonetwork.

Chapter 6

SUM RATE ANALYSIS OF MULTIPLE-ACCESS NEURO-SPIKE COMMUNICATION CHANNEL WITH DYNAMIC SPIKING THRESHOLD

6.1 Introduction

In pyramidal neurons multiple pre-synaptic neurons contribute to fire a spike in the postsynaptic neuron [Bear et al., 2007]. Therefore, the information transfer rate for MISO neuro-spike communication is derived in [Malak and Akan, 2013a]. Brain is one of the most expensive organs of any living organism in terms of energy consumption [Laughlin and Sejnowski, 2003, Sengupta et al., 2013]. The generation of the spike and changes in membrane potential consume most of the energy reserved for the brain as it involves opening and closing of numerous ionic channels on the cell membrane [Attwell and Laughlin, 2001]. Thus, the maximum achievable sum rate of the MISO channel is analyzed in chapter 5 [Ramezani et al., 2018b] considering a realistic channel model with metabolic energy constraint. This study uses spike generation model for the postsynaptic neuron with constant spiking threshold.

It is evident from different neurological studies that the spiking threshold of cortical neurons displays large variability over time, profoundly influencing the encoding of information into a spike train [Platkiewicz and Brette, 2010, Kobayashi et al., 2009, Fontaine et al., 2014]. Thus, the adaptive nature of the spiking threshold causes variation in neuronal response with respect to time, i.e., it is responsible for short-term plasticity [Mejias and Torres, 2011]. Short-term synaptic plasticity leads to short-term changes in synaptic function, lasting from milliseconds to minutes, and regulates the moment-to-moment information flow through a neural circuit. Although in [Ramezani et al., 2018a], a SISO time-variant channel with

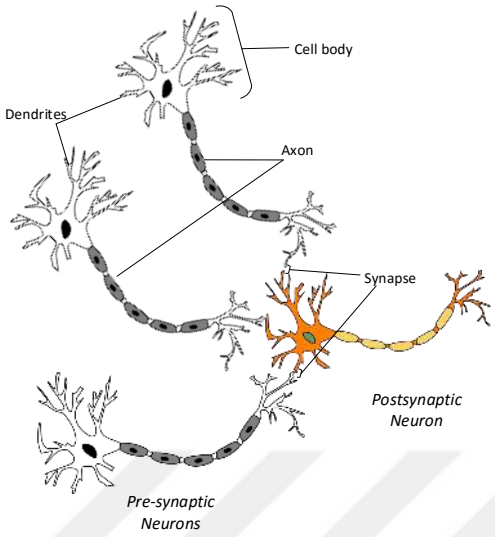

Figure 6.1: MISO Neuro-spike Communication Channel.

variable vesicle release probability has been analyzed, however, the effect of the dynamic spiking threshold on the information flow has not been addressed in any of the studies so far. Therefore, in this article we aim to quantify the variation in the mutual information with respect to time caused by the adaptive spiking threshold in MISO neuro-spike communication channel.

The brain consists of a variety of neurons having different characteristics. Thus, we need a model that incorporates dynamics of the spiking threshold into its responses as well as capable of reproducing spike response of any type of neuron. In INCF *Quantitative Single-Neuron Modeling* competition, participants were challenged to develop a model that fits to the spiking data from different neurons [Rossant et al., 2011]. The most accurate one on the training data was the multi-timescale adaptive threshold (MAT)-model predicting 86% of the reliable spikes [Kobayashi et al., 2009]. MAT-model is a simple integrate-and-fire model having adaptive threshold comprising of a summation of two components that increase at the occurrence of every spike and decay towards a resting value with different time constants. Therefore, in this chapter, we enumerate maximum achievable sum rate of the MISO neuro-spike communication channel by integrating MAT-model as spike generation mechanism under metabolic energy constraints. Furthermore, we analyze

the responses of three types of postsynaptic neurons, i.e., regular spiking (RS) neuron, intrinsic bursting (IB) neuron and fast spiking (FS) neuron, and compare their achievable rates. Moreover, we analyze the trade-off between achievable sum rates and the metabolic cost incurred, by calculating information-cost efficiency. Thus, the main objective of this study is to analyze time varying MISO neuro-spike communication channel by incorporating the effect of complex adaptive nature of the spiking threshold as well as available metabolic energy on the achievable sum rate of multiple access neuro-spike communication. Such analysis is necessary to provide the theoretical foundations on the performance of the neuronal networks before the practical implementation of bio-inspired nanonetworks. Moreover, the performance analysis of the neuronal network with different types of neurons are important in order to develop ICT-based diagnosis and treatment techniques for neurological diseases in future. Furthermore, the models of different types of neurons would enable us to select the best suited neuron type for a particular application of the bio-inspired nanonetworks based on neuron characteristics, such as, less power consumption or high encoding/transmission rates.

The rest of the chapter is organized as follows. In Section 6.2, we describe the MISO neuro-spike communication model. In Section 6.3, we formulate the mutual information and sum rate of MISO neuro-spike communication channel under metabolic cost constraints. In Section 6.4, we present the numerical results. Finally, we conclude the chapter in Section 6.5.

6.2 Model Description

The basic morphology of neurons is shown in Fig. 6.1. The spike is generated at the soma or the cell body of a neuron and propagates through its axon to reach axonal terminal. There exists a small gap, called synapse, between any two neurons. Thus, the information transfer between neurons occurs through chemical messengers known as neurotransmitters. The axonal terminal contains vesicles, i.e., the packets of neurotransmitters, which are released in response to the spike. These neurotransmitters diffuse through the synaptic cleft to reach postsynaptic neuron [Bear et al.,

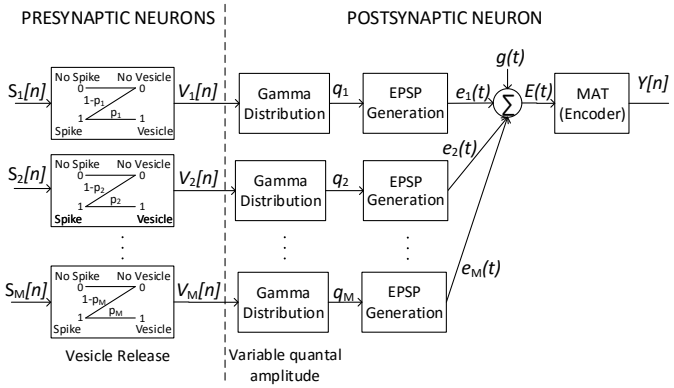

Figure 6.2: Block diagram of the MISO neuro-spike communication channel.

2007]. The binding of neurotransmitters with the receptors present on the post-synaptic terminal opens ionic channels causing ionic influx or efflux. This ionic flow changes the post-synaptic membrane potential. If this change is greater than the threshold value, the spike is generated in the post-synaptic neuron. This study is based on a MISO neuro-spike communication channel, where a single post-synaptic neuron receives and processes information from the multiple pre-synaptic neurons as shown in Fig. 6.1. In this section, we define individual subprocesses of the MISO neuro-spike communication channel model shown in Fig. 6.2.

6.2.1 Vesicle Release Process

Each pre-synaptic neuron generates a spike train, $S_i(t)$, $i \in [1, M]$, where M is the number of pre-synaptic neurons. In [Malak and Akan, 2013a] and [Aghababaiyan et al., 2018b], these spike trains are modeled as doubly Poisson process, i.e., a Poisson process with a time-varying spiking rate. However, to highlight the impact of the adaptive spiking threshold on the information transfer, we simplify the model by ignoring the variation in rate with time. Thus, the spike trains generated by pre-synaptic neurons are modeled by Poisson processes with constant rate λ_i [Ramezani and Akan, 2017e]. Few information and communication theoretical studies have focused on modeling the memory and signal transmission errors during axonal transmission and their impact on the performance of neuro-spike communica-

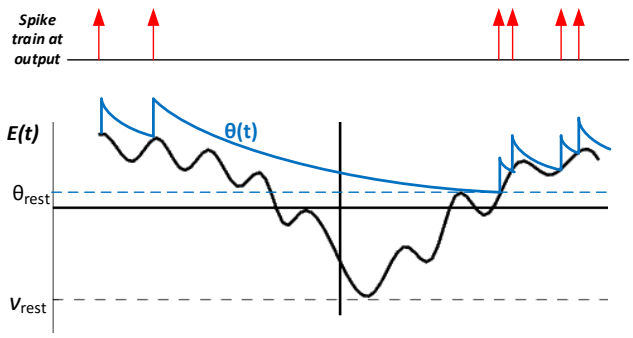

Figure 6.3: Spike generation with MAT model: $\theta(t)$ represents the threshold dynamics with the resting value θ_{rest} and $E(t)$ is the membrane potential with the resting value V_{rest} (adapted from [Kobayashi et al., 2009]).

tion [Aghababaiyan et al., 2018b, Ramezani and Akan, 2017a, Ramezani and Akan, 2018]. However, the pyramidal neurons have myelinated axons, thus, the axonal transmission is highly reliable in these neurons when they are healthy. Thus, the axon is considered as all pass filter. Therefore, the same spike train is assumed to be received at the pre-synaptic terminal.

The spike arrival at each pre-synaptic terminal causes vesicle release, which is modeled using pool-based release and replenishment model in the literature [Matveev and Wang, 2000]. The available vesicles in the pre-synaptic terminal are divided into at least two groups or pools depending on their distance from the membrane and their mobility. The group comprising the vesicles that are ready to be released upon the arrival of spike and are the nearest to the membrane is called readily releasable pool (RRP) with size N_i in i-th pre-synaptic terminal. The remaining vesicles are in reserve pool, which are used to refill the RRP after each release. In this work, we consider the instantaneous replenishment of the ready pool same as in [Malak and Akan, 2013a], thus, N_i does not change with time.

We divide time in windows of equal duration, Δt, which is small enough to have only one spike. Thus, Δt is selected equal to refractory period, i.e., 2 ms [Kobayashi et al., 2009], which is the minimum allowed time interval between two consecutive spikes. During refractory period neuron does not fire even if the potential exceeds the

threshold. Thus, the probability of vesicle release from i-th pre-synaptic terminal during n-th window is derived based on pool-based release model [Ramezani and Akan, 2017e] as

$$P\{V_i[n] = 1 | S_i[n] = 1\} = 1 - \exp\left(-\alpha_i N_i\right) \triangleq p_i, \tag{6.1}$$

where $\alpha_i = 0.06\sqrt{N_i}$ is the rate at which vesicles are fused with the membrane to get released [Dobrunz and Stevens, 1997], $S_i[n] = 1$ and $V_i[n] = 1$ indicate the spike arrival and vesicle release, respectively.

6.2.2 Postsynaptic response at each synapse

After each release, the post-synaptic potential caused by i-th synapse is modeled as [Malak and Akan, 2013a]

$$e_i(t) = \begin{cases} q_i h_i \frac{t}{t_p} \exp\left(1 - \frac{t}{t_p}\right), & \text{if } t \geq 0 \\ 0, & \text{if } t < 0 \end{cases} \tag{6.2}$$

where t_p is the time to reach the peak amplitude, h_i is the peak EPSP amplitude generated at i-th synapse and q_i introduces the trial to trial variability in the magnitude of EPSP at each synapse due to random variations in the synaptic parameters such as the number of neurotransmitters per vesicle, number of neurotransmitters reaching post-synaptic membrane, number and state of available receptors and binding probability of receptors. In this work, q_i is modeled as Gamma random variable as in [Malak and Akan, 2013a].

6.2.3 Spike Generation

The total membrane potential $E(t)$ at post-synaptic neuron contributed by all the inputs is given as

$$E(t) = v_{rest} + \sum_{i=1}^{M} \sum_{t_n \leq t, \forall n} V_i[n] e_i(t - t_n) + g(t), \tag{6.3}$$

where v_{rest} is the membrane resting potential, t_n is the beginning of n-th time window and $g(t)$ is the synaptic noise modeled by Gaussian distribution with zero mean and variance σ_n^2 [Malak and Akan, 2013a]. The inner sum in (6.3) accounts for the temporal summation of the membrane potential at individual synapses and the outer sum gives the spatial summation of membrane potential across all synapses. A spike occurs in the post-synaptic neuron, i.e., $Y[n] = 1$, when $E(t)$ reaches spiking threshold called $\theta(t)$, i.e., $E(t) \geq \theta(t)$ for $(n-1)\Delta t \leq t < \Delta t$.

In this work, we use the spike generation model developed in [Kobayashi et al., 2009] called multiple-timescale adaptive threshold (MAT) model. This model offers low computational cost as compared to other nonlinear complex biophysical models for spike generation. In adaptive threshold models, the threshold is not assumed constant since it has been observed to be varied with time [Fontaine et al., 2014]. Therefore, in MAT model, a dynamic threshold, i.e., $\theta(t)$, is considered that increases when spike occurs and then decays exponentially with multiple timescales towards the resting value θ_{rest} as shown in Fig. 3. The adaptive threshold, $\theta(t)$, is given as

$$\theta(t) = \sum_{k} H(t - t_k) + \theta_{rest}, \tag{6.4}$$

where

$$H(t) = \sum_{j=1}^{L} \beta_j \exp\left(-t/\tau_j\right), \tag{6.5}$$

where t_k is the time for generation of k-th spike in post-synaptic neuron, L is the number of timescales or exponential functions, τ_j is the j-th time constant for exponential function, β_j is the weight of the j-th exponential function and θ_{rest} is the resting value for the threshold. In [Kobayashi et al., 2009], these parameters were

optimized to maximize the degree of coincidence of a model spike train with a real spike train.

As apparent from its name, MAT model utilizes multiple timescales, i.e., multiple τ_j's to predict the spike timings. Thus, in (6.4), $\theta(t)$ decays exponentially with L time constants. In [Kobayashi et al., 2009], τ_j are selected from 10, 50 and 200 ms and the optimal performance was achieved with the combination of two timescales, i.e., L=2, with $\tau_1 = 10$ ms and $\tau_2 = 200$ ms. The performance of the MAT model found to be superior than the standard models like HH, LIF and SRM models in predicting the spike timings with the score of 0.89 ± 0.21.

6.3 Rate Region Analysis with Metabolic Energy constraint on neuronal signaling

In this section, we analyze information transmission rate of the MISO neuro-spike communication channel. The input spike generated at the i-th pre-synaptic neuron is defined as $S_i[n]$ and the output spike generated by a post-synaptic neuron is denoted as $Y[n]$ in the n-th time slot. Thus, the mutual information between $S^M[n] = \{S_1[n], S_2[n], ..., S_M[n]\}$, as input, and $Y[n]$ can be written as

$$I(S^M[n]; Y[n]) = H(Y[n]) - H(Y[n]|S^M[n]). \tag{6.6}$$

The total capacity of the MISO channel is the $I(S^M[n]; Y[n])$ maximized over all input distribution, $p(S^M[n])$. Since we are considering the spike generation in all pre-synaptic neurons based on Poisson distribution, the mutual information can be maximized over λ_i for $\forall i$ to find the maximum achievable sum rate. Defining $R_i[n]$ as the achievable rate for the i-th pre-synaptic neuron in n-th window, the upper bound on the achievable sum rate of the MISO channel is derived as

$$\sum_{i=1}^{M} R_i[n] \leq \max_{\forall i,\ \lambda_i} I(S^M[n]; Y[n]) \triangleq C[n]. \tag{6.7}$$

Since the spiking threshold is changing over time, the mutual information, thus,

$C[n]$, would change in each time step. Therefore, the maximum achievable sum rate of the time-varying MISO channel is defined as

$$C = \lim_{n\to\infty} \max_{\forall i,\ \lambda_i} \sum_{l=1}^{n} \frac{I(S^M[l]; Y[l])}{n}, \tag{6.8}$$

where n increases with the number of time slots. However, in neuro-spike communication channel the achievable rate is limited by the metabolic cost of neural activities, in terms of number of ATP molecules used. Major portion of these ATP molecules are used for maintaining the resting membrane potential as well as spike generation. For the given MISO channel with M pre-synaptic and one post-synaptic neuron, the metabolic energy consumed in the n-th time interval can be calculated as [Attwell and Laughlin, 2001],

$$w(S^M[n], Y[n]) = (M+1)\beta\Delta t + \kappa(Y[n] + \sum_{i=1}^{M} S_i[n]), \tag{6.9}$$

where $\beta = 0.342 \times 10^9$ ATP molecules per second required to maintain resting potential and $\kappa = 0.71 \times 10^9$ ATP molecules required to generate a single spike [Kostal and Kobayashi, 2015]. Thus, the average metabolic energy consumed during the n-th time step is

$$w_p[n] = \sum_{S^M, Y} w(S^M[n], Y[n]) p(S^M[n], Y[n]). \tag{6.10}$$

According to the energy consumption explained above, the maximum achievable rate of the MISO channel would become a function of maximum possible value of $w_p[n]$, i.e, W, hence,

$$C(W) = \lim_{n\to\infty} \max_{\substack{\forall i:\ \lambda_i, \\ \forall l\in[1,n]:\ w_p[l]\le W}} \sum_{l=1}^{n} \frac{I(S^M[l]; Y[l])}{n}. \tag{6.11}$$

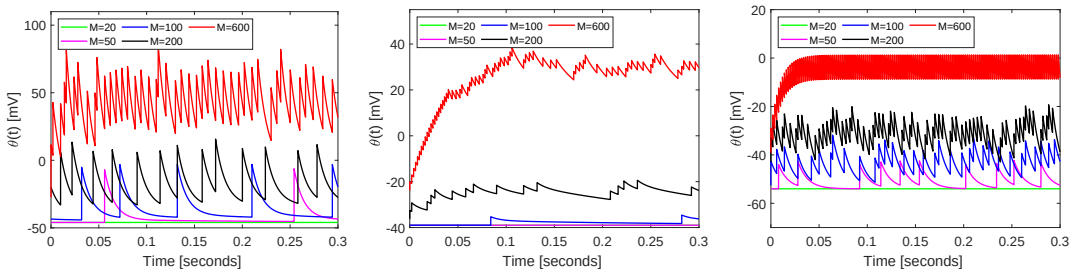

(a) Regular spiking neurons. (b) Intrinsically bursting neurons. (c) Fast spiking neurons.

Figure 6.4: Threshold dynamics of different types of postsynaptic neurons for spiking rate, $\lambda = 100$, and different number of pre-synaptic neurons, M.

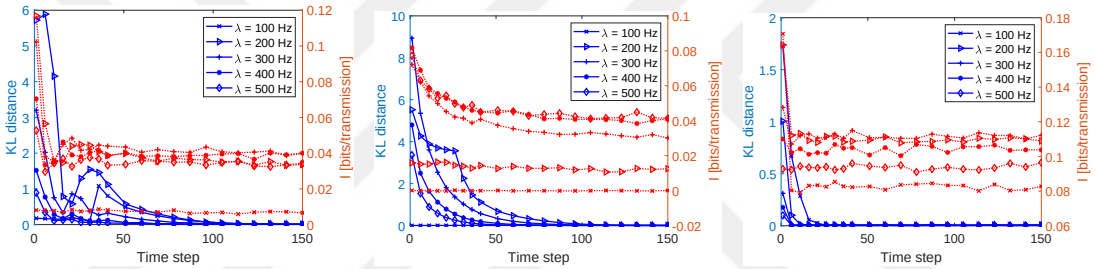

(a) Regular spiking neurons. (b) Intrinsically bursting neurons. (c) Fast spiking neurons.

Figure 6.5: Convergence of $I(S^M[n]; Y[n])$ (dotted lines) and Kullback Leibler distances (solid lines) between the distribution of $\theta(t)$ in different time steps ($p(x)$) and the distribution in 150-th time step ($q(x)$) for $M = 50$ and different spiking rates λ.

6.4 Simulation Results and Discussion

In this section, we simulate the MISO neuro-spike communication channel model described in Section 6.2 with the numerical data available in the literature as given in Table 6.1. We consider M pre-synaptic neurons terminating at a single post-synaptic neuron. We generate spike train in each pre-synaptic neuron using Poisson distribution with the same rate for all inputs, i.e, $\lambda_i = \lambda$.

6.4.1 Dynamic Spiking Threshold

We simulate our model for three different types of postsynaptic neurons, i.e., regular spiking (RS) neuron ($\theta_{rest} = 19$ mV, $\beta_1 = 37$ mV, $\beta_2 = 2$ mV), intrinsic bursting

(IB) neuron ($\theta_{rest} = 26$ mV, $\beta_1 = 1.7$ mV, $\beta_2 = 2$ mV) and fast spiking (FS) neuron ($\theta_{rest} = 11$ mV, $\beta_1 = 10$ mV, $\beta_2 = 0.002$ mV) [Kobayashi et al., 2009]. Note that the given values of θ_{rest} in all three cases are with reference to v_{rest}. The values and the number of timescales, i.e., τ_j and L, respectively, are the same for each type of neuron as mentioned in Section 6.2.3 and the model has been tailored to suit individual neuron by adjusting the amount of fast ($\tau_1 = 10$ ms) and slow ($\tau_2 = 200$ ms) dynamics, i.e., by tuning β_j's [Kobayashi et al., 2009]. The variation in dynamic spiking threshold with respect to time is shown in Fig. 6.4 for different number of pre-synaptic neurons, M.

According to (6.4), the spiking threshold rises whenever spike is generated and decays back towards the resting value. It is shown in Fig. 6.4(c) that FS neuron can produce high number of output spikes with a very few inputs due to lower resting threshold and fast decay of the threshold. However, in IB neuron, resting value is very high and the decay is very slow as compared to RS and FS neurons, thus, it takes longer to produce spike with fewer inputs. However, as the number of inputs increases, the number of output spikes also increases approaching the behavior of FS neuron. Moreover, as can be observed in Fig. 6.4(a), the RS neuron maintains

Table 6.1: Simulation Parameters for Dynamic Threshold

Parameters	**Symbols**	**Values**
Normalized EPSP amplitude	h_i for $\forall i$	1 mV [Malak and Akan, 2013a]
Time to peak of EPSP	t_p	3.85 μs [Khan et al., 2017]
Size of RRP	N_i for $\forall i$	10 [Schikorski and Stevens, 1997]
# of Threshold time constants	L	2 [Kobayashi et al., 2009]
Threshold time constants	τ_1, τ_2	10, 200 ms [Kobayashi et al., 2009]
Threshold exponents Weights	α_1, α_2	37, 2 mV [Kobayashi et al., 2009]
Resting Potential	v_{rest}	-65 mV
Resting threshold (w.r.t v_{rest})	θ_{rest}	19 mV [Kobayashi et al., 2009]
Mean and variance of q_i	$\bar{q}$, σ_q^2	1, 0.6 [Malak and Akan, 2013a]
Noise standard deviation	σ_n	0.1 mV [Malak and Akan, 2013a]

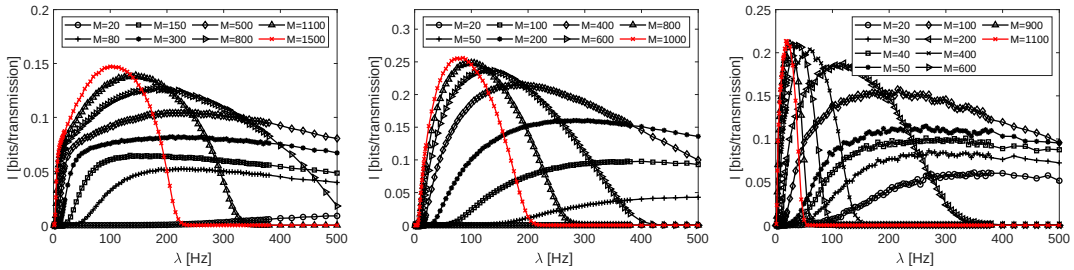

(a) Regular spiking neurons. (b) Intrinsically bursting neurons. (c) Fast spiking neurons.

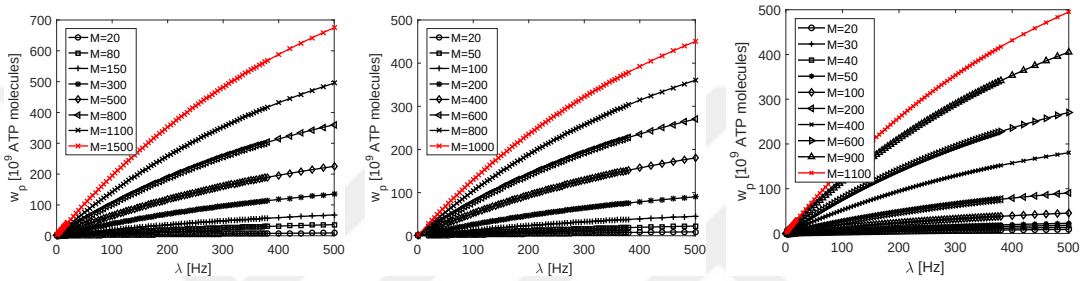

(d) Regular spiking neurons. (e) Intrinsically bursting neurons. (f) Fast spiking neurons.

Figure 6.6: (a-c) Mutual information, I, and (d-f) average metabolic cost, w_p, for different number of pre-synaptic neurons, M, and spiking rates, λ.

regular spiking behavior over a large range of inputs for the given input spiking rate, λ. However, RS behavior will also approach FS neuron with further increase in number of inputs or for higher values of lambda since it increases the probability of input spike.

6.4.2 Mutual Information

We simulate our model to find mutual information between $S^M[n]$ and $Y[n]$. Since we are using MAT-model for the spike generation, the spiking threshold, $\theta(t)$, thus, the mutual information between input and output, changes over time. To evaluate how the distribution of the spiking threshold changes over time, we use Kullback Leibler distance (KL distance) given as

$$KL\ distance = \int p(x) \log_2 \frac{p(x)}{q(x)} dx + \int q(x) \log_2 \frac{q(x)}{p(x)} dx,$$

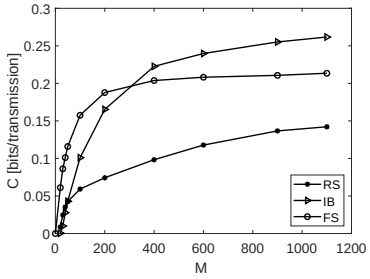

Figure 6.7: Maximum achievable sum rate for MISO neuro-spike communication channel for different number of input neurons.

where $p(x)$ and $q(x)$ are two distributions and the KL distance shows the distance between them. In Fig. 6.5, the change in the distribution of $\theta(t)$ for different types of neurons with $M = 50$ is shown using the KL distance. Here, the $p(x)$ is the distribution of $\theta(t)$ in different time steps and $q(x)$ is the distribution in 150-th time step. We can observe that the distribution of $\theta(t)$ is converging to its steady state value in less than 150 time steps for all types of the postsynaptic neurons. Thus, we can conclude that the mutual information also converges to its steady state in the same time. To verify this conclusion, the mutual information $I(S^M[n]; Y[n])$ is also plotted (dotted lines) in Fig. 6.5 against time steps where its convergence can be observed. Therefore, to calculate the maximum achievable sum rate of the MISO channel, we can maximize the mutual information after reaching the steady state instead of utilizing (6.8). Hence, we calculate mutual information between $S^M[n]$ and $Y[n]$ after significant time has passed allowing the mutual information to converge for each value of M and maximize it over λ to find the maximum achievable sum rate of the MISO channel.

The mutual information, I, between input and output of the channel is shown in Fig. 6.6(a)-(c) for RS, IB and FS neurons, respectively. Increase in either spiking rate, λ, or the number of inputs, M, increases the number of spikes at the input, thus increasing th probability of output spike, which in turn increases the mutual information until reaching its maximum value as shown in Fig. 6.6(a)-(c). Moreover, this maximum mutual information is achieved with higher λ as M decreases since the

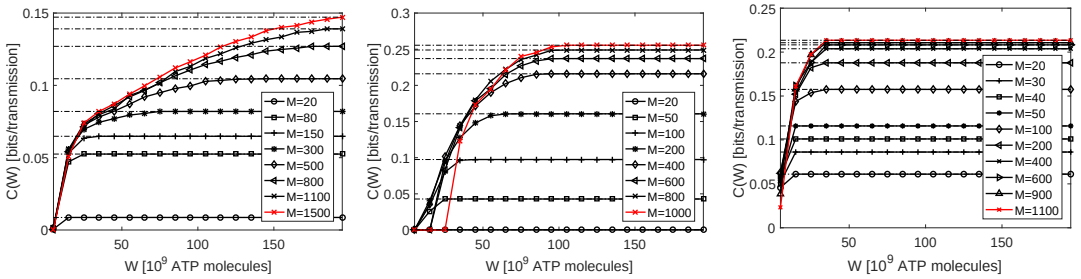

(a) Regular spiking neurons. (b) Intrinsically bursting neurons. (c) Fast spiking neurons.

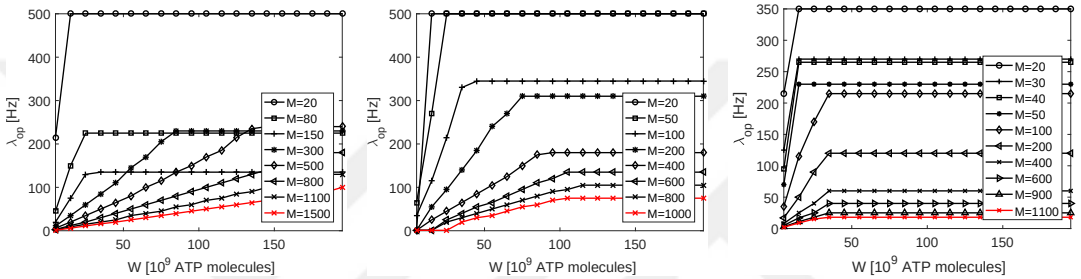

(d) Regular spiking neurons. (e) Intrinsically bursting neurons. (f) Fast spiking neurons.

Figure 6.8: (a-c) Maximum achievable sum rate for MISO neuro-spike communication channel with metabolic cost constraint, $C(W)$, and (d-f) the spiking rate that maximizes the sum rate, λ_{op}.

reduction in M reduces the number of spikes at the input, which is compensated by higher λ. We can also observe that after reaching the maximum mutual information, increasing λ decreases I since it causes more number of input spikes, which in turn decreases the chance of receiving 0 at the output, i.e., decreasing the uncertainty in the output. This argument is true for the values of M as well since increasing M also contributes in increase in the number of input spikes. This observation can be made in Fig. 6.6 for any value of λ.

The mutual information is not only dependent on input spiking rate and the number of inputs M, but is also affected by the inherent characteristics of a neuron. Thus, different types of the postsynaptic neurons exhibit different amount of variation in I in various ranges of M. For instance, it can be observed from Fig. 6.6(b) and 6.6(c) that the FS Neuron shows large variation in maximum mutual information for $M < 50$, however, for RS neuron, the variation in not significant for

$M < 50$. Thus, different simulation scenarios are considered for different types of neurons to show the variation in mutual information with respect to M. By comparing the three types of neurons, we notice that IB neurons achieves highest value of maximum mutual information for the given number of input neurons, closely followed by FS neurons. Moreover, we observe that for lower values of M, maximum mutual information is higher in FS neurons since its resting threshold is lower than the IB neurons.

The average metabolic cost, w_p, for different spiking rates, λ, and number of input neurons, M, is shown in Fig. 6.6(d)-(f). Since either increasing λ or M increases the number of spikes at the input, it increases the average metabolic energy consumed, w_p, based on (6.10) in either type of neurons. Moreover, since w_p includes energy consumption by input spikes and all types of postsynaptic neurons are receiving same inputs, thus, for any given number of inputs, w_p is similar for all types of postsynaptic neurons as presence or absence of one output spike would not affect the energy consumption significantly.

6.4.3 Maximum achievable sum rate versus number of pre-synaptic inputs

In this section, we maximize the mutual information, shown in Fig. 6.6(a)-(c), over λ to estimate the maximum achievable sum rate of the MISO channel without applying the metabolic cost constraint. The relation between maximum achievable rate and the number of pre-synaptic inputs is shown in Fig. 6.7. It is observed that the maximum achievable sum rate, C, increases with increasing number of inputs, i.e., M, since the average number of spikes in the input increases. However, after certain value of M, the maximum achievable sum rate of the channel saturates, i.e, increasing the number of pre-synaptic inputs does not increase information being transmitted.

By comparing the maximum achievable sum rate of MISO channel with the three types of postsynaptic neurons in Fig. 6.7, we can thus conclude that IB neurons are achieving highest value of maximum achievable sum rate, C, for the given number of input neurons, M. Although the rate of increase in C is higher in FS neurons for

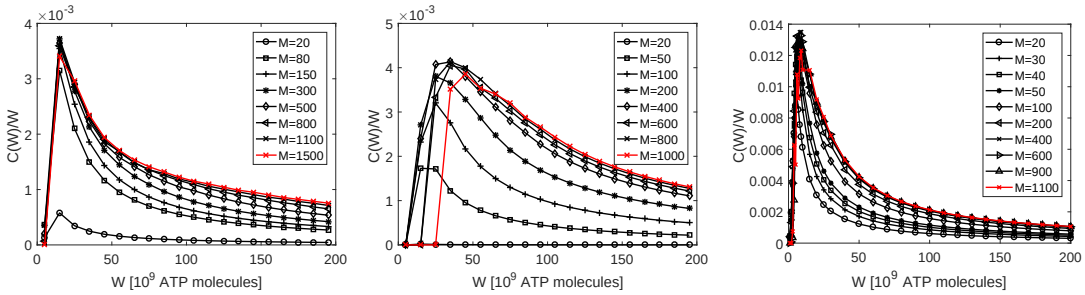

(a) Regular spiking neurons. (b) Intrinsically bursting neurons. (c) Fast spiking neurons.

Figure 6.9: The maximum achievable sum rate per unit metabolic energy.

lower values of M. However, for $M > 400$, the mutual information in FS neurons saturates while in IB neurons it continues to increase with a bit higher rate. The rate of increase of C in RS neurons is slower for all values of M as compared to the other neurons, thus, we can conclude that maximum achievable sum rate of MISO channel with RS neuron acting as postsynaptic neuron will saturate at a lower value than the other two neurons.

6.4.4 Maximum achievable sum rate versus metabolic cost

To enumerate the maximum achievable sum rate of the multiple access channel under metabolic cost constraint, we simulate our model for different number of presynaptic neurons and the results are shown in Fig. 6.8(a)-(c). The dotted lines in this figure show the maximum achievable sum rate that can be achieved for a particular number of inputs in the absence of metabolic cost constraint.

By increasing available metabolic energy, W, more number of spikes are allowed at the input while satisfying the metabolic cost constraint. Moreover, in Fig. 6.6, we observed that increasing the spiking rate at the input, i.e., number of spikes at the input, increases the mutual information. Hence, as shown in Fig. 6.8(a)-(c), the maximum achievable sum rate of the channel increases as we relax the upper bound on the average metabolic cost, i.e., W. Moreover, the maximum achievable sum rate, $C(W)$, increases with the same rate for each M since $C(W)$ is a function of average number of spikes allowed at the input, which is not affected by varying

number of pre-synaptic neurons, M, but is limited by a given value of metabolic energy, W. However, $C(W)$ saturates after the maximum mutual information is achieved for each value of M.

Enforcing metabolic cost constraint, i.e., $w_p < W$, limits the possible values of spiking rate, λ, used to calculate sum rate in Fig. 6.8. The values of λ that achieve maximum sum rate of the MISO channel, i.e., λ_{op}, are shown in Fig. 6.8(d)-(f) for different amounts of metabolic energy, W. For each M, we can observe that higher λ_{op} is obtained for more available energy since it allows occurrence of more spikes at the input. However, λ_{op} for any value of M does not increase as soon as maximum mutual information is achieved. Moreover, we can also observe in Fig. 6.8(d)-(f) that maximum sum rate is achieved at lower λ_{op} for higher values of M since it increases the average number of spikes at the input for any value of λ. It is observed that maximum achievable sum rate, $C(W)$ as well as the optimum spiking rate, λ_{op}, that achieve this sum rate, follow same pattern with respect to metabolic energy for all types of postsynaptic neurons.

Comparing these results with [Ramezani et al., 2018b], which is based on the constant spiking threshold, we conclude that very large number of inputs are needed to generate a spike in the postsynaptic neuron with dynamic spiking threshold. Thus, very high amount of energy is being consumed to achieve only half of the maximum achievable sum rate.

6.4.5 Information-Cost efficiency

As observed in Fig. 6.8(a)-(c), maximum achievable sum rate stops increasing after certain value of metabolic energy, i.e., no matter how much energy is provided, information transmission rate would not increase. Therefore, we find a trade-off between the sum rate and the available metabolic energy, W, in terms of information-cost efficiency, $E = \frac{C(W)}{W}$, as shown in Fig. 6.9. It is observed that relaxing upper bound on W beyond the optimum value would reduce the information-cost efficiency. Thus, the efficiency of the system is an important factor to optimize energy consumption of nanonetwork based on MISO neuro-spike communication model.

If we compare the three types of postsynaptic neurons, we conclude that FS neuron transfers information most efficiently, i.e., it achieves the similar information transfer rate as IB neuron, however, consuming far less amount of energy. It can be observed in Fig. 6.8(b) and (c) that for IB neuron, maximum sum rate of ≈ 0.26 bits/transmission is achieved for $\approx 105 \times 10^9$ ATP molecules and on the other hand for FS neuron, maximum sum rate of ≈ 0.22 bits/transmission is achieved for $\approx 35 \times 10^9$ ATP molecules. This makes FS neurons 67% more efficient than the IB neurons.

6.5 Conclusion

Neurons use spikes to encode information form the outside world to be processed inside the brain. The cortical neurons receive inputs from the multiple pre-synaptic neurons and generate a spike when its membrane potential reaches a spiking threshold. The researchers succeeded in regenerating the spike trains considering the adaptive spiking threshold that depends on previous spike generation. Adaptive threshold is also an important factor in causing short-term plasticity in the brain, which is used to control the information flow between neurons. Thus, in this chapter, we analyzed information transmission in the multiple-access neuro-spike communication channel with dynamic spiking threshold model for spike generation. Furthermore, neuro-spike communication has a major constraint in terms of metabolic energy required by the brain cells to carry out their routine processing. Therefore, we quantified the maximum achievable sum rate taking into account the metabolic cost in terms of ATP molecules consumed. Moreover, we analyzed different types of cortical neurons, i.e., RS, IB and FS neurons and concluded that FS neurons are the most efficient in terms of energy consumption, however, IB neurons provide highest data transmission rates. This analysis would help us to select the neuron with suitable characteristics for a particular application of the nanonetworks.

Chapter 7

IMPACT OF LONG TERM PLASTICITY ON INFORMATION TRANSMISSION OVER NEURONAL NETWORKS

7.1 Introduction

Neuro-spike communication has inherent characteristics to be utilized as the means of communication between artificial bio-inspired nano devices such as the artificial neuron described in [Simon et al., 2015]. Moreover, the information theoretical tools we have developed during our work assisted in the development of the first macro-to-nano-scale communication scheme based on the nervous system [Abbasi et al., 2018]. In [Balasubramaniam et al., 2011], the use of cultured neuronal network is proposed for the communication between nanodevices. Thus, design of interface between nanomachine and neuron as well as the protocol for transmission scheduling has been proposed. Furthermore, the idea of using nanomachines for in situ monitoring and treatment of neurodegenerative diseases has been put forward in [Mesiti and Balasingham, 2013] where the feasibility of neuron-to-nanomachine interface has been investigated to develop a nanoscale stimulator device.

Thus, to utilize neuro-spike communication model in various biomedical applications, we need to investigate different factors affecting the information transmission over neuronal network. There are several information and communication theoretical studies that focus on modeling the processes involved in neuro-spike communication and evaluating its performance [Galluccio et al., 2013, Manwani and Koch, 2001, Ramezani et al., 2017, Veletić et al., 2016b, Aghababaiyan et al., 2018b, Malak and Akan, 2013a, Ramezani and Akan, 2017e, Ramezani et al., 2018a, Ramezani et al., 2018b]. More recently, realistic communication models are used in [Ramezani and

Akan, 2017e, Ramezani et al., 2018a] to study the capacity of vesicle release process and synaptic transmission, respectively. Moreover, maximum achievable sum rate of a MISO neuro-spike communication channel is calculated with constant and dynamic spiking threshold in [Ramezani et al., 2018b] and [Khan and Akan, 2019], respectively.

Synaptic plasticity is a fundamental property of the mammalian brain and refers to the capability of synapses to change their strength [Citri and Malenka, 2008]. It is involved in the control of information flow between neurons on different temporal scales and can be divided into two main categories, (i) short term plasticity, which lasts on the order of milliseconds to several minutes [Crabtree and Gogos, 2014], and (ii) long-term plasticity, which refers to changes that can last from hours to the lifetime of the synapse and is thought to play a central role in the mechanisms involved in memory and learning [Citri and Malenka, 2008]. Moreover, aberrant synaptic plasticity contributes to several neuropsychiatric disorders [Citri and Malenka, 2008, Bliss et al., 2014]. Hence, studying synaptic plasticity in both healthy and diseased conditions is an important step towards understanding brain functions and the development of novel diagnostic and treatment techniques.

The strength of synapse can either increase, known as synaptic potentiation, making it more reliable, or decrease, known as synaptic depression, to inhibit information transfer [Citri and Malenka, 2008]. Both potentiation and depression depends on various pre- and postsynaptic mechanisms. Thus, synaptic plasticity is involved in the control of information flow between neurons. While the impact of short-term plasticity on mutual information is considered in [Ramezani and Akan, 2017e, Khan and Akan, 2019, Ramezani et al., 2018a], none of the existing studies in the literature have considered the impact of long-term synaptic plasticity on the performance of neuro-spike communication channel.

Our main motivation in this work is to study and analyze natural neural network (NN), which will provide a communication paradigm for the realization of the bio-inspired man-made NNs, that behave as real neurons, having vast range of applications described at the end of this article. Since in natural NNs, synaptic plasticity

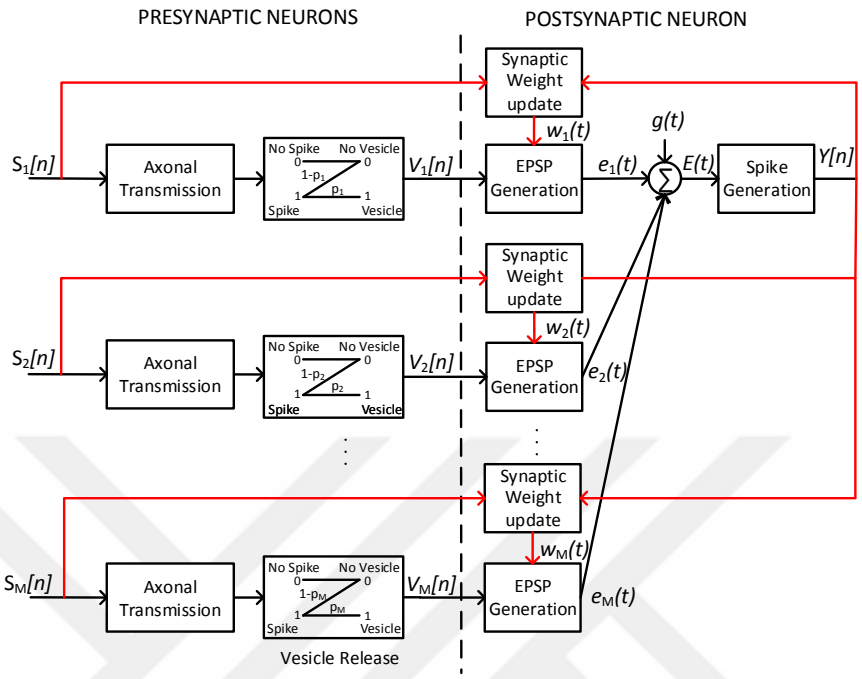

Figure 7.1: MISO Synaptic Channel Model.

is a common phenomenon that exhibits learning and memory, we aim to provide a comprehensive analysis of neuro-spike communication channel including the impact of plasticity and the parameters that govern this behavior. Hence, we select the pyramidal neurons in Cornu Ammonis (CA) area of hippocampus location in the brain for our work as this area is heavily investigated in physiology, which provides experimental data for our work, and is responsible for learning and memory, thus, inherently possesses the property of plasticity. In this work, for the first time in the literature, we study the impact of the long-term synaptic plasticity on neuro-spike communication channel among hippocampal pyramidal neurons. Since pyramidal neurons receive input form multiple neurons, our study is based on MISO communication channel. Moreover, long-term plasticity can be expressed in two forms, (i) long term potentiation (LTP) and (ii) long term depression (LTD) [Citri and Malenka, 2008]. Thus, in this work, we are using bidirectional STDP model that either depresses or strengthens the synapses depending on the temporal correlation between pre and postsynaptic spikes [Gerstner and Kistler, 2002].

Learning occurs through cooperation between synaptic inputs and the plasticity rules select inputs which are correlated with other inputs [van Rossum and Turrigiano, 2001]. Thus, we analyze the influence of correlation among presynaptic spike trains on the strengthening of synapses and its impacts on the signal transmission over this channel. To do so, we calculate the mutual information between input and output of the channel and observe its evolution with time as a result of synaptic plasticity. Moreover, impacts of input spiking rate, number of correlated presynaptic neurons and the correlation factor on the mutual information is observed.

The remainder of this chapter is organized as follows. In Section 7.2, the MISO neuro-spike communication channel model is explained. Then, STDP and its impact on the synaptic channel strength is explained in Section 7.3. Performance evaluation is provided in Section 7.4 and some key applications of bio-inspired neuronal networks are given in Section 7.5. Finally, the chapter is concluded in Section 7.6.

7.2 Neuro-spike Communication Channel Model

This study is based on the MISO synaptic channel model of information transmission among hippocampal pyramidal neurons described in this section. In this MISO channel, a single postsynaptic neuron receives and processes information from multiple presynaptic neurons as shown in Fig. 7.1.

7.2.1 Input Spike Trains and Axonal Transmission

Each presynaptic neuron generates a spike train, $S_i(t)$, $i \in [1, M]$, where M is the number of presynaptic neurons, that travel through axon to reach presynaptic terminal. These spike trains are modeled by Poisson processes with rate λ_i in the literature [Ramezani and Akan, 2017e]. If there is a spike at input neuron, the binary signal 1 will be transmitted through neuro-spike communication channel, otherwise, 0 will be sent. By discretizing time into windows of equal length, i.e., Δt, the spiking probability, i.e., the probability of transmitting 1, in each time step n can be calculated as $P\{S_i[n] = 1\} = 1 - exp(-\lambda_i \Delta t)$, where $S_i[n] = 1$ indicates the spike arrival. Moreover, after firing one spike, the neuron is not able to

generate another spike for a certain period of time, which is called refractory period τ_{ref} [Kobayashi et al., 2009]. Hence, $P\{S_i[n] = 1\} = 0$ for $\frac{\tau_{ref}}{\Delta t}$ consecutive time steps after firing one spike. Here, we are considering only regular spiking neurons for our analysis. The other common types of neurons are intrinsic bursting and fast spiking neurons, which have different spiking patterns and may have different τ_{ref}. Furthermore, since spikes propagate reliably through axons in hippocampal neurons [Veletić et al., 2016a], we model axonal transmission as ideal all pass filter with zero transmission delay.

7.2.2 Vesicle Release Process

Each spike can initiate the release of at most one vesicle from each presynaptic terminal in hippocampal pyramidal neurons [Alabi and Tsien, 2012]. Hence, we use the univesicular release model of [Malak and Akan, 2013a] to derive the vesicle release probability, i.e., p_i, as follows,

$$P\{V_i[n] = 1 | S_i[n] = 1\} = 1 - exp(-\alpha_i N_i) \triangleq p_i,$$

where $\alpha_i = 0.06\sqrt{N_i}$ is the rate at which vesicles are fused with the membrane to get released [Dobrunz and Stevens, 1997], N_i is the number of available vesicles for release and $V_i[n] = 1$ indicate the vesicle release from ith presynaptic terminal.

7.2.3 Postsynaptic Response at Each Synapse

The type of neuron is defined by its spiking threshold and the EPSP shape [Kobayashi et al., 2009]. Since we are considering regular spiking neurons, the spiking threshold will be selected accordingly. Moreover, after each release, the postsynaptic potential caused by ith synapse is modeled in [Malak and Akan, 2013a] as

$$e_i(t) = w_i(t) h_i \frac{t}{t_p} exp(1 - \frac{t}{t_p}), \tag{7.1}$$

where t_p is the time to reach the peak amplitude of EPSP, $w_i(t)h_i$ is the peak EPSP amplitude generated at ith synapse and $w_i(t)$ is the synaptic weight, which

can increase or decrease according to the synaptic activity. In the following, we explain the STDP model for updating synaptic weights, $w_i(t)$, according to memory of synaptic transmission.

7.2.4 Evolution of Synaptic Weights due to STDP

Strong depolarization of postsynaptic neuron is required for induction of LTP while weaker depolarization leads to LTD. Therefore, the change in synaptic efficacy is driven by temporal correlations between presynaptic spike arrival and postsynaptic firing and it is termed as STDP. STDP is order dependent, i.e., if the presynaptic spike arrives before postsynaptic spike, the synapse is strengthened, while the opposite order weakens the synapse. This kind of long term synaptic plasticity is prevalent in cortical neurons especially in excitatory hippocampal pyramidal neurons [Feldman, 2012]. Hence, in this section, we provide the model for updating the synaptic wights, governed by a variable weight $w_i(t)$ as shown in (7.1), using STDP model.

Considering $S_i(t) = \sum_f \delta(t - t_{i,pre}^{(f)})$ and $Y(t) = \sum_f \delta(t - t_{post}^{(f)})$ as pre- and postsynaptic spike trains, respectively, and $t' = t_{i,pre}^{(f)} - t_{post}^{(f)}$ as the time difference between pre- and postsynaptic spikes, the change in synaptic weight is given in [Gerstner and Kistler, 2002] as,

$$\frac{d}{dt}w_i(t) = a_0 + S_i(t)\left(a_1^{pre} + \int_0^\infty a_2^{pre,post}(t')Y(t-t')dt'\right) + Y(t)\left(a_1^{post} + \int_0^\infty a_2^{post,pre}(t')S_i(t-t')dt'\right), \quad (7.2)$$

where the parameter $a_0 < 0$ represents an activity independent constant decrease in the synaptic weight, i.e., irrespective of the presence of a spike on pre and postsynaptic terminal, a_1^{pre} and a_1^{post} represent the non-Hebbian effect on synaptic weight resulting due to the occurrence of pre- and postsynaptic spike, respectively. If a presynaptic spike occurs at a particular time instant, $a_2^{pre,post}(t')$ governs the weight change that depends on the time since the last postsynaptic spike arrival. This factor is supposed to reduce the weight according to Hebbian learning. On the other hand,

if a postsynaptic spike occurs at a certain time instant, the time since last presynaptic spike arrival dictates strengthening of the synapse with the factor $a_2^{post,pre}(t')$. Both $a_2^{pre,post}(t')$ and $a_2^{post,pre}(t')$ together describe a *learning window* $W(t')$, i.e., a rule for updating synaptic weight $w_i(t)$, as follows [Gerstner and Kistler, 2002],

$$W(t') = \begin{cases} a_2^{post,pre}(-t') = A_+ \exp\left(t'/\tau_1\right), & \text{if } t' < 0 \\ a_2^{pre,post}(t') = A_- \exp\left(-t'/\tau_2\right), & \text{if } t' > 0 \end{cases} \tag{7.3}$$

where $t' < 0$ shows the arrival of presynaptic spike before postsynaptic spike and $t' > 0$ shows otherwise. The simple exponential learning window used in (7.3), is fitted to the experimental data in [Zhang et al., 1998].

7.2.5 Spike Generation

The total membrane potential $E(t)$ at postsynaptic neuron contributed by all the inputs is given as

$$E(t) = v_{rest} + \sum_{i=1}^{M} \sum_{t_n \leq t, \forall n} V_i[n] e_i(t - t_n) + g(t), \tag{7.4}$$

where v_{rest} is the membrane resting potential, t_n is the beginning of nth time window and $g(t)$ is the synaptic noise modeled by Gaussian distribution with zero mean and variance σ_n^2 [Malak and Akan, 2013a]. A spike occurs in the postsynaptic neuron, i.e., $Y[n] = 1$, when $E(t)$ reaches spiking threshold called θ, i.e., $E(t) \geq \theta$ for $(n-1)\Delta t \leq t < n\Delta t$.

7.3 Information Transmission Rate and Correlated Users

For analyzing the achievable rate of information transmission over our model, we use basic definitions from information theory. The input and output of our model are the spike train, $S_i[n]$ and the generated spikes at output, $Y[n]$, respectively. Thus, the mutual information of the channel is derived as

$$I(S^M[n]; Y[n]) = H(Y[n]) - H(Y[n]|S^M[n]), \tag{7.5}$$

where $S^M[n] = \{S_1[n], S_2[n], ..., S_M[n]\}$. Since the synaptic weight can change in each time step depending on both input spike train and previously fired spike at output neuron, the channel transmission probability, i.e., $P\{Y[n]|S^M[n]\}$, and the probability of spike generation at the output neuron, i.e., $P\{Y[n] = 1\}$, thus, the mutual information among input and output of the channel, i.e., $I(S^M[n]; Y[n])$, can change in each time step. Thus, deriving closed form equations for $P\{Y[n]|S^M[n]\}$ and $P\{Y[n] = 1\}$ seems not feasible. Therefore, we will use Monte Carlo simulations to derive average changes in synaptic weights, the channel transmission probability, the output spike generation probability and the mutual information between input and output of the channel.

We are interested in increasing the information transmission rate over neuronal network, thus, we study the input characteristics that leads to LTP generation. Since STDP is governed by timing of input and output spike trains and the correlated activity of presynaptic neurons affects the output spike generation probability, we study impact of correlation among input spike trains on the input selectivity induced by STDP and ICT-based performance of the network. To introduce this correlation, we divide inputs into two groups G_1 and G_2, where $M_c \in \{5, 10, 15, 20, 50\}$ and $M - M_c$ neurons are assigned to G_1 and G_2, respectively. Let $T_i \sim Poiss(\lambda_i)$, where $\lambda_i = \lambda$ for $i \in [1, M]$, be independent random variables. In G_1, the spike trains are defined as $S_i = T_i + C$ where $i \in G_1$ and $C \sim Poiss(\lambda_c)$. Hence, the spike train of neurons in G_1 are correlated with correlation coefficient given as,

$$\rho_{ij} = corr(S_i, S_j) = \begin{cases} \dfrac{\lambda_c}{\lambda + \lambda_c}, & \text{if } i \neq j \\ 1, & \text{if } i = j \end{cases} \tag{7.6}$$

where $i, j \in G_1$. For neurons in G_2, i.e., $i \in G_2$, the spike trains are defined as $S_i = T_i$, thus, they are uncorrelated. Note that spike trains of neurons assigned to different groups are independent.

Table 7.1: Simulation Parameters for STDP model

Parameters	**Symbols**	**Values**
Normalized EPSP amplitude	$h_i w_{rest}$	1 mV [Malak and Akan, 2013a]
Initial synaptic weight	w_{rest}	0.5
Time to reach EPSP peak	t_p	0.2 ms [Khan et al., 2017]
Number of available vesicles	N_i for $\forall i$	10 [Schikorski and Stevens, 1997]
Resting Potential	v_{rest}	-65 mV
Noise standard deviation	σ_n	0.1 mV [Malak and Akan, 2013a]
Refractory period	τ_{ref}	2 ms [Kobayashi et al., 2009]
Time-step		0.1 ms [Kobayashi et al., 2009]
Number of inputs	M	100
Spiking threshold	θ	-45 mV [Plonsey and Barr, 2007]
STDP parameters	a_0, a_1^{pre}, a_1^{post}	-1, 0.01, 0
	A_+, A_-	0.24, -0.1
	τ_1, τ_2	12.2,13.6 ms

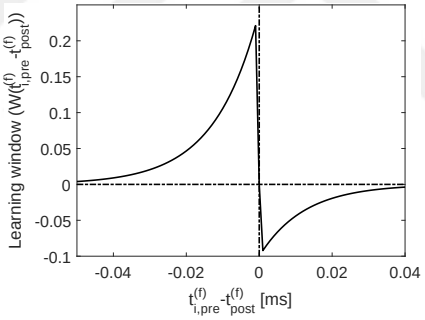

Figure 7.2: Learning Window.

7.4 Performance Evaluation

We evaluate the neuro-spike communication channel considering M presynaptic neurons making only one synapse each with the output neuron as shown in Fig. 7.1 and utilizing parameters given in Table 7.1, which are extracted from experimental data reported in the literature for hippocampal pyramidal neurons. Changes in synaptic efficacy based on STDP model are defined using (7.2) and (7.3) and the learning window is shown in Fig. 7.2. To induce realistic synaptic plasticity, we need to ensure that synaptic weights remain in certain bounds. Thus, we consider initial values of $w_i(0) = w_{rest}$ and restrict them in the interval [0,1] for each synapse [Kistler and

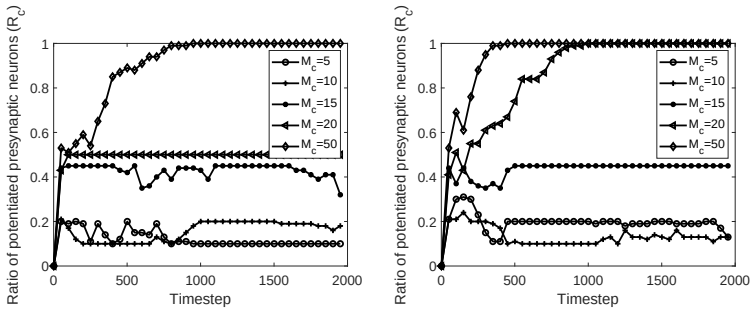

(a) All presynaptic neurons, $\lambda =$ 25 Hz and $\lambda_c = 25$ Hz.

(b) All presynaptic neurons, $\lambda =$ 25 Hz and $\lambda_c = 50$ Hz.

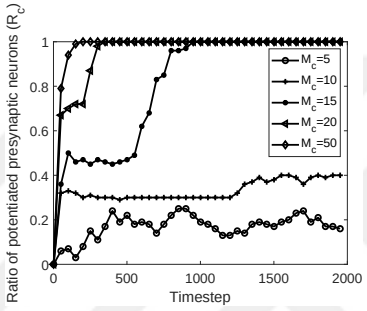

(c) All presynaptic neurons, $\lambda =$ 25 Hz and $\lambda_c = 100$ Hz.

Figure 7.3: Changes in percentage of potentiated presynaptic neurons due to STDP.

Hemmen, 2000]. Moreover, the parameters of STDP model are selected according to studies fitting the STDP model to experimental data [Hayashi and Igarashi, 2009].

In this section, we investigate the impact of system parameters, i.e., input spike rate, λ, correlation factor, λ_c, and number of correlated presynaptic neurons, M_c, on the performance of MISO neuro-spike communication channel, which inherently has plasticity. The simulation results provide a guideline for selecting these parameters in future uses of the bio-inspired neuronal networks for information transmission towards different biomedical applications.

7.4.1 Evolution of Synaptic Weights due to Plasticity

To investigate the evolution of synaptic strength, we simulate the MISO neuro-spike communication channel for 2000 time-steps and calculate the change in synaptic weights over a period of time based on (7.2). By repeating this simulation for 1000

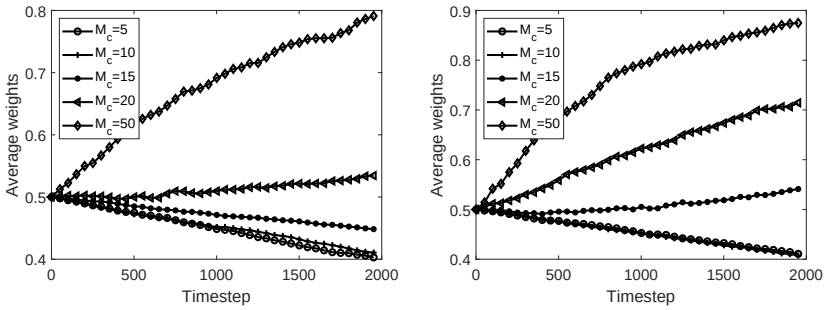

(a) All presynaptic neurons, $\lambda = 25$ Hz and $\lambda_c = 25$ Hz.

(b) All presynaptic neurons, $\lambda = 25$ Hz and $\lambda_c = 50$ Hz.

Figure 7.4: Changes in average synaptic weights due to STDP.

iterations, we derive the average synaptic weights in each time-step. Defining the strengthened or potentiated presynaptic neurons as the one with average synaptic weight grater than w_{rest}, the ratio of strengthened synapses, R_c, with respect to time is plotted in Fig. 7.3 for $\lambda = 25$ Hz. As can be observed, for a constant value of λ_c, higher number of correlated presynaptic neurons, i.e., M_c, leads to higher ratio of potentiated presynaptic neurons. Moreover, the ratio of potentiated presynaptic neurons, R_c, increases by increasing the correlation among the presynaptic neurons in G_1, thus, we have the highest number of potentiated presynaptic neurons for $\lambda_c = 100$ Hz as shown in Fig. 7.3(c). In addition, increasing λ_c causes faster potentiation of synapses. Comparing the ratio of correlated presynaptic neurons with ratio of potentiated synapses shown in Fig. 7.3, we observe that the uncorrelated presynaptic neurons are also strengthened due to the presence of correlated presynaptic neurons in the network. Furthermore, more uncorrelated presynaptic neurons are potentiated if there are higher number of correlated presynaptic neurons in the network or the correlation among presynaptic neurons is stronger, i.e., λ_c is higher. Note that for low values of M_c small changes in number of potentiated preynaptic neurons changes R_c largely. Thus, more fluctuation are observed in R_c for lower value of M_c in Fig. 7.3. Moreover, these fluctuations are more at the beginning of simulations as the synaptic weights are still around w_{rest} and small changes in $t_{i,pre}^{(f)} - t_{post}^{(f)}$ can easily change the synaptic weight from potentiated to depressed and vice versa.

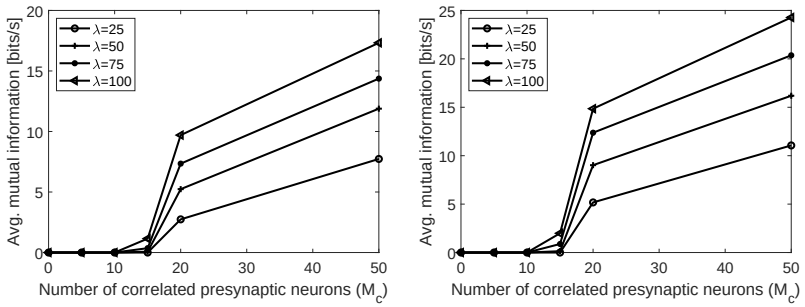

(a) $\lambda_c = 25$ Hz. (b) $\lambda_c = 50$ Hz.

Figure 7.5: Changes in average synaptic weights for different number of correlated presynaptic neurons when synaptic weights are constant, i.e., no STDP.

Although Fig. 7.3 shows the ratio of potentiated presynaptic neurons, the changes in actual magnitude of weights with time are not shown. Thus, we calculate the average of synaptic weights of all presynaptic neurons in each time-step as illustrated in Fig. 7.4. We can observe that synapses are potentiated at higher magnitudes of weights as either M_c or λ_c is increased.

7.4.2 Impact of STDP and Correlated Inputs on Mutual Information

Two factors affect the average mutual information for different number of correlated presynaptic neurons, M_c, first the correlation factor and then the changes in synaptic weights as a result of plasticity. We first ignore the existence of STDP and use constant synaptic weights, w_{rest}, for all presynaptic neurons to identify the impact of correlation on the achievable rate when there is no plasticity as shown in Fig. 7.5. It is observed that if we increase λ, λ_c or the number of correlated presynaptic neurons, M_c, the mutual information among input and output of MISO neuro-spike channel improves as it leads to the generation of more output spikes.

By including STDP along with correlation, we observe in Fig. 7.6 that for low and high values of M_c the mutual information does not change with time. The reason is that enough number of synapses are not potentiated for low values of M_c as shown in Fig. 7.3, thus, there is no changes in probability of output spike generation as a result of plasticity. For very high number of correlated presynaptic neurons, almost

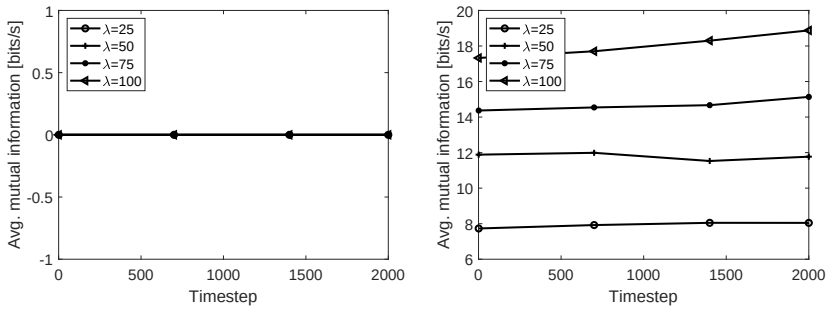

(a) STDP with $M_c = 5$. (b) STDP with $M_c = 50$.

Figure 7.6: Average mutual information for $\lambda_c = 25$Hz and different number of correlated presynaptic neurons.

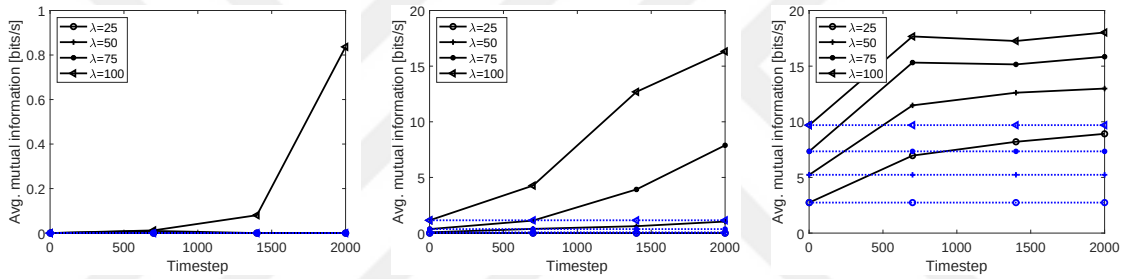

(a) $\lambda_c = 25$Hz and $M_c = 10$. (b) $\lambda_c = 25$Hz and $M_c = 15$. (c) $\lambda_c = 25$Hz and $M_c = 20$.

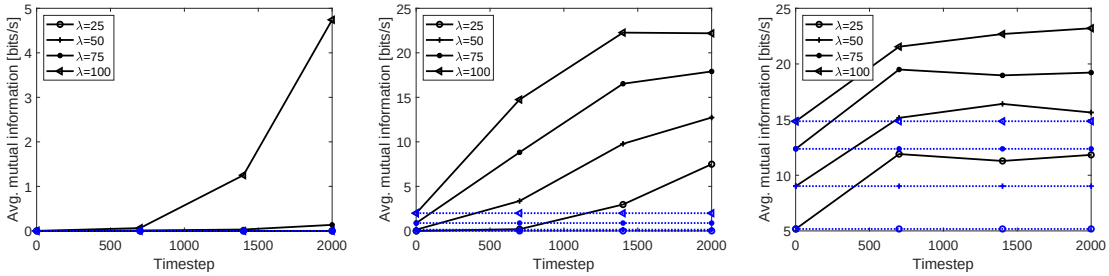

(d) $\lambda_c = 50$Hz and $M_c = 10$. (e) $\lambda_c = 50$Hz and $M_c = 15$. (f) $\lambda_c = 50$Hz and $M_c = 20$.

Figure 7.7: Average mutual information for different λ_c and number of correlated presynaptic neurons (dotted line: without STDP, solid line: with STDP).

all of the synapses undergo potentiation, which is time-dependent, as shown in Fig. 7.3. However, the mutual information remains constant over time as shown in Fig. 7.6 since the required changes in postsynaptic potential for spike generation is 20 mV in regular spiking neurons and we have enough number of correlated inputs for spike generation even without synaptic potentiation.

The average mutual information for medium values of M_c and both with and without STDP scenarios is depicted in Fig. 7.7. When there is no plasticity, the synaptic weights stay constant during signal transmission. Thus, as shown with dotted lines in Fig. 7.7, the average mutual information does not change with time. Comparing Fig. 7.6 and Fig. 7.7, we observe that the mutual information is most affected by synaptic plasticity when the number of correlated presynaptic neurons is close to $M_{spike} = \frac{\theta}{h_i w_{rest}}$. The reason is that $h_i w_{rest}$ is the EPSP generated by a synapse in absence of plasticity, thus, M_{spike} represents the required number of active inputs in a time-step for spike generation. Hence, when number of correlated presynaptic neurons is close to M_{spike}, even small changes in synaptic weights affect the probability of output spike generation, which in turn affects the mutual information. Considering the synaptic weight changes for $\lambda = 25$ Hz and $M_c = 15$ shown in Fig. 7.4, we observe that average mutual information is 0 for $\lambda_c = 25$ Hz in Fig. 7.7 as the synaptic weights are depressed. However, the mutual information increases with time for higher λ_c as it is enhancing the synaptic weights. Moreover, as illustrated in Fig. 7.7, the mutual information among input and output of the channel increases for higher values of λ_c or M_c, which is due to the increment in synaptic weights observed in Fig. 7.3 and 7.4.

As shown if Fig. 7.3, the synapses of uncorrelated presynaptic neurons are also strengthened with time in case of strong correlation among correlated inputs. Thus, we study the impact of changes in synaptic weights on the information transmission by correlated and uncorrelated presynaptic neurons. To this aim, we simulate the network for 2000 time-steps with all presynaptic neurons contributing in weight update and derive the network with updated weights. Then, we calculate the information transmission rate in this updated network for three scenarios: (i) all of the input presynaptic neurons, (ii) only correlated presynaptic neurons, and (iii) only uncorrelated presynaptic neurons transmitting information at four specific time-steps, i.e., $0, 750, 1500$ and 2000. As shown in Fig. 7.8, the mutual information among input and output of the system improves with time even when only the uncorrelated presynaptic neurons utilize the updated network. However, the improvement

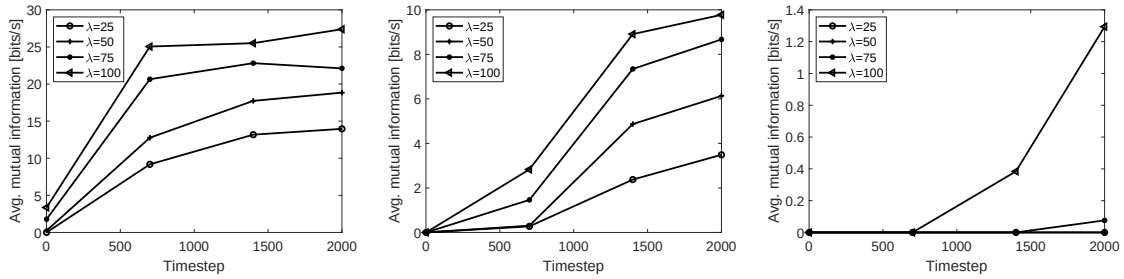

(a) All presynaptic neurons. (b) Correlated presynaptic neurons. (c) Uncorrelated presynaptic neurons.

Figure 7.8: Effect of weight changes due to STDP on correlated and uncorrelated presynaptic neurons when $M_c = 15$ and $\lambda_c = 100$ Hz.

in the mutual information is most when all of the presynaptic neurons are active as it improves the probability of generating enough EPSP for spike firing.

7.5 Applications of Bio-inspired Neural Networks

As discussed earlier, synaptic plasticity in natural neural networks (NNs) is the key reason behind the growth of human memory and intellect. The true potential of bio-inspired NNs, which are composed of bio-compatible nanomachines acting same as real neurons, is too extensive to be summarized in a short passage, however, in this section we note some of their interesting applications. Before we proceed to identify these applications, it is imperative that we address the distinction between artificial neural networks (ANNs), a concept used in the field of Artificial intelligence, and the bio-inspired NNs. This is important since ANNs are very hot topic currently and it is sometimes not easy to identify the differences between both the networks.

7.5.1 Bio-inspired NN vs ANN

We present some key differences between the both in the text below, and discuss key advantages bio-inspired NNs hold over ANNs.

- **Learning:** A key difference between both the types of networks lies in the methods of their learning. While ANNs operate on algorithms such as gradient descent [Bottou, 2010] on a global scale, bio-inspired NNs operate on

a local decentralized scales with methods such as Hebbian learning [Kempter et al., 1999]. The exact mechanisms of bio-inspired NN operation are still not understood completely, however, many local methods operate simultaneously, and thus provide them with more flexibility in terms of learning for various problems at the same time. Although many of the differences between brains and processing machines pointed out by *John von Neumann* in [Von Neumann, 2012] have been integrated into modern ANN-based systems, the architectures and connections schemes of the nervous system are still too complex to be implemented via computing machines.

- **Network structure:** The structures for ANNs are fixed and usually defined before a problem is solved through them. Bio-inspired NNs, on the other hand, can change their network structures based on plasticity between their nodes. This is especially true for long term memories that may end up removing or adding new connections to the system. Thus, in terms of network structures, bio-inspired NNs are more versatile since they are even able to change their structures over the course of time.

- **Data processing rate:** At first glance it may seem that ANNs can process data at a rate much larger than bio-inspired NNs. For instance, in our prior work [Abbasi et al., 2018], we found that a maximum data rate of 66 bps could be achieved during data transmission over a simple nervous system. However, as we noted in that study, if the simple nervous system of an earthworm is scaled up to the level of a human brain even by a simple multiplicative method, the amount of data processing increases a billion fold. Most ANNs are not capable of operation on these scales.

- **Information processing scale:** The amount of information processing and transfer in any process depends on both the process itself and the limit of observation in sampling it. Thus, in an ANN, the connection or synapse between two neurons is the limit that identifies the information processing ability. On

the other hand, in bio-inspired NNs we know that synaptic information exchange occurs as a result of neurotransmitter propagation through the synaptic cleft. This process itself is governed by a number of ion exchanges between cells. Therefore, purely from a synaptic point of view, the scales of information processing and exchange for bio-inspired NN are very large as compared to any existing ANN.

- **Power consumption:** The biggest advantage bio-inspired NNs have over ANNs, or rather any biological network has over its artificial counterpart, is their use of very low power. bio-inspired NNs are mostly based on molecular communication, which is inherently very low-powered [Akyildiz et al., 2008, Akan et al., 2016b]. This point is especially amplified when we look at the power consumption of larger neural network operating on the order of complexity of the human brain where billions of neurons are synapsing with each other.

7.5.2 Applications

Now that we have identified some key advantages bio-inspired NNs provide over ANNs, we discuss some of the key applications they have in various fields.

Pattern Recognition

The ability to recognize patterns has allowed life forms to sustain over billions of years. We observe a large set of patterns during our daily lives from various stimuli around us by means of sensors such as the eyes, ear and noses. These stimuli are then translated by a vast network of neurons employing plasticity into our memories, and thus assist us in making decisions. Specific portions of bio-inspired NNs have learned over billions of years of evolution and are highly optimized in performing recognition tasks. From just a training perspective, any neural network, artificial or biological, that has had longer training, can perform better at recognition tasks.

Thus, existing pattern recognition systems cannot compare to bio-inspired NNs in terms of their abilities of generalization in specific tasks.

For instance, emotion recognition is an important aspect of man-machine interface research. To date, no generalized method exists that can operate over multiple databases and provide good accuracy over all of them. On the other hand, Amygdala is a small portion of the human brain that is related to our emotional intelligence. Using this portion, the annotations provided by the human annotators working on the aforementioned databases have provided us with the gold standard that no machine is able to match. The case with face identification, voice identification and signal classification is also similar. Thus, it makes a lot of sense to think towards the use of bio-inspired NNs in pattern recognition tasks.

Nanonetworks

Most future communication networks aim to process large amount of data while maintaining operations on very low power. This is especially true for application such as nanosensor networks which have to sustain themselves over long periods of times without power sources. Many Internet of things (IoT) applications have similar goals as well. Bio-inspired NNs offer these capabilities along with naturally built systems that are able to maintain their energy needs for extended periods, and thus offer a viable solution for energy efficient nanonetworks.

Biomedical Applications

Understanding natural NNs and implementing bio-inspired NNs finds its major applications in life science as it provides the way for novel and more effective ICT-based diagnosis and treatment techniques for nervous system diseases. This promising approach covers a wide range of research avenues ranging from revealing the correlation between diseases and underlying communication mechanisms to ICT-based abstraction of diagnosis and treatment techniques for improved efficiency [Akan et al., 2016b]. Bio-inspired NNs can also be used for re-establishing the brain body connection in spinal cord injury patients [Capogrosso et al., 2016, Wenger et al., 2014].

Moreover, formation of Intenet of bio-nano things (IoBNT) by connecting biological entities and nano-devices to the Internet would play a vital role in healthcare [Akyildiz et al., 2015]. One such application is remote monitoring of patients' health through IoBNT, which can be achieved by connecting bio-sensors and actuators operating inside or near human body to Internet [Seyedi et al., 2013]. IoBNT can also be used to administer drugs to patients requiring frequent or periodic dosages [Seyedi et al., 2013]. A very big challenge in IoBNT is the ability of macro-scale devices to interface with micro- and nano-scale biological things. Since the nervous systems is already biological in nature, its interfacing with other such networks is completely bio-compatible. Moreover, the network is already used extensively in the human body to transmit and receive information from other systems in the body (sensory and motor pathways). This direction of research has the potential to open a large number of avenues for the expansion of the IoBNT paradigm and make the realization a reality. For instance, application of IoBNT systems may be realized in the insulin-glucose system for smart drug delivery using bio-inspired NNs interfaces [Abbasi and Akan, 2017].

7.6 Conclusion

In this chapter, we studied the impact of STDP on the performance of multiple access neuro-spike communication channel for correlated as well as uncorrelated input spike trains. STDP depends on timing of input and output spike trains and the correlated activity of presynaptic neurons affects the output spike generation probability. Thus, we analyzed the role of correlation among input spike trains on the strengthening of synaptic weights induced by STDP and ICT-based performance of the network. We observed that the existence of correlated presynaptic neurons in the network improves the synaptic weights of the uncorrelated presynaptic neurons as well. Moreover, we analyzed the evolution of synaptic weights over time and its impact on mutual information. We observed that average mutual information improves with time as the number of correlated inputs or the correlation factor increases, however, these changes are finally saturated when there are sufficient

spikes at the input to guarantee the generation of spike at the output. Our analysis signifies the importance of a comprehensive model for neuro-spike communication channel consisting of long-term plasticity to fully evaluate the performance of the nanonetwork using neuro-spike communication paradigm. Note that studying the combined effect of short term and long term plasticity stays as an open direction.

This study gives insights to realize appropriate structure of a bio-inspired NN by adjusting its synaptic weights for a particular biomedical application through selection of suitable control parameters such as input spike rate, number of correlated inputs and degree of correlation among them. Moreover, in applications where bio-inspired NNs need to interface with real neurons, the synaptic weights of real neurons can be manipulated by adjusting control parameters through bio-inspired NNs acting as input neurons.

Chapter 8

COMMUNICATION THEORETICAL MODELING AND ANALYSIS OF TRIPARTITE SYNAPSES WITH ASTROCYTES IN SYNAPTIC MOLECULAR COMMUNICATION

8.1 Introduction

To realize a fully functional nanonetwork inspired by neuronal communication, we need to study every phenomenon affecting information transmission through neuronal network. One of such important phenomena is synaptic plasticity, which is the ability of neurons to modify the strength of their synapses depending on various factors. This property of a neuron controls the information flow through the network, either facilitating or inhibiting the information flow [Citri and Malenka, 2008]. The information transmission reduces when there is synaptic depression (weakening of synapse) and increases in presence of synaptic potentiation (strengthening of synapse), as neurons that strongly wired together are capable of passing more information with less chances of error. Moreover, abnormalities in plasticity leads to several neuropshychiatric disorders [Bliss et al., 2014]. Thus, modeling plasticity in healthy as well as diseased neuronal network is fundamental for the development of novel diagnostic and treatment techniques. Plasticity is divided into two categories, (i) short-term plasticity, which lasts on the order of milliseconds to several minutes [Crabtree and Gogos, 2014], and (ii) long-term plasticity, which refers to changes that can last from hours to the lifetime of the synapse and is thought to play a central role in the mechanisms involved in memory and learning [Citri and Malenka, 2008].

The causes of plasticity range from different pre-synaptic to postsynaptic mech-

anisms, thus, its difficult to include all types of plasticity in a single model. In [Ramezani and Akan, 2017e], capacity of a vesicle release process has been evaluated under the influence of short-term synaptic depression caused by slower replenishment of readily releasable vesicles. In [Ramezani et al., 2018a], complete SISO channel is analyzed under the influence of short-term synaptic depression and capacity of the channel with memory is evaluated. In chapter 6 of this thesis [Khan and Akan, 2019], short-term synaptic plasticity due to post-synaptic factor, i.e., dynamic nature of spiking threshold, is considered and the capacity of the MISO channel with different types of neurons is analyzed. In the previous chapter [Khan et al., 2019], MISO neural channel is analyzed with spike timing dependent plasticity (STDP). All of these studies considered bipartite synapses, i.e., a synapse consisting of only pre- and postsynaptic neurons largely ignoring the presence of glial cells that greatly out number the neurons. Astrocytes are the most abundant of glial cells that are historically known as support cells [Kandel et al., 2000] and form tripartite synapses as shown in Fig. 8.1. However, this classical view has been changed due to two observations. First, astrocytes respond to the neurotransmitters released from presynaptic neuron by elevating the intracellular calcium levels in astrocytes. Second, in response to calcium elevations, astrocytes release gliotransmitters that include glutamate which may bind to receptors on neuron [Santello and Volterra, 2009]. This two way astro-neuro communication indicates the active role of astrocytes in neural signaling, specifically synaptic plasticity [Perea et al., 2009].

The glutamate released from the neuron binds with metabotropic glutamate receptors (mGluR) present on astrocyte. This leads to production of inositol triphosphate (IP3), a second messenger in astrocyte. The IP3 binds with IP3 receptors present on Endoplasmic Reticulum (ER) which releases calcium inside astrocyte. Elevation in intracellular calcium of astrocytes causes glutamate release which bind to presynaptic mGluRs that leads to potentiation of synaptic transmission [Nadkarni and Jung, 2007] that lasts for minutes, most likely through release of calcium from presynaptic stores. The prolonged increase in intracellular calcium concentration of neuron facilitates the spontaneous vesicle release process by increasing the release

probability, giving rise to synaptic facilitation or potentiation. Though considering bipartite synapse while modeling neuro-spike communication greatly simplifies the calculations, however, ignoring astrocytes' contribution in neural signaling drags away from realistic scenario as well as underestimates the effect of plasticity on information transmission.

There is an existing literature that considered astrocytes' contribution while modeling neuro-spike communication. In [Mesiti et al., 2015b, Mesiti et al., 2015a], channel models for neuronal communication including astrocytes are proposed. A tripartite synapse is analyzed in [Lotter et al., 2020], where astrocytes are considered as an insulator protecting the synapse from synaptic crosstalk and clearing the residual neurotransmitters from the synapse. In [Veletić et al., 2016b], tripartite synapse is analyzed from communication theoretical perspective. However, in these studies, plasticity caused by astrocytes and its effect on transmission rate has not been analyzed.In [Veletić et al., 2016b], tripartite synapse is analyzed from communication theoretical perspective.

In this chapter, for the first time, we analyze the effect of long-term synaptic plasticity caused by astrocytes' feedback on vesicle release process in a tripartite synapse. Since vesicle release process is also affected by short-term depression (STD) caused by depletion of vesicles with every single release, it is unavoidable to include the impact of this type of STD while analyzing vesicle release process. Thus, in this chapter, we consider the combined effect of short and long-term synaptic plasticity on information transmission through vesicle release. The focus of this research is on hippocampal pyramidal neurons due to the availability of vast number of studies. In [Ramezani and Akan, 2017e], a pool-based model for vesicle release and replenishment process is used that quantifies the effect of short-term synaptic depression due to slow replenishment of released neurotransmitters. In this chapter, we use the same model and integrate the model of long-term plasticity caused by astrocytic feedback on vesicle release process by changing calcium concentration in pre-synaptic terminal. Moreover, we evaluate the probability of vesicle release and mutual information between input spike and vesicle release, to compare the effect of

both types of plasticities on these quantities. We also manipulate different synaptic parameters such as input spike rate, maximum number of releasable vesicles and replenishment rate of these vesicles to see their effect on the information transmission rate of the vesicle release process in the presence and absence of synaptic plasticity.

The rest of the chapter is organized as follows. In Section 8.2, we formulate our model that includes long and short term plasticity simultaneously. In Section 8.3, we formulate mutual information of the vesicle release process. In Section 8.4, we describe the simulation set up and present the numerical result of our formulated system. Finally, in Section 8.5, we conclude this chapter.

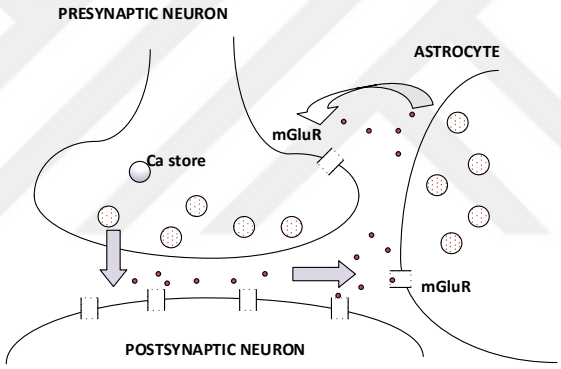

Figure 8.1: Tripartite Synapse

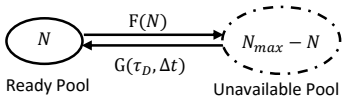

Figure 8.2: Pool-based model for neurotransmitter release and replenishment.

8.2 Model Description

8.2.1 Pre-synaptic Vesicle Release

In synaptic transmission, the arrival of spike to the axonal terminal can be modeled by a non-homogeneous Poisson process with rate $\lambda(t)$ [Malak and Akan, 2013a].

After firing a spike, due to inactivation of sodium channels, a neuron cannot generate another spike for a short time, no matter how strong stimulus is given. This time duration that initiates with action potential (AP) and lasts until its peak is called absolute refractory period [Kobayashi et al., 2009, Kandel et al., 2000]. Hence, we can divide time into n windows of equal duration Δt, where Δt is smaller than the absolute refractory period so that each window may contain only one spike at most.Thus, the probability of spike arrival at nth time slot can be calculated as [Malak and Akan, 2013a]

$$P\{S[n] = 1\} = 1 - \exp\left(-\lambda(t)\Delta t\right). \tag{8.1}$$

The above equation can be approximated as $P\{S[n] = 1\} = \lambda(t)\Delta t$ for small values of the product $\lambda(t)\Delta t$. However, in our simulations, we are using more general form given in (8.1).

8.2.2 Pre-synaptic Vesicle Release

Most of the neuron to neuron transmission occurs through chemical synapses using neurotransmitters present in the form of small packets, i.e., vesicles, in pre-synaptic terminal. We consider these vesicles to be divided into two distinct pools [Matveev and Wang, 2000]. One is the ready pool (RP) with vesicles near release site called readily releasable vesicles (RRVs), and the other one is called unavailable pool which is larger having the vesicles farther from the release site. This pool-based vesicle release and replenishment model is shown in Fig. 8.2 [Ramezani and Akan, 2017e] where the capacity of RP, i.e., the maximum number of RRVs when no vesicle is released, is denoted by N_{max}. The time for replenishment of one vesicle vacancy is τ_D and $G(\tau_D, \Delta t)$ is the probability of refilling one vesicle after Δt seconds.

The number of vesicles that are available to refill RP exceeds N_{max} by a large number [Matveev and Wang, 2000], thus, the replenishment of one released vesicle can be modeled by the first event of a Poisson process [De La Rocha and Parga,

2005]. Therefore, the probability of one vacancy replenishment is derived as

$$G(\tau_D, \Delta t) = 1 - \exp\big(-\tau_D^{-1}\ \Delta t\big), \tag{8.2}$$

and the number of recovered vesicles after Δt seconds is derived based on Binomial distribution given by $B(N_{\max} - N, G(\tau_D, \Delta t))$ [Ramezani et al., 2018a].

Vesicles can be released spontaneously or upon arrival of a spike. Hence, we consider both of these scenarios while deriving the vesicle release probability.

Evoked Vesicle Release

The arrival of AP to the pre-synaptic terminal initiates the influx of calcium ions by opening the voltage dependent calcium channels (VDCCs). These calcium ions diffuse into the pre-synaptic terminal where they bind to calcium buffers or sensors. When enough calcium ions are attached to the sensor, which is in the vicinity of the available vesicles for release, the fusion of vesicles with the membrane is initiated. This causes vesicle release to the synaptic cleft [Bear et al., 2007]. We use Bertram model [Bertram et al., 1996, Veletić et al., 2016b] to quantify vesicle release probability upon arrival of AP. In this model, it is assumed that there are four binding sites for calcium, namely, $(j = 1, 2, 3, 4)$, with different opening and closing rates. Thus, the probability that the release site is activated, $P_v(t)$, is given as [Bertram et al., 1996],

$$P_v(t) = O_1(t)O_2(t)O_3(t)O_4(t) \tag{8.3}$$

where O_j is an opening probability associated with site j and

$$\frac{dO_j(t)}{dt} = k_j^+ Ca_{pre}(t) - \frac{O_j(t)}{\tau_j}, \quad j = 1, 2, 3, 4$$

where $Ca_{pre}(t)$ is a pre-synaptic calcium concentration that is affected by the astrocytic feedback, $k_1^+ = 3.75 \times 10^{-3}$, $k_2^+ = 2.5 \times 10^{-3}$, $k_3^+ = 5 \times 10^{-4}$, $k_4^+ = 7.5 \times 10^{-3}$,

$k_1^- = 4 \times 10^{-4}$, $k_2^- = 1 \times 10^{-3}$, $k_3^- = 0.1$, $k_4^- = 10$ and $\tau_j = \frac{1}{(k_j^+ Ca_{pre}(t) + k_j^-)}$ [Veletić et al., 2016b].

The vesicle release is also governed by Poisson process with rate $\lambda_v(t)$, thus, by using splitting property of non-homogeneous Poisson processes [Chahibi and Akyildiz, 2014] we have,

$$\lambda_v(t) = P_v(t)\lambda(t)$$

Fusion rate for each vesicle during Δt is

$$\alpha_v(\Delta t) = \int_{t_0}^{t_0+\Delta t} \lambda_v(t)dt = \int_{t_0}^{t_0+\Delta t} P_v(t)\lambda(t)dt$$

The probability of univesicular release in hippocampal neurons, when RP contains N vesicles is given as [Matveev and Wang, 2000],

$$P\{\, V[n]{=}1 | S[n]{=}1\} = \begin{cases} 1 - \exp(-N\alpha_v(\Delta t)), & \Delta t \leq \Delta t_s \\ 1 - \exp(-N\alpha_v(\Delta t_s)), & \Delta t > \Delta t_s \end{cases} \tag{8.4}$$

where Δt_s is the spike duration.

Spontaneous Vesicle Release

The spontaneous release event is generated by Poisson process with rate $\lambda_0(t)$ [Nadkarni and Jung, 2007]. The spontaneous release probability from a synapse with N vesicles during Δt seconds is

$$P\{\, V[n]{=}1 | S[n]{=}0\} = 1 - exp(-N\lambda_0(t)\Delta t) \tag{8.5}$$

where

$$\lambda_0(t) = a_3\Big(1 + exp\big(\frac{a_1 - Ca_{pre}(t)}{a_2}\big)\Big)^{-1}$$

and a_1, a_2 and a_3 are coefficients that depend on number of active zones [Nadkarni and Jung, 2007]. In this chapter, we are considering only one active zone and the corresponding values of these coefficients are given in Table 8.1.

8.2.3 Astrocytic Calcium Response due to presynaptic vesicle release

Neurotransmitters released from pre-synaptic neuron, in addition to binding with the postsynaptic neuron, also bind with metabotropic glutamate receptors (mGluRs) present on astrocytes. This binding leads to a production of inositol triphosphate (IP3), a second messenger, which causes release of calcium from internal stores in astrocyte. The IP3 concentration p degrades with time and is given by the following equation [Nadkarni and Jung, 2007],

$$\begin{aligned}\frac{dp}{dt} &= -\frac{1}{\tau}(p - p_0) + v_p\frac{(Ca_{Astro}(t) + 0.2k_p)}{k_p + Ca_{Astro}(t)} + \\ v&\frac{g^n}{{k_g}^n + g^n}(\Theta(t - t_i) - \Theta(t - t_i - 2ms))\end{aligned} \tag{8.6}$$

where $Ca_{Astro}(t)$ is the concentration of calcium in astrocyte, $-1/\tau_p$ is a degradation rate of p, p_0 is the basal level of p, g denotes the glutamate concentration coming in contact with astrocyte. It is fixed as 200 μM for 2 ms. Other parameters are defined in [Nadkarni and Jung, 2007] in detail.

A simple stochastic model for calcium concentration in astrocyte is given by modifying Li-Rinzel model [Shuai and Jung, 2002],

$$\begin{aligned}\frac{dCa_{Astro}(t)}{dt} &= -J_c(q) - J_s - J_l \\ \frac{dq}{dt} &= \alpha_q(1 - q) - \beta_q q + \zeta(t)\end{aligned} \tag{8.7}$$

where $J_c(q), J_s$ and J_l are three major fluxes that change calcium concentration in astrocytes. When cytosolic calcium rises too high, calcium induced inhibition to the rising calcium flux is represented by q, where α_q and β_q are the activation and inactivation rates, respectively, that control the inhibition. The definitions of the variables in (8.7) their respective equations are detailed in [Nadkarni and Jung, 2007].

Gliotransmitters that include glutamate molecules are released from the astrocytes when its cytosolic calcium concentration exceeds a threshold of approximately 200 nM.

8.2.4 Feedback from Astrocyte to Neuron

Glutamate released by astrocyte bound to glutamate receptors present on the pre-synaptic terminal. This binding increases intracellular calcium in pre-synaptic neuron through release of calcium from internal stores. The rise of calcium supports spontaneous vesicle release leading to potentiation of synaptic transmission that can last for minutes [Fiacco and McCarthy, 2004, Perea and Araque, 2007]. However, it is a slow process that lasts from seconds to minutes or maybe even longer. On the other hand, calcium entering the pre-synaptic terminal through voltage-gated calcium channels opened during an action potential changes calcium concentration such that it decays within about 100 ms after action potential, by diffusion and buffer kinetics. To differentiate between these two types of calcium inflows, we divide the total pre-synaptic calcium concentration Ca_{pre} into the calcium concentration due to AP, i.e., $Ca_{pre,AP}$, entering through voltage gated calcium channels and the calcium concentration released from the stores, i.e., $Ca_{pre,st}$ and decaying on a time scale of about a minute, i.e.,

$$Ca_{pre}(t) = Ca_{pre,AP}(t) + Ca_{pre,st}(t), \tag{8.8}$$

$$\frac{dCa_{pre,st}(t)}{dt} = -\gamma Ca_{pre,st}(t) + \quad \alpha Ca_{Astro}(t)\Theta(Ca_{Astro}(t) - Ca_{thresh}), \tag{8.9}$$

Table 8.1: Simulation Parameters for Tripartite Synapse

Parameters	**Symbols**	**Values**
Refractory period	τ_{ref}	2 ms [Kobayashi et al., 2009]
Time-step duration	Δt	0.02 ms
Vesicle replenishment time	τ_D	$\frac{600}{N_{max}}$ ms [Ramezani and Akan, 2017e]
Spontaneous release parameters	a_1, a_2, a_3	$7181\mu M$, $606\mu M$, $100ms^{-1}$ [Nadkarni and Jung, 2007]
Ca_{pre} *due to AP*	$Ca_{pre,AP}$	$300\mu M$ [Nadkarni and Jung, 2007]
Threshold of Ca_{Astro}	Ca_{thresh}	$196.4nM$ [Nadkarni and Jung, 2007]
Rate constant	γ	$0.02\times10^{-3}ms^{-1}$ [Nadkarni and Jung, 2007]
Feedback strength for one Active Zone	α	$0.101ms^{-1}$ [Nadkarni and Jung, 2007]

where γ is the rate constant representing the time-scale of astrocytic potentiation. The second term in Eq. (8.9) with $Theta$ function represents linear increase in pre-synaptic calcium as soon as astrocytic calcium exceeds its threshold value, i.e., Ca_{thresh}. α is the feedback strength in calculated in presence of one active zone [Nadkarni and Jung, 2007].

8.3 Information Transmission Rate

For analyzing the achievable rate of information transmission over our model, we use basic definitions from information theory. The input and output of our model are the spike train, $S[n]$ and the generated vesicle release at output, $V[n]$, respectively. Thus, the mutual information of the vesicle release process is derived as

$$I(S[n];V[n]) = H(V[n]) - H(V[n]|S[n]), \tag{8.10}$$

where the entropies in (8.10) follow the following general formula,

$$H(\zeta[n]) = \sum_i P\{\zeta[n]=i\}.\log_2 P\{\zeta[n]=i\}$$

.

Since the probability of vesicle release is dependent on calcium concentration

in pre-synaptic terminal, which is changing over time due to astrocytic feedback as explained in Section 8.2, $P\{V[n]|S[n]\}$, thus, $H(V[n]|S[n])$, will change over time. Hence, the mutual information between input and output of the vesicle release process. i.e., $I(S[n];V[n])$, will also change over time. Consequently, deriving closed form equations for probabilities and mutual information is not feasible in this scenario. Thus, vesicle release in response to action potential, i.e., $P\{V[n]=1|S[n]=1\}$ as well as spontaneous vesicle release, i.e., $P\{V[n]=1|S[n]=0\}$, are calculated through Monte Carlo simulations by using (8.4) and (8.5), respectively. The probabilities in (8.4) and (8.5) depend on instantaneous pre-synaptic calcium concentration, i.e., $Ca_{pre}(t)$, which is given by (8.8). As explained in Section 8.2, $Ca_{pre}(t)$ is affected by feedback from astrocyte and this effect is evaluated by using (8.6) through (8.9).

Finally, we will use these simulation results to calculate average changes in the mutual information over time, between input and output of the process, i.e.,

$$I_{avg} = \sum_{l=1}^{n} \frac{I(S[l];V[l]}{n}, \tag{8.11}$$

In hippocampal neurons, once a vesicle is released, whether it be evoked or spontaneous, the vesicle release machinery renders inactive for almost 6.3 ms. This is referred to as very short-term plasticity in [Dobrunz et al., 1997]. Thus, this plasticity is also included in our simulation set-up.

8.4 Simulation results

In our simulation set-up, we are considering a vesicle release process in a hippocampal neuron. In this section, we are simulating vesicle release process to evaluate the combined effect of short and long-term plasticity on vesicle release probability, which ultimately affects the information transmission through the neuronal channel. We are considering a pool-based vesicle release model as described in section II. This pool-based model incorporates the rates of vesicle depletion and replenishment

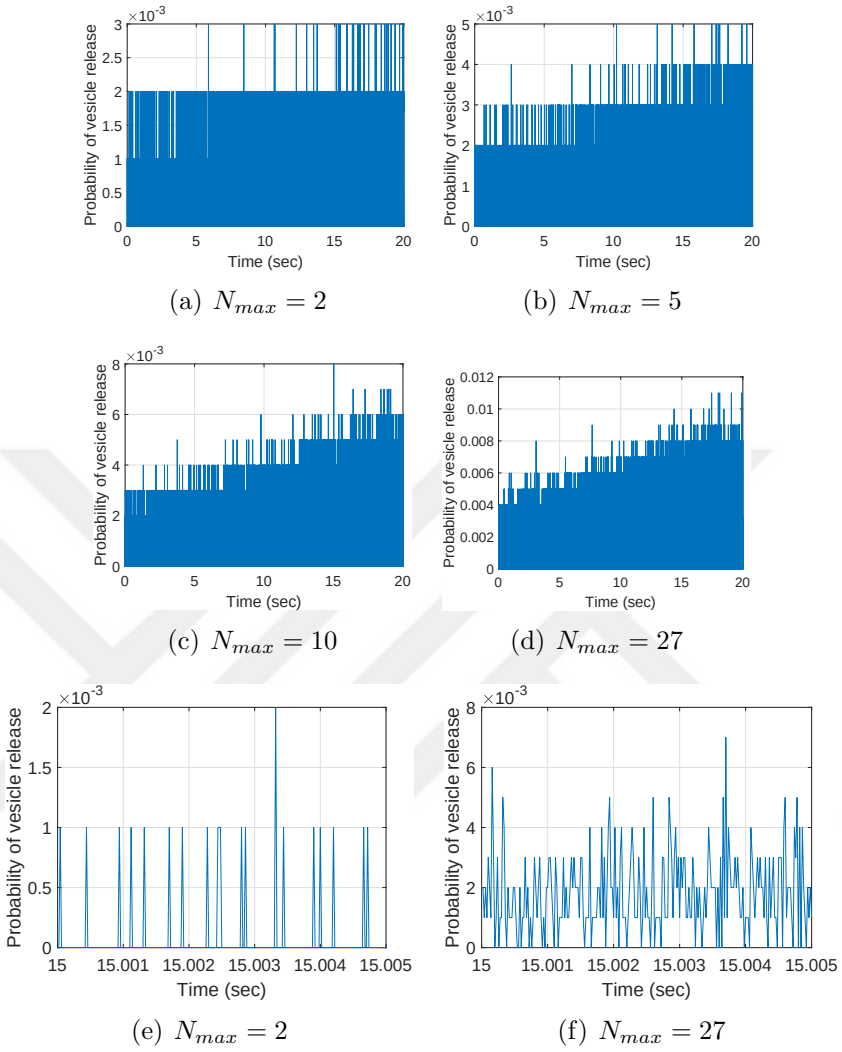

(a) $N_{max} = 2$ (b) $N_{max} = 5$

(c) $N_{max} = 10$ (d) $N_{max} = 27$

(e) $N_{max} = 2$ (f) $N_{max} = 27$

Figure 8.3: (a)-(d) Vesicle release probability for different values of N_{max} with LTP and STD, (e)-(f) Vesicle release probability for $N_{max} = 2$ and $N_{max} = 27$, respectively, for 5 ms window. ($\lambda = 500Hz$).

which happens with a certain delay i.e. the rates of depletion and replenishment are not same. This phenomenon varies vesicle release probability with time but on short time scale. Thus, this effect is considered to cause short-term depression in the signal transmission [De La Rocha and Parga, 2005].

Since vesicle release, both evoked and spontaneous, is dependent on calcium concentration in pre-synaptic terminal on molecular level as explained in section II, slight variation in calcium concentration greatly affect the probability of release.

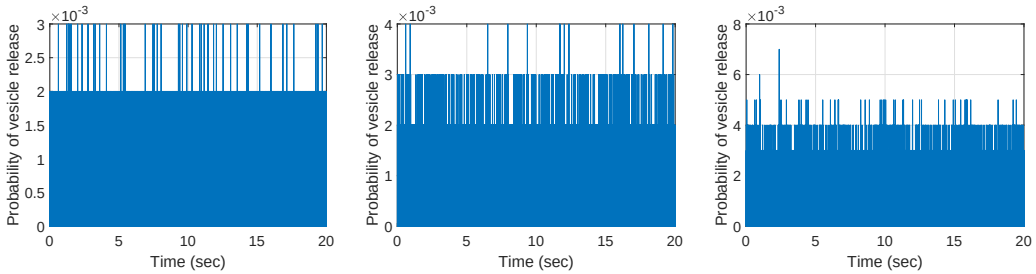

(a) $N_{max} = 5$ (b) $N_{max} = 10$ (c) $N_{max} = 27$

Figure 8.4: Vesicle release probability for different values of N_{max} without Astrocyte, i.e., with only STD ($\lambda = 500Hz$).

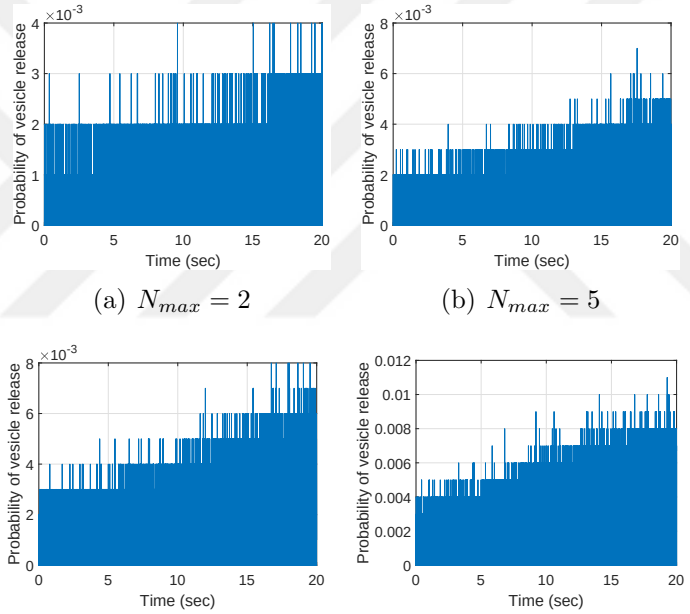

(a) $N_{max} = 2$ (b) $N_{max} = 5$

(c) $N_{max} = 10$ (d) $N_{max} = 27$

Figure 8.5: Release probability for different values of N_{max} with instantaneous vesicle replenishment, i.e., with only LTP ($\lambda = 500Hz$).

Thus,we use calcium based model for vesicle release probability for simulations.

To investigate the impact of plasticity on vesicle release probability, thus, on information flow through the neuron, we simulate the vesicle release process along with the feedback from astrocyte for tens of seconds since the effects of long term plasticity lasts for longer times. By discretizing time into n time slots, we did 1000 iterations for each time slot and calculated release probability and the average

mutual information between the input and output of the vesicle release process,i.e., input spike, $S[n]$, and vesicle release, $V[n]$, respectively. Since, we are dealing with the differential equations in our simulation, we need to keep the simulation time-step very small.

8.4.1 Variation in Vesicle Release Probability w.r.t N_{max}

In our model, for any value of N_{max}, there are two phenomena working at the same time to vary the information flow through the neuron. One is the depletion of vesicle after each vesicle release that causes short-term synaptic depression (STD) and the other one is increase in calcium concentration with time in pre-synaptic terminal due to astrocytic feedback causing long-term potentiation (LTP). Both types of plasticities are included in simulation set up to obtain Fig. 8.3. The values of N_{max} are selected corresponding to the range reported in biological studies of hippocampal neurons [Matveev and Wang, 2000]. We can see that for lower values of N_{max} probability build up is slower as compare to the higher values of N_{max} since number of available vesicle is higher at any time causing more chances of vesicle release. Thus, frequent release of vesicles will generate more positive feedback from asrtocytes in any given time. Ultimately, the probability achieves higher values for higher N_{max} for the same time window. In Fig. 8.3 (e) and (f), the change in probability for two extreme values of N_{max}, i.e., 2 and 27, are shown for 5 ms window after 15 seconds of simulation. It is clearly observed that for smaller value of N_{max}, probability is going to zero for longer intervals of time owing to the slower vesicle replenishment.

In Fig. 8.4, we simulate the system without astrocytic feedback, i.e., without LTP. It can be observed that in the absence of LTP, there is no probability build up due to STD for any value of N_{max}, however, the basal value of probability is higher for greater N_{max} as expected. In presence of STD, reduction in release probability with time is expected. However, our results are shown larger time-scale, thus, we cannot observe the short-term changes, happening over time-scale of milliseconds due to STD in these figures.

Next, for comparison purpose, we consider the instantaneous replenishment of vesicles after release, i.e., N_{max} vesicles would be available in each time slot, thus, there will be no STD. The system is simulated only with LTP. This should increase the vesicle release probability in each time slot, thus, probability build up is expected to increase with time. In Fig. 8.5, we can observe that probability build up is slower for very low values of N_{max} as compared to very high N_{max}. This is because for very large N_{max} with slow replenishment rates there will be enough number of vesicles to keep high probability build up even at the start of the process.

8.4.2 Variation in Vesicle Release Probability w.r.t λ

We also simulate our model for different input spike frequencies, λs, keeping N_{max} constant at 10 to observe its effect on build up of release probability. The changes in probability with λ are not significant as can be observed in Fig. 8.6. The trend of probability is same for all values of frequencies for a fixed N_{max}. This is due to fact that even if there are more spikes at the input at high input frequency λ, the release probability still depends on N_{max} which is reducing with each release and the replenishment is slower as compare to the release rate. Therefore, probability build up is not high for high frequency due to unavailability of the releasable vesicles. Moreover, we can observe in Fig. 8.3 that higher values of release probability were achieved for higher N_{max} at the same input spike rate. Thus, it can be concluded that the release probability saturates after certain spike rate depending on the value of N_{max} as a result of insufficient releasable vesicles to cater high frequency stimulus. Also, the saturation value would be higher for higher values of N_{max}.

8.4.3 Mutual Information

In this section, we calculate the average mutual information between input spike and vesicle release for different values of maximum available vesicles, N_{max} and input spike frequencies λ. In Fig. 8.7, we can observe that for each value of N_{max}, the average information transmission rate is increasing with time. In our model we aim to observe the impact of short as well as long term plasticity on the vesicle

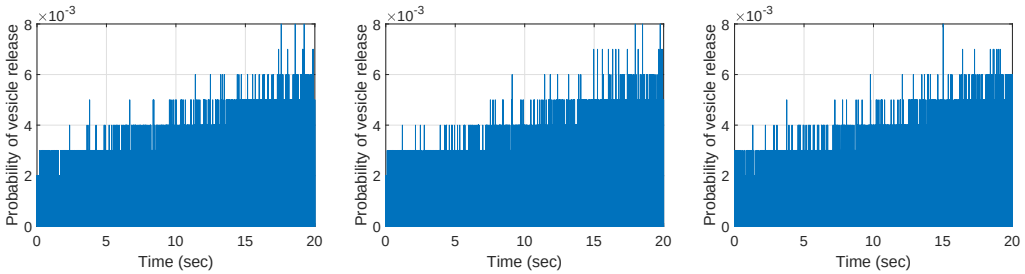

(a) $\lambda = 20Hz$ (b) $\lambda = 200Hz$ (c) $\lambda = 500Hz$

Figure 8.6: Release probability for different values of λ with LTP and STD ($N_{max} = 10$).

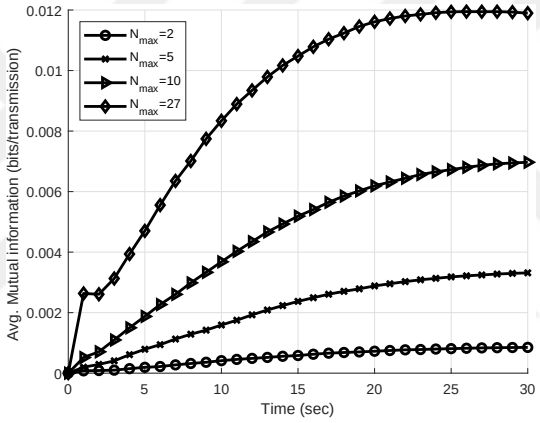

Figure 8.7: Mutual Information for different values of N_{max} with LTP and STD ($\lambda = 500Hz$).

release process. According to [Ramezani and Akan, 2017e], the short term depression occurs due to pool-based model of vesicle release where the replenishment rate of vesicles has been observed to be slower than the release rate. Moreover, the long-term effect is caused by increase in calcium concentration in neuron contributed by astrocytes over a long period of time. To make it more obvious, we simulated the system without astrocytic feedback and we observe in Fig. 8.8 that the average rate is almost constant over time achieving very low values. Thus, as we can see in Fig. 8.7, the strengthening of the synapse over the time period of 30 seconds is due to the effect of long term plasticity contributed by astrocytes. Moreover, average mutual information is increasing faster for higher values of N_{max} as the probability of release is higher for high number of available vesicles at a time.

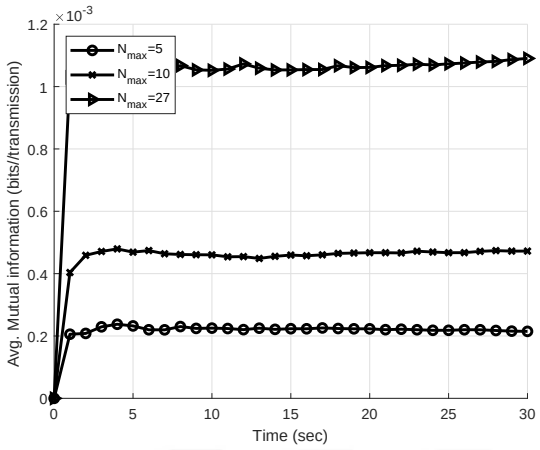

Figure 8.8: Mutual Information for different values of N_{max} without Astrocyte, i.e., with only STD ($\lambda = 500Hz$).

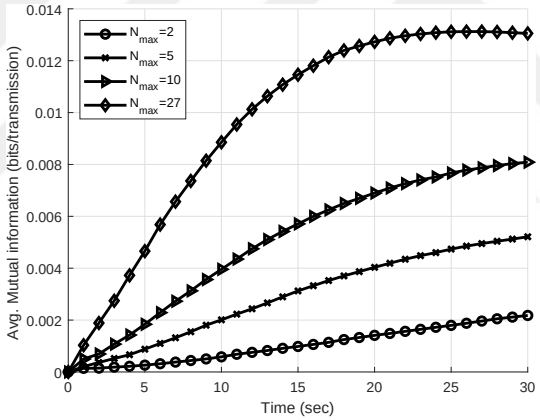

Figure 8.9: Mutual Information for different values of N_{max} with instantaneous replenishment of vesicles, i.e., with only LTP ($\lambda = 500Hz$).

In Fig. 8.9, the system is simulated with vesicle replenishment occurring instantaneously, thus, ignoring the effect of short-term depression on mutual information. Therefore, by comparing Fig. 8.7 and Fig. 8.9, we can observe that in absence of depression, the average mutual information has higher steady state values for each N_{max}.

In Fig. 8.10, the effect of varying input spiking rate is shown on the average mutual information for a fixed value of $N_{max} = 10$. Since at higher input spiking frequency, the chances of evoked vesicle release are higher, thus, we can see an increase in average mutual information. With time, more number of vesicle releases

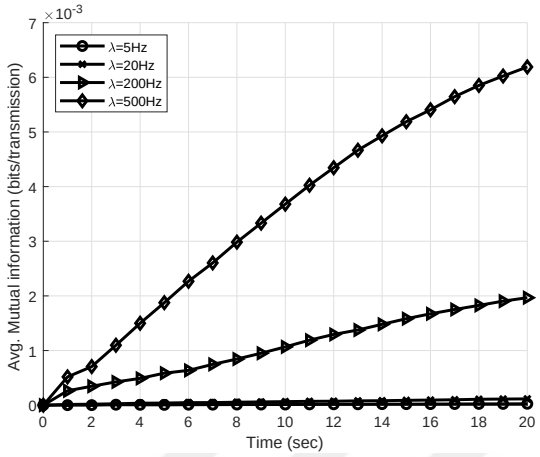

Figure 8.10: Mutual Information for different spiking frequencies (λ) and $N_{max} = 10$ with LTP and STD.

would generate more positive feedback from the astrocytes resulting in high calcium concentration in pre-synaptic terminal further increasing the probability of spontaneous vesicle release, thus, increasing the average mutual information. However, it is also obvious that the build up of average rate with the increase in input spike frequency is comparatively far less than what is caused by increasing the maximum number of available vesicles N_{max} as shown in Fig. 8.7.

8.5 Conclusion

Synaptic plasticity is the ubiquitous phenomenon in central nervous system that is responsible for learning and memory. Thus, it is inevitable to include plasticity while modeling the neuro-spike communication to completely understand the brain functions as well as to develop novel diagnostic and treatment techniques for nervous system diseases. Studies have shown that astrocytes play a vital role in the regulation of synaptic plasticity, thus, it is crucial to evaluate the effects of plasticity on neural signaling in the presence of feedback from astrocyte. Therefore, in this chapter, we focused on the vesicle release process in a tripartite synapse to evaluate the impact of LTP caused by astrocyte on information flow. Since vesicle release process inherently possesses STD due to the depletion of vesicles with every

single release, we studied the combined effect of STD and LTP on vesicle release process for the first time in literature from the perspective of communication theory. Moreover, we evaluated the changes in release probability and average mutual information between input spikes and vesicle release with time, for different synaptic parameters such as number of available RRVs, input spike rate and replenishment rate of vesicles. We have the following observations:

- In absence of astrocyte (i.e., in bipartite synapse), transmission rate is far less than what is achieved with the tripartite synapse, thus, information rates are underestimated when we ignore the presence of astrocytes in the network.

- Although LTP's effect is more prominent on release probability than STD over longer time-scales, the removal of STD from the model, i.e., having instantaneous replenishment causes increase in overall value of average mutual information over time. This effect is more pronounced for higher values of N_{max}. Thus, studying combined effect of different types of plasticity is crucial.

- Release probability was expected to achieve higher values with time for higher input frequencies. However, we observe that the release probability saturates as the spiking frequency is increased for fixed value of N_{max}. This is due to the fact that RRVs are reducing with each release and the replenishment is slower as compare to the release rate. Thus, insufficient RRVs would not allow increase in release probability with the increase in input frequency.

Our analysis highlights the importance of a comprehensive and realistic model for neuro-spike communication channel consisting of a tripartite synapse analyzing combined effects of different types of synaptic plasticity to fully evaluate the performance of neuro-spike communication paradigm. However, studying complete neuro-spike communication channel with plasticities caused by various synaptic phenomena is still an open research question.

Chapter 9

CONCLUSION

The recent advancements in nanotechnology has enabled the development of nano-scale devices with unique and useful characteristics. These nanodevices are one of the frontiers of the scientific research in the current age, and have a huge set of applications in diverse domains. Some of these include nanoscale sensing, intelligent drug delivery, body area networks (BANs), Internet of Bio-nano Things (IoBNT) and other industrial and environmental monitoring applications. However, a nanodevice itself has operational limitations due its size, which can be overcome by operating in the form of a network. These nanonetworks call for novel communication paradigm due to their unconventional nature.

Neurons are biological nano-scale devices that use molecular communication to carry out the most complicated functions of the human body. Thus, studying nervous nanonetworks from communication theoretical perspective would lay the foundation of a novel bio-inspired communication paradigm for the nanonetworks. Hence, in this thesis, we analyzed the nervous nanonetworks from communication and informational theoretical perspective. We focused on realistically modeling and analyzing neuro-spike communication including the most important phenomenon called synaptic plasticity. In the following, we elaborate the detailed conclusion reached in each chapter.

9.1 Fundamentals of Molecular Information and Communication Science

In this chapter, we introduced an entirely novel perception of molecular communication paradigms to lay down the foundations of science of molecular information and communication. Human body is an epitome of molecular signaling that is be-

ing investigated to design and optimize nanonetworks. Therefore, we seized this opportunity to analyze recent literature on intra-body nanonetworks and molecular communication and present open issues that need to be addressed in order to define and extract the fundamentals of molecular information and communication science. Based on this investigation we proposed a framework to unveil fundamental limits of molecular information science by relating ICT-based characteristics of molecular communication channel to its physical and chemical properties. Finally, we highlighted the significance of molecular information and communication science in life sciences focusing on its applications in developing ICT-based diagnosis and treatment techniques for the diseases caused by malfunction of intra-body nanonetworks.

9.2 Diffusion-based Model for Synaptic Molecular Communication Channel

In this chapter, we investigated one of the most advanced mechanism of molecular communication that exists in nature. We focused on the point-to-point synaptic channel in hippocampal neuron and introduced a novel mathematical formulation of neurotransmitters' diffusion in synaptic cleft that encompasses the effects of geometrical structure of synapse and re-uptake phenomenon. As a result of this mathematical achievement we have developed a deterministic code, which calculates the expected behavior of synaptic molecular communication channel. The predictions of this code are successfully verified by a corresponding Monte Carlo simulation. This is one of the main contributions of this work, as the code developed takes much less time for the same task compared to the Monte Carlo approach.

Moreover, we observed the effects of variations in various synaptic parameters on number of maximum bound receptors and time to reach this maximum, which together determine EPSP profile. The results obtained in this analysis comply with the outcomes of existing physiological studies and simulations in literature. We also discussed the possible causes of trial-to-trial variability in peak amplitude of EPSP. Eventually, we performed communication theoretical analysis of our model by evaluating error probability in output detection.

9.3 Information Theoretical Analysis of SISO Synaptic Communication

In this chapter, we analyzed a realistic physical reference model as the most basic realization of nanonetworks that utilize neuro-spike communication paradigm from information theoretical perspective. We formulated the mutual information between input and output of a SISO synaptic communication for a single transmission. Since this system has memory, we found the average mutual information over multiple transmissions to evaluate its overall capacity. Moreover, we derived a closed-form expression for the capacity of synaptic transmission and calculated the capacity-achieving spiking probability. Finally, we found the effects of change in various synaptic parameters, such as spiking probability, number of readily releasable vesicles (RRVs) and number of neurotransmitters in a vesicle, on the information capacity of the system.

9.4 Sum Rate of MISO Neuro-spike Communication Channel with Constant Spiking Threshold

Certain limitations and constraints exist on the transmission capacity of a MISO neuro-spike communication system as a result of different stochastic processes involved in it and the available metabolic energy for neurons to carry out their routine processing. In this chapter, we derived the closed form equation for the mutual information between input and output of a MISO neuro-spike communication system. Moreover, we quantified the maximum rate of information transmission after taking into account the consumed metabolic energy in terms of ATP molecules. Furthermore, we have studied impacts of number of pre-synaptic terminals, biological parameters of the channel and available metabolic energy on the maximum achievable sum rate of the MISO neuro-spike communication. The results provided in this chapter gives insights on (i) selecting channel parameters while designing bio-inspired nanonetworks based on neuro-spike communication and (ii) the impact of diseases that change the neuro-spike communication channel characteristics on the

performance of nervous nanonetwork.

9.5 Sum Rate Analysis of Multiple-Access Neuro-Spike Communication Channel with Dynamic Spiking Threshold

Neurons use spikes to encode information form the outside world to be processed inside the brain. The cortical neurons receive inputs from the multiple pre-synaptic neurons and generate a spike when its membrane potential reaches a spiking threshold. The researchers succeeded in regenerating the spike trains considering the adaptive spiking threshold that depends on previous spike generation. Adaptive threshold is also an important factor in causing short-term plasticity in the brain, which is used to control the information flow between neurons. Thus, in this chapter, we analyzed information transmission in the multiple-access neuro-spike communication channel with dynamic spiking threshold model for spike generation. Furthermore, neuro-spike communication has a major constraint in terms of metabolic energy required by the brain cells to carry out their routine processing. Therefore, we quantified the maximum achievable sum rate taking into account the metabolic cost in terms of ATP molecules consumed. Moreover, we analyzed different types of cortical neurons, i.e., RS, IB and FS neurons and concluded that FS neurons are the most efficient in terms of energy consumption, however, IB neurons provide highest data transmission rates. This analysis would help us to select the neuron with suitable characteristics for a particular application of the nanonetworks.

9.6 Impact of Long Term Plasticity on Information Transmission over Neuronal Networks

In this chapter, we studied the impact of STDP on the performance of multiple access neuro-spike communication channel for correlated as well as uncorrelated input spike trains. STDP depends on timing of input and output spike trains and the correlated activity of presynaptic neurons affects the output spike generation probability. Thus, we analyzed the role of correlation among input spike trains on

the strengthening of synaptic weights induced by STDP and ICT-based performance of the network. We observed that the existence of correlated presynaptic neurons in the network improves the synaptic weights of the uncorrelated presynaptic neurons as well. Moreover, we analyzed the evolution of synaptic weights over time and its impact on mutual information. We observed that average mutual information improves with time as the number of correlated inputs or the correlation factor increases, however, these changes are finally saturated when there are sufficient spikes at the input to guarantee the generation of spike at the output. Our analysis signifies the importance of a comprehensive model for neuro-spike communication channel consisting of long-term plasticity to fully evaluate the performance of the nanonetwork using neuro-spike communication paradigm. Note that studying the combined effect of short term and long term plasticity stays as an open direction.

This study gives insights to realize appropriate structure of a bio-inspired NN by adjusting its synaptic weights for a particular biomedical application through selection of suitable control parameters such as input spike rate, number of correlated inputs and degree of correlation among them. Moreover, in applications where bio-inspired NNs need to interface with real neurons, the synaptic weights of real neurons can be manipulated by adjusting control parameters through bio-inspired NNs acting as input neurons.

9.7 Communication Theoretical Modeling and Analysis of Tripartite Synapses with Astrocytes in Synaptic Molecular Communication

Synaptic plasticity is the ubiquitous phenomenon in central nervous system that is responsible for learning and memory. Thus, it is inevitable to include plasticity while modeling the neuro-spike communication to completely understand the brain functions as well as to develop novel diagnostic and treatment techniques for nervous system diseases. Studies have shown that astrocytes play a vital role in the regulation of synaptic plasticity, thus, it is crucial to evaluate the effects of plasticity on neural signaling in the presence of feedback from astrocyte. Therefore, in this chapter, we focused on the vesicle release process in a tripartite synapse to

evaluate the impact of LTP caused by astrocyte on information flow. Since vesicle release process inherently possesses STD due to the depletion of vesicles with every single release, we studied the combined effect of STD and LTP on vesicle release process for the first time in literature from the perspective of communication theory. Moreover, we evaluated the changes in release probability and average mutual information between input spikes and vesicle release with time, for different synaptic parameters such as number of available RRVs, input spike rate and replenishment rate of vesicles. We have the following observations:

- In absence of astrocyte (i.e., in bipartite synapse), transmission rate is far less than what is achieved with the tripartite synapse, thus, information rates are underestimated when we ignore the presence of astrocytes in the network.

- Although LTP's effect is more prominent on release probability than STD over longer time-scales, the removal of STD from the model, i.e., having instantaneous replenishment causes increase in overall value of average mutual information over time. This effect is more pronounced for higher values of N_{max}. Thus, studying combined effect of different types of plasticity is crucial.

- Release probability was expected to achieve higher values with time for higher input frequencies. However, we observe that the release probability saturates as the spiking frequency is increased for fixed value of N_{max}. This is due to the fact that RRVs are reducing with each release and the replenishment is slower as compare to the release rate. Thus, insufficient RRVs would not allow increase in release probability with the increase in input frequency.

Our analysis highlights the importance of a comprehensive and realistic model for neuro-spike communication channel consisting of a tripartite synapse analyzing combined effects of different types of synaptic plasticity to fully evaluate the performance of neuro-spike communication paradigm. However, studying complete neuro-spike communication channel with plasticities caused by various synaptic phenomena is still an open research question.

BIBLIOGRAPHY

[Abbasi and Akan, 2015] Abbasi, N. A. and Akan, O. B. (2015). A queueing-theoretical delay analysis for intra-body nervous nanonetwork. *Nano Com. Net.*

[Abbasi and Akan, 2017] Abbasi, N. A. and Akan, O. B. (2017). An information theoretical analysis of human insulin-glucose system toward the internet of bio-nano things. *IEEE transactions on nanobioscience*, 16(8):783–791.

[Abbasi et al., 2018] Abbasi, N. A., Lafci, D., and Akan, O. B. (2018). Controlled information transfer through an in vivo nervous system. *Scientific reports*, 8(1):2298.

[Aghababaiyan et al., 2018a] Aghababaiyan, K., Shah-Mansouri, V., and Maham, B. (2018a). Asynchronous neuro-spike array-based communication. In *2018 IEEE International Black Sea Conference on Communications and Networking (BlackSeaCom)*, pages 1–5. IEEE.

[Aghababaiyan et al., 2018b] Aghababaiyan, K., Shah-Mansouri, V., and Maham, B. (2018b). Axonal channel capacity in neuro-spike communication. *IEEE transactions on nanobioscience*, 17(1):78–87.

[Aghababaiyan et al., 2018c] Aghababaiyan, K., Shah-Mansouri, V., and Maham, B. (2018c). Capacity bounds of neuro-spike communication by exploiting temporal modulations. In *Wireless Communications and Networking Conference (WCNC), 2018 IEEE*, pages 1–6. IEEE.

[Aghababaiyan et al., 2018d] Aghababaiyan, K., Shah-Mansouri, V., and Maham, B. (2018d). Joint optimization of input spike rate and receiver decision threshold to maximize achievable bit rate of neuro-spike communication channel. *IEEE transactions on nanobioscience*.

[Aghababaiyan et al., 2019] Aghababaiyan, K., Shah-Mansouri, V., and Maham, B. (2019). Capacity and error probability analysis of neuro-spike communication exploiting temporal modulation. *IEEE Transactions on Communications*, 68(4):2078–2089.

[Agmon and Edelstein, 1997] Agmon, N. and Edelstein, A. L. (1997). Collective binding properties of receptor arrays. *Biophys. J.*, 72(4):1582.

[Akan et al., 2016b] Akan, O. B., Ramezani, H., Khan, T., Abbasi, N. A., and Kuscu, M. (2016b). Fundamentals of molecular information and communication science. *Proceedings of the IEEE*.

[Akan et al., 2016a] Akan, O. B., Ramezani, H., Khan, T., Abbasi, N. A., and Kuscu, M. (to be published, 2016a). Fundamentals of molecular information and communication science. *Proc. of the IEEE*.

[Akyildiz et al., 2015] Akyildiz, I., Pierobon, M., Balasubramaniam, S., and Koucheryavy, Y. (2015). The internet of bio-nano things. *Com. Mag., IEEE*, 53(3):32–40.

[Akyildiz et al., 2008] Akyildiz, I. F., Brunetti, F., and Blázquez, C. (2008). Nanonetworks: A new communication paradigm. *Comp. Net.*, 52(12):2260–2279.

[Akyildiz and Jornet, 2010] Akyildiz, I. F. and Jornet, J. M. (2010). The internet of nano-things. *Wireless Comm., IEEE*, 17(6):58–63.

[Alabi and Tsien, 2012] Alabi, A. A. and Tsien, R. W. (2012). Synaptic vesicle pools and dynamics. *Cold Spring Harbor perspectives in biology*, 4(8).

[Atakan et al., 2012] Atakan, B., Akan, O. B., and Balasubramaniam, S. (2012). Body area nanonetworks with molecular communications in nanomedicine. *Comm. Mag., IEEE*, 50(1):28–34.

[Attwell and Laughlin, 2001] Attwell, D. and Laughlin, S. B. (2001). An energy budget for signaling in the grey matter of the brain. *Journal of Cerebral Blood Flow & Metabolism*, 21(10):1133–1145.

[Balasubramaniam et al., 2011] Balasubramaniam, S., Boyle, N. T., Della-Chiesa, A., Walsh, F., Mardinoglu, A., Botvich, D., and Prina-Mello, A. (2011). Development of artificial neuronal networks for molecular communication. *Nano Com. Net.*, 2(2):150–160.

[Balasubramaniam and Lio, 2013] Balasubramaniam, S. and Lio, P. (2013). Multi-hop conjugation based bacteria nanonetworks. *NanoBiosci., IEEE Tran.*, 12(1):47–59.

[Balasubramaniam et al., 2014] Balasubramaniam, S., Lyamin, N., Kleyko, D., Skurnik, M., Vinel, A., and Koucheryavy, Y. (2014). Exploiting bacterial properties for multi-hop nanonetworks. *Com. Mag., IEEE*, 52(7):184–191.

[Balevi and Akan, 2013] Balevi, E. and Akan, O. B. (2013). A physical channel model for nanoscale neuro-spike communications. *Com.s, IEEE*, 61(3):1178–1187.

[Bavamian et al., 2007] Bavamian, S., Klee, P., Britan, A., Populaire, C., Caille, D., Cancela, J., Charollais, A., and Meda, P. (2007). Islet-cell-to-cell communication as basis for normal insulin secretion. *Diabetes, Obesity and Metabolism*, 9(s2):118–132.

[Bear et al., 2007] Bear, M. F., Connors, B. W., and Paradiso, M. A. (2007). *Neuroscience: Exploring the Brain*. Lippincott Williams & Wilkins, 3 edition.

[Benninger et al., 2011] Benninger, R. K., Head, W. S., Zhang, M., Satin, L. S., and Piston, D. W. (2011). Gap junctions and other mechanisms of cell–cell communication regulate basal insulin secretion in the pancreatic islet. *The J. of physiology*, 589(22):5453–5466.

[Bertram et al., 1996] Bertram, R., Sherman, A., and Stanley, E. F. (1996). Single-domain/bound calcium hypothesis of transmitter release and facilitation. *Journal of Neurophysiology*, 75(5):1919–1931.

[Blalock, 1994] Blalock, J. E. (1994). The syntax of immune-neuroendocrine communication. *Immunology today*, 15(11):504–511.

[Bliss et al., 2014] Bliss, T., Collingridge, G., and Morris, R. (2014). Synaptic plasticity in health and disease: introduction and overview.

[Borst and Theunissen, 1999] Borst, A. and Theunissen, F. E. (1999). Information theory and neural coding. *Nature neuroscience*, 2(11):947–957.

[Bottou, 2010] Bottou, L. (2010). Large-scale machine learning with stochastic gradient descent. In *Proceedings of COMPSTAT'2010*, pages 177–186. Springer.

[Cacciapuoti and Caleffi, 2015] Cacciapuoti, A. and Caleffi, M. (2015). Receiver design for a bionic nervous system: Modeling the dendritic processing power. *Internet of Things J., IEEE*, PP(99):1–1.

[Capogrosso et al., 2016] Capogrosso, M., Milekovic, T., Borton, D., Wagner, F., Moraud, E. M., Mignardot, J.-B., Buse, N., Gandar, J., Barraud, Q., Xing, D., et al. (2016). A brain–spine interface alleviating gait deficits after spinal cord injury in primates. *Nature*, 539(7628):284.

[Chahibi et al., 2015] Chahibi, Y., Akyildiz, I., Balasubramaniam, S., and Koucheryavy, Y. (2015). Molecular communication modeling of antibody-mediated drug delivery systems. *Biomed. Eng., IEEE Tran.*, 62.

[Chahibi and Akyildiz, 2014] Chahibi, Y. and Akyildiz, I. F. (2014). Molecular communication noise and capacity analysis for particulate drug delivery systems. *Comm., IEEE Tran.*, 62(11):3891–3903.

[Chahibi et al., 2013] Chahibi, Y., Pierobon, M., Song, S. O., and Akyildiz, I. F. (2013). A molecular communication system model for particulate drug delivery systems. *Biomed. Eng., IEEE Tran.*, 60(12):3468–3483.

[Chude-Okonkwo et al., 2014] Chude-Okonkwo, U. et al. (2014). Diffusion-controlled enzyme-catalyzed molecular communication system for targeted drug delivery. In *Global Com. Conf. (GLOBECOM), IEEE*, pages 2826–2831. IEEE.

[Citri and Malenka, 2008] Citri, A. and Malenka, R. C. (2008). Synaptic plasticity: multiple forms, functions, and mechanisms. *Neuropsychopharmacology*, 33(1):18.

[Civas and Akan, 2020] Civas, M. and Akan, O. B. (2020). Rate of information flow across layered neuro-spike network in the spinal cord. *IEEE transactions on nanobioscience*, 19(3):368–377.

[Clements, 1996] Clements, J. (1996). Transmitter timecourse in the synaptic cleft: its role in central synaptic function. *Trends Neurosci.*, 19(5):163–171.

[Cobo and Akyildiz, 2010] Cobo, L. C. and Akyildiz, I. F. (2010). Bacteria-based communication in nanonetworks. *Nano Com. Net.*, 1(4):244–256.

[Collaborators et al., 2003] Collaborators, M. W. S. et al. (2003). Breast cancer and hormone-replacement therapy in the million women study. *The Lancet*, 362(9382):419–427.

[Cooke and Bliss, 2006] Cooke, S. and Bliss, T. (2006). Plasticity in the human central nervous system. *Brain*, 129(7):1659–1673.

[Crabtree and Gogos, 2014] Crabtree, G. W. and Gogos, J. A. (2014). Synaptic plasticity, neural circuits, and the emerging role of altered short-term information processing in schizophrenia. *Frontiers in synaptic neuroscience*, 6:28.

[Crotty and Levy, 2005] Crotty, P. and Levy, W. B. (2005). Energy-efficient inter-spike interval codes. *Neurocomputing*, 65:371–378.

[Cussler, 2009] Cussler, E. L. (2009). *Diffusion: mass transfer in fluid systems*. Cambridge university press.

[Danbolt, 2001] Danbolt, N. C. (2001). Glutamate uptake. *Prog. Neurobiol.*, 65(1):1–105.

[Dayan and Abbott, 2003] Dayan, P. and Abbott, L. (2003). Theoretical neuroscience: computational and mathematical modeling of neural systems. *Journal of Cognitive Neuroscience*, 15(1):154–155.

[Dayan and Abbott, 2001] Dayan, P. and Abbott, L. F. (2001). *Theoretical Neuroscience: Computational and Mathematical Modeling of Neural Systems*. MIT Press.

[De La Rocha and Parga, 2005] De La Rocha, J. and Parga, N. (2005). Short-term synaptic depression causes a non-monotonic response to correlated stimuli. *J. Neurosci.*, 25(37):8416–8431.

[Dennerstein et al., 1978] Dennerstein, L., Laby, B., Burrows, G. D., and Hyman, G. J. (1978). Headache and sex hormone therapy. *Headache: The J. of Head and Face Pain*, 18(3):146–153.

[Destexhe et al., 2002] Destexhe, A., Mainen, Z., and Sejnowski, T. (2002). "kinetic models for synaptic interactions. *The Handbook of Brain Theory and Neural Networks*, pages 1126–1130.

[Dobelle, 2000] Dobelle, W. H. (2000). Artificial vision for the blind by connecting a television camera to the visual cortex. *ASAIO J.*, 46(1):3–9.

[Dobrunz et al., 1997] Dobrunz, L. E., Huang, E. P., and Stevens, C. F. (1997). Very short-term plasticity in hippocampal synapses. *Proceedings of the National Academy of Sciences*, 94(26):14843–14847.

[Dobrunz and Stevens, 1997] Dobrunz, L. E. and Stevens, C. F. (1997). Heterogeneity of release probability, facilitation, and depletion at central synapses. *Neuron*, 18(6):995–1008.

[Eddington et al., 1977] Eddington, D. K., Dobelle, W., Brackmann, D., Mladejovsky, M., and Parkin, J. (1977). Auditory prostheses research with multiple channel intracochlear stimulation in man. *The Annals of otology, rhinology, and laryngology*, 87(6 Pt 2):1–39.

[Enomoto et al., 2011] Enomoto, A., Moore, M. J., Suda, T., and Oiwa, K. (2011). Design of self-organizing microtubule networks for molecular communication. *Nano Com. Net.*, 2(1):16–24.

[Farsad et al., 2012] Farsad, N., Eckford, A. W., and Hiyama, S. (2012). Channel design and optimization of active transport molecular communication. In *Bio-Inspired Models of Net., Info., and Computing Sys.*, pages 213–223. Springer.

[Farsad et al., 2014] Farsad, N., Eckford, A. W., and Hiyama, S. (2014). A markov chain channel model for active transport molecular communication. *Signal Processing, IEEE Tran.*, 62(9):2424–2436.

[Farsad et al., 2011] Farsad, N., Eckford, A. W., Hiyama, S., and Moritani, Y. (2011). A simple mathematical model for information rate of active transport molecular communication. In *Comp. Com.s Workshops (INFOCOM WKSHPS), IEEE Conf.*, pages 473–478. IEEE.

[Feldman, 2012] Feldman, D. E. (2012). The spike-timing dependence of plasticity. *Neuron*, 75(4):556–571.

[Fernandez and Williams, 2010] Fernandez, M. and Williams, S. (2010). Closed-form expression for the poisson-binomial probability density function. *Aerospace and Electronic Systems, IEEE Transactions on*, 46(2):803–817.

[Fiacco and McCarthy, 2004] Fiacco, T. A. and McCarthy, K. D. (2004). Intracellular astrocyte calcium waves in situ increase the frequency of spontaneous ampa receptor currents in ca1 pyramidal neurons. *Journal of Neuroscience*, 24(3):722–732.

[Filippi and Agosta, 2015] Filippi, M. and Agosta, F. (2015). Motor neuron diseases. *Oxford Textbook of Neuroimaging*, pages 279–294.

[Fontaine et al., 2014] Fontaine, B., Peña, J. L., and Brette, R. (2014). Spike-threshold adaptation predicted by membrane potential dynamics in vivo. *PLoS Comput Biol*, 10(4):e1003560.

[Franks et al., 2002] Franks, K. M., Bartol, T. M., and Sejnowski, T. J. (2002). A monte carlo model reveals independent signaling at central glutamatergic synapses. *Biophysical journal*, 83(5):2333–2348.

[Franks et al., 2003] Franks, K. M., Stevens, C. F., and Sejnowski, T. J. (2003). Independent sources of quantal variability at single glutamatergic synapses. *J.Neurosci.*, 23(8):3186–3195.

[Galluccio et al., 2013] Galluccio, L., Palazzo, S., and Santagati, G. E. (2013). Characterization of molecular communications among implantable biomedical neuro-inspired nanodevices. *Nano Communication Networks*, 4(2):53–64.

[Gao et al., 2011] Gao, Y., Lakshmanan, S., and Sivakumar, R. (2011). On attractant scheduling in networks based on bacterial communication. In *Comp. Com. Workshops (INFOCOM WKSHPS), IEEE Conf.*, pages 419–424.

[Geiger and Jonas, 2000] Geiger, J. R. and Jonas, P. (2000). Dynamic control of presynaptic ca 2+ inflow by fast-inactivating k+ channels in hippocampal mossy fiber boutons. *Neuron*, 28(3):927–939.

[Gerozissis, 2004] Gerozissis, K. (2004). Brain insulin and feeding: a bi-directional communication. *European J. of pharmacology*, 490(1):59–70.

[Gerstner and Kistler, 2002] Gerstner, W. and Kistler, W. M. (2002). *Spiking neuron models: Single neurons, populations, plasticity*. Cambridge university press.

[Giné and Akyildiz, 2009] Giné, L. P. and Akyildiz, I. F. (2009). Molecular communication options for long range nanonetworks. *Comp. Net.*, 53(16):2753–2766.

[Goldberg and Andreou, 2004] Goldberg, D. H. and Andreou, A. G. (2004). Spike communication of dynamic stimuli: rate decoding versus temporal decoding. *Neurocomputing*, 58:101–107.

[Goldberg et al., 2003] Goldberg, D. H., Sripati, A. P., and Andreou, A. G. (2003). Energy efficiency in a channel model for the spiking axon. *Neurocomputing*, 52:39–44.

[Gregori and Akyildiz, 2010] Gregori, M. and Akyildiz, I. F. (2010). A new nanonetwork architecture using flagellated bacteria and catalytic nanomotors. *Selected Areas in Com., IEEE J.*, 28(4):612–619.

[Gregori et al., 2010] Gregori, M., Llatser, I., Cabellos-Aparicio, A., and Alarcón, E. (2010). Physical channel characterization for medium-range nanonetworks using catalytic nanomotors. *NanoCom. Net.*, 1(2):102–107.

[Gregori et al., 2011] Gregori, M., Llatser, I., Cabellos-Aparicio, A., and Alarcón, E. (2011). Physical channel characterization for medium-range nanonetworks using flagellated bacteria. *Comp. Net.*, 55(3):779–791.

[Guney et al., 2012] Guney, A., Atakan, B., and Akan, O. B. (2012). Mobile ad hoc nanonetworks with collision-based molecular communication. *Mobile Computing, IEEE Tran.*, 11(3):353–366.

[Harnois and Di Paolo, 1990] Harnois, C. and Di Paolo, T. (1990). Decreased dopamine in the retinas of patients with parkinson's disease. *Investigative ophthalmology & visual sci.*, 31(11):2473–2475.

[Harris et al., 2015] Harris, J. J., Jolivet, R., Engl, E., and Attwell, D. (2015). Energy-efficient information transfer by visual pathway synapses. *Current Biology*, 25(24):3151–3160.

[Hayashi and Igarashi, 2009] Hayashi, H. and Igarashi, J. (2009). Ltd windows of the stdp learning rule and synaptic connections having a large transmission delay enable robust sequence learning amid background noise. *Cognitive neurodynamics*, 3(2):119–130.

[He et al., 2015] He, P., Mao, Y., Liu, Q., and Yang, K. (2015). A diffusion-neuron hybrid system for molecular communication. *arXiv preprint arXiv:1507.01060*.

[Hodgkin and Huxley, 1952] Hodgkin, A. and Huxley, A. (1952). Propagation of electrical signals along giant nerve fibres. *Proc R Soc Lond B Biol Sci.*, pages 177–183.

[Hornykiewicz, 1998] Hornykiewicz, O. (1998). Biochemical aspects of parkinson's disease. *Neurology*, 51(2 Suppl 2):S2–S9.

[Jezewski et al., 2014] Jezewski, A. J., Larson, J. J., Wysocki, B., Davis, P. H., and Wysocki, T. (2014). A novel method for simulating insulin mediated glut4 translocation. *Biotech. and bioeng.*, 111(12):2454–2465.

[Jongsma and Wilders, 2000] Jongsma, H. J. and Wilders, R. (2000). Gap junctions in cardiovascular disease. *Circulation Research*, 86(12):1193–1197.

[Jornet and Akyildiz, 2011] Jornet, J. M. and Akyildiz, I. F. (2011). Channel modeling and capacity analysis for electromagnetic wireless nanonetworks in the terahertz band. *Wireless Communications, IEEE Transactions on*, 10(10):3211–3221.

[Kadloor et al., 2012] Kadloor, S., Adve, R. S., and Eckford, A. W. (2012). Molecular communication using brownian motion with drift. *NanoBiosci., IEEE Tran.*, 11(2):89–99.

[Kagan et al., 2009] Kagan, D., Calvo-Marzal, P., Balasubramanian, S., Sattayasamitsathit, S., Manesh, K. M., Flechsig, G.-U., and Wang, J. (2009). Chemical sensing based on catalytic nanomotors: motion-based detection of trace silver. *J. of the American Chem. Soc.*, 131(34):12082–12083.

[Kandel et al., 2000] Kandel, E. R., Schwartz, J. H., Jessell, T. M., Siegelbaum, S., and Hudspeth, A. (2000). *Principles of neural science*, volume 4. McGraw-hill New York.

[Kempter et al., 1999] Kempter, R., Gerstner, W., and Van Hemmen, J. L. (1999). Hebbian learning and spiking neurons. *Physical Review E*, 59(4):4498.

[Khan and Akan, 2019] Khan, T. and Akan, O. B. (2019). Sum rate analysis of multiple-access neuro-spike communication channel with dynamic spiking threshold. *Nano Communication Networks*, 19:110–118.

[Khan et al., 2017] Khan, T., Bilgin, B. A., and Akan, O. B. (2017). Diffusion-based model for synaptic molecular communication channel. *IEEE Transactions on NanoBioscience*.

[Khan et al., 2019] Khan, T., Ramezani, H., Abbasi, N. A., and Akan, O. B. (2019). Impact of long term plasticity on information transmission over neuronal networks. *IEEE transactions on nanobioscience*, 19(1):25–34.

[Kilinc and Akan, 2013a] Kilinc, D. and Akan, O. B. (2013a). An information theoretical analysis of nanoscale molecular gap junction communication channel between cardiomyocytes. *Nanotech., IEEE Tran.*, 12(2):129–136.

[Kilinc and Akan, 2013b] Kilinc, D. and Akan, O. B. (2013b). Receiver design for molecular communication. *Selected Areas in Com., IEEE J.*, 31(12):705–714.

[Kistler and Hemmen, 2000] Kistler, W. M. and Hemmen, J. L. v. (2000). Modeling synaptic plasticity in conjunction with the timing of pre-and postsynaptic action potentials. *Neural Computation*, 12(2):385–405.

[Kline et al., 2005] Kline, T. R., Paxton, W. F., Mallouk, T. E., and Sen, A. (2005). Catalytic nanomotors: remote-controlled autonomous movement of striped metallic nanorods. *Angew. Chemie*, 117(5):754–756.

[Kobayashi et al., 2009] Kobayashi, R., Tsubo, Y., and Shinomoto, S. (2009). Made-to-order spiking neuron model equipped with a multi-timescale adaptive threshold. *Front. in comp. neuroscience*, 3:9.

[Koldovskỳ et al., 1994] Koldovskỳ, O., Illnerova, H., Macho, L., Strbak, V., and Stěpánková, R. (1994). Milk-borne hormones: possible tools of communication between mother and suckling. *Physiological research/Academia Scientiarum Bohemoslovaca*, 44(6):349–351.

[Kostal and Kobayashi, 2015] Kostal, L. and Kobayashi, R. (2015). Optimal decoding and information transmission in hodgkin–huxley neurons under metabolic cost constraints. *Biosys.*, 136:3–10.

[Kostal et al., 2013] Kostal, L., Lansky, P., and McDonnell, M. D. (2013). Metabolic cost of neuronal information in an empirical stimulus-response model. *Biological cybernetics*, 107(3):355–365.

[Kumar and Gilula, 1996] Kumar, N. M. and Gilula, N. B. (1996). The gap junction communication channel. *Cell*, 84(3):381–388.

[Kuran et al., 2011] Kuran, M. S., Yilmaz, H. B., Tugcu, T., and Akyildiz, I. F. (2011). Modulation techniques for communication via diffusion in nanonetworks. In *Com. (ICC), IEEE Int. Conf.*, pages 1–5. IEEE.

[Kuran et al., 2012] Kuran, M. Ş., Yilmaz, H. B., Tugcu, T., and Akyildiz, I. F. (2012). Interference effects on modulation techniques in diffusion based nanonetworks. *Nano Com. Net.*, 3(1):65–73.

[Kuscu and Akan, 2012] Kuscu, M. and Akan, O. B. (2012). A physical channel model and analysis for nanoscale molecular communications with förster resonance energy transfer. *Nanotech., IEEE Tran.*, 11(1):200–207.

[Kuscu and Akan, 2014] Kuscu, M. and Akan, O. B. (2014). A communication theoretical analysis of fret-based mobile ad hoc molecular nanonetworks. *NanoBiosci., IEEE Tran.*, 13(3):255–266.

[Lakowicz, 2013] Lakowicz, J. R. (2013). *Principles of fluorescence spectroscopy*. Springer Science & Business Media.

[Laughlin and Sejnowski, 2003] Laughlin, S. B. and Sejnowski, T. J. (2003). Communication in neuronal networks. *Science*, 301(5641):1870–1874.

[Leef and Thomas, 2013] Leef, G. and Thomas, S. M. (2013). Molecular communication between tumor-associated fibroblasts and head and neck squamous cell carcinoma. *Oral oncology*, 49(5):381–386.

[Levy and Baxter, 1996] Levy, W. B. and Baxter, R. A. (1996). Energy efficient neural codes. *Neural Computation*, 8(3):531–543.

[Liu et al., 2014] Liu, Q., He, P., Yang, K., and Leng, S. (2014). Inter-symbol interference analysis of synaptic channel in molecular communications. In *Com. (ICC), IEEE Int. Conf.*, pages 4424–4429. IEEE.

[Locker, 1998] Locker, G. (1998). Hormonal therapy of breast cancer. *Cancer treatment reviews*, 24(3):221–240.

[Longden et al., 2017] Longden, K. D., Wicklein, M., Hardcastle, B. J., Huston, S. J., and Krapp, H. G. (2017). Spike burst coding of translatory optic flow and depth from motion in the fly visual system. *Current Biology*, 27(21):3225–3236.

[Lotter et al., 2020] Lotter, S., Ahmadzadeh, A., and Schober, R. (2020). Synaptic channel modeling for dmc: Neurotransmitter uptake and spillover in the tripartite synapse. *IEEE Transactions on Communications*, 69(3):1462–1479.

[Mahfuz et al., 2010] Mahfuz, M. U., Makrakis, D., and Mouftah, H. T. (2010). On the characterization of binary concentration-encoded molecular communication in nanonetworks. *Nano Com. Net.*, 1(4):289–300.

[Malak and Akan, 2013a] Malak, D. and Akan, O. (2013a). A communication theoretical analysis of synaptic multiple-access channel in hippocampal-cortical neurons. *Com., IEEE Tran.*, 61(6):2457–2467.

[Malak and Akan, 2012] Malak, D. and Akan, O. B. (2012). Molecular communication nanonetworks inside human body. *Nano Com. Net.*, 3(1):19–35.

[Malak and Akan, 2013b] Malak, D. and Akan, O. B. (2013b). Synaptic interference channel. In *Com. Workshops (ICC), IEEE Int. Conf.*, pages 771–775. IEEE.

[Malak and Akan, 2014] Malak, D. and Akan, O. B. (2014). Communication theoretical understanding of intra-body nervous nanonetworks. *IEEE Communications Magazine*, 52(4):129–135.

[Man et al., 2007] Man, C. D., Rizza, R., Cobelli, C., et al. (2007). Meal simulation model of the glucose-insulin system. *Biomed. Eng., IEEE Tran.*, 54(10):1740–1749.

[Mann and Yates, 1986] Mann, D. and Yates, P. (1986). Neurotransmitter deficits in alzheimer's disease and in other dementing disorders. *Human neurobiology*, 5(3):147–158.

[Manwani and Koch, 1998] Manwani, A. and Koch, C. (1998). Synaptic transmission: An information-theoretic perspective. *Adv. in neural infor. proc. syst.*, pages 201–207.

[Manwani and Koch, 2001] Manwani, A. and Koch, C. (2001). Detecting and estimating signals over noisy and unreliable synapses: information-theoretic analysis. *Neural comput.*, 13(1):1–33.

[Matveev and Wang, 2000] Matveev, V. and Wang, X.-J. (2000). Implications of all-or-none synaptic transmission and short-term depression beyond vesicle depletion: a computational study. *J. Neurosci.*, 20(4):1575–1588.

[McGregor, 2005] McGregor, P. K. (2005). *Animal communication networks*. Cambridge University Press.

[Mejias and Torres, 2011] Mejias, J. F. and Torres, J. J. (2011). Emergence of resonances in neural systems: the interplay between adaptive threshold and short-term synaptic plasticity. *PloS one*, 6(3):e17255.

[Meng et al., 2014] Meng, L.-S., Yeh, P.-C., Chen, K.-C., and Akyildiz, I. F. (2014). On receiver design for diffusion-based molecular communication. *Signal Processing, IEEE Tran.*, 62(22):6032–6044.

[Mesiti and Balasingham, 2013] Mesiti, F. and Balasingham, I. (2013). Nanomachine-to-neuron communication interfaces for neuronal stimulation at nanoscale. *IEEE Journal on Selected Areas in Communications*, 31(12):695–704.

[Mesiti et al., 2015a] Mesiti, F., Floor, P. A., and Balasingham, I. (2015a). Astrocyte to neuron communication channels with applications. *IEEE Transactions on Molecular, Biological and Multi-Scale Communications*, 1(2):164–175.

[Mesiti et al., 2015b] Mesiti, F., Veletić, M., Floor, P. A., and Balasingham, I. (2015b). Astrocyte–neuron communication as cascade of equivalent circuits. *Nano communication networks*, 6(4):183–197.

[Mlynarski, 2014] Mlynarski, W. (2014). Efficient coding of spectrotemporal binaural sounds leads to emergence of the auditory space representation. *Frontiers in Computational Neuroscience*.

[Montes et al., 2015] Montes, J., Peña, J. M., DeFelipe, J., Herreras, O., and Merchan-Perez, A. (2015). The influence of synaptic size on ampa receptor activation: A monte carlo model. *PloS one*, 10(6):e0130924.

[Moore et al., 2009] Moore, M. J., Suda, T., and Oiwa, K. (2009). Molecular communication: modeling noise effects on information rate. *NanoBiosci., IEEE Tran.*, 8(2):169–180.

[Moritani et al., 2007] Moritani, Y., Hiyama, S., Nomura, S., Akiyoshi, K., and Suda, T. (2007). A communication interface using vesicles embedded with channel forming proteins in molecular communication. In *Bio-Inspired Models of Net., Info. and Comp. Sys., Bionetics*, pages 147–149. IEEE.

[Moritani et al., 2006] Moritani, Y., Hiyama, S., and Suda, T. (2006). Molecular communication among nanomachines using vesicles. In *Proceedings of NSTI nanotechnology conference*.

[Moujahid et al., 2011] Moujahid, A., d'Anjou, A., Torrealdea, F., and Torrealdea, F. (2011). Energy and information in hodgkin-huxley neurons. *Physical Review E*, 83(3):031912.

[Murad et al., 2010] Murad, M. H., Elamin, M. B., Garcia, M. Z., Mullan, R. J., Murad, A., Erwin, P. J., and Montori, V. M. (2010). Hormonal therapy and sex reassignment: a systematic review and meta-analysis of quality of life and psychosocial outcomes. *Clinical endocrinology*, 72(2):214–231.

[Murthy and Stevens, 1999] Murthy, V. N. and Stevens, C. F. (1999). Reversal of synaptic vesicle docking at central synapses. *Nature neuroscience*, 2:503–507.

[Nadkarni and Jung, 2007] Nadkarni, S. and Jung, P. (2007). Modeling synaptic transmission of the tripartite synapse. *Physical biology*, 4(1):1.

[Nakano et al., 2008] Nakano, T., Hsu, Y.-H., Tang, W. C., Suda, T., Lin, D., Koujin, T., Haraguchi, T., and Hiraoka, Y. (2008). Microplatform for intercellular communication. In *Nano/Micro Eng. and Molec. Sys., 2008. NEMS, 3rd IEEE Int. Conf.*, pages 476–479. IEEE.

[Nakano et al., 2012a] Nakano, T., Moore, M., Okaie, Y., Enomoto, A., and Suda, T. (2012a). Swarming biological nanomachines through molecular communication for targeted drug delivery. *SCIS-ISIS 2012*.

[Nakano et al., 2012b] Nakano, T., Moore, M. J., Wei, F., Vasilakos, A. V., and Shuai, J. (2012b). Molecular communication and networking: Opportunities and challenges. *NanoBiosci., IEEE Tran.*, 11(2):135–148.

[Nakano et al., 2007] Nakano, T., Suda, T., Koujin, T., Haraguchi, T., and Hiraoka, Y. (2007). Molecular communication through gap junction channels: System design, experiments and modeling. In *Bio-Inspired Models of Net., Info. and Computing Sys., 2007. Bionetics 2007. 2nd*, pages 139–146. IEEE.

[Nakano et al., 2014] Nakano, T., Suda, T., Okaie, Y., Moore, M. J., and Vasilakos, A. V. (2014). Molecular communication among biological nanomachines: A layered architecture and research issues. *NanoBiosci., IEEE Tran.*, 13(3):169–197.

[Nielsen et al., 2004] Nielsen, T. A., DiGregorio, D. A., and Silver, R. A. (2004). Modulation of glutamate mobility reveals the mechanism underlying slow-rising ampar epscs and the diffusion coefficient in the synaptic cleft. *Neuron*, 42(5):757–771.

[Noel et al., 2014] Noel, A., Cheung, K. C., and Schober, R. (2014). A unifying model for external noise sources and isi in diffusive molecular communication. *Selected Areas in Com., IEEE J.*, 32(12):2330–2343.

[Opie, 2004] Opie, L. H. (2004). *Heart physiology: from cell to circulation*. Lippincott Williams & Wilkins.

[Paxton et al., 2004] Paxton, W. F., Kistler, K. C., Olmeda, C. C., Sen, A., St. Angelo, S. K., Cao, Y., Mallouk, T. E., Lammert, P. E., and Crespi, V. H. (2004). Catalytic nanomotors: autonomous movement of striped nanorods. *J. of the American Chemical Society*, 126(41):13424–13431.

[Perea and Araque, 2007] Perea, G. and Araque, A. (2007). Astrocytes potentiate transmitter release at single hippocampal synapses. *Science*, 317(5841):1083–1086.

[Perea et al., 2009] Perea, G., Navarrete, M., and Araque, A. (2009). Tripartite synapses: astrocytes process and control synaptic information. *Trends in neurosciences*, 32(8):421–431.

[Pierobon and Akyildiz, 2010] Pierobon, M. and Akyildiz, I. F. (2010). A physical end-to-end model for molecular communication in nanonetworks. *Selected Areas in Com., IEEE J.*, 28(4):602–611.

[Pierobon and Akyildiz, 2013] Pierobon, M. and Akyildiz, I. F. (2013). Capacity of a diffusion-based molecular communication system with channel memory and molecular noise. *Info. Theory, IEEE Tran.*, 59(2):942–954.

[Platkiewicz and Brette, 2010] Platkiewicz, J. and Brette, R. (2010). A threshold equation for action potential initiation. *PLoS Comput Biol*, 6(7):e1000850.

[Plonsey and Barr, 2007] Plonsey, R. and Barr, R. C. (2007). *Bioelectricity: a quantitative approach*. Springer.

[Ramezani and Akan, 2015a] Ramezani, H. and Akan, ozgur, B. (2015a). Synaptic channel model including effects of spike width variation. In *Nanoscale Computing and Com. (NANOCOM), 2nd ACM Int. Conf.* ACM.

[Ramezani and Akan, 2015b] Ramezani, H. and Akan, O. B. (2015b). Synaptic channel model including effects of spike width variation. In *Proc. of ACM NANOCOM*, page 11.

[Ramezani and Akan, 2017a] Ramezani, H. and Akan, O. B. (2017a). A communication theoretical modeling of axonal propagation in hippocampal pyramidal neuron. *IEEE Trans. on NanoBiosci.*

[Ramezani and Akan, 2017b] Ramezani, H. and Akan, O. B. (2017b). A communication theoretical modeling of axonal propagation in hippocampal pyramidal neurons. *IEEE Trans. NanoBiosci.*, 16(4):248–256.

[Ramezani and Akan, 2017c] Ramezani, H. and Akan, O. B. (2017c). Importance of vesicle release stochasticity in neuro-spike communication. In *Proc. of IEEE EMBC'17*.

[Ramezani and Akan, 2017d] Ramezani, H. and Akan, O. B. (2017d). Information capacity of vesicle release in neuro-spike communication. *IEEE Communications Letters*.

[Ramezani and Akan, 2017e] Ramezani, H. and Akan, O. B. (2017e). Information capacity of vesicle release in neuro-spike communication. *IEEE Communications Letters*.

[Ramezani and Akan, 2018] Ramezani, H. and Akan, O. B. (2018). Impacts of spike shape variations on synaptic communication. *IEEE Transactions on NanoBioscience*, 17(3):260–271.

[Ramezani et al., 2018a] Ramezani, H., khan, T., and Akan, O. B. (2018a). Information theoretical analysis of synaptic communication for nanonetworks. In *Proc. 37th IEEE INFOCOM*. IEEE.

[Ramezani et al., 2018b] Ramezani, H., Khan, T., and Akan, O. B. (2018b). Sum rate of miso neuro-spike communication channel with constant spiking threshold. *IEEE Transactions on NanoBioscience*, 17(3):342–351.

[Ramezani et al., 2017] Ramezani, H., Koca, C., and Akan, O. B. (2017). Rate region analysis of multi-terminal neuronal nanoscale molecular communication channel. In *Proc. of IEEE Nano'17*.

[Rohr, 2004] Rohr, S. (2004). Role of gap junctions in the propagation of the cardiac action potential. *Cardiovascular research*, 62(2):309–322.

[Rosenberg, 2012] Rosenberg, G. A. (2012). Neurological diseases in relation to the blood–brain barrier. *J. of Cerebral Blood Flow & Metabolism*, 32(7):1139–1151.

[Rossant et al., 2011] Rossant, C., Goodman, D. F., Fontaine, B., Platkiewicz, J., Magnusson, A. K., and Brette, R. (2011). Fitting neuron models to spike trains. *Frontiers in neuroscience*, 5:9.

[Rusakov et al., 2011] Rusakov, D. A., Savtchenko, L. P., Zheng, K., and Henley, J. M. (2011). Shaping the synaptic signal: molecular mobility inside and outside the cleft. *Trends Neurosci.*, 34(7):359–369.

[Santello and Volterra, 2009] Santello, M. and Volterra, A. (2009). Synaptic modulation by astrocytes via ca2+-dependent glutamate release. *Neuroscience*, 158(1):253–259.

[Savtchenko and Rusakov, 2007] Savtchenko, L. P. and Rusakov, D. A. (2007). The optimal height of the synaptic cleft. *Proc Natl Acad Sci U S A*, 104(6):1823–1828.

[Sayer et al., 1990] Sayer, R., Friedlander, M., and Redman, S. (1990). The time course and amplitude of epsps evoked at synapses between pairs of ca3/ca1 neurons in the hippocampal slice. *J. Neurosci.*, 10(3):826–836.

[Schikorski and Stevens, 1997] Schikorski, T. and Stevens, C. F. (1997). Quantitative ultrastructural analysis of hippocampal excitatory synapses. *J. Neurosci.*, 17(15):5858–5867.

[Sengupta et al., 2013] Sengupta, B., Laughlin, S. B., and Niven, J. E. (2013). Balanced excitatory and inhibitory synaptic currents promote efficient coding and metabolic efficiency. *PLoS Comput Biol*, 9(10):e1003263.

[Sengupta and Stemmler, 2014] Sengupta, B. and Stemmler, M. B. (2014). Power consumption during neuronal computation. *Proc. IEEE*, 102(5):738–750.

[Severs, 2000] Severs, N. J. (2000). The cardiac muscle cell. *Bioessays*, 22(2):188–199.

[Seyedi et al., 2013] Seyedi, M., Kibret, B., Lai, D. T., and Faulkner, M. (2013). A survey on intrabody communications for body area network applications. *Biomed. Eng., IEEE Tran.*, 60(8):2067–2079.

[ShahMohammadian et al., 2012] ShahMohammadian, H., Messier, G. G., and Magierowski, S. (2012). Optimum receiver for molecule shift keying modulation in diffusion-based molecular communication channels. *Nano Com. Net.*, 3(3):183–195.

[Shannon, 1948] Shannon, C. E. (1948). A mathematical theory of communication. *Bell System Technical Journal, 27 (1948),*, 27:379–423.

[Sheng et al., 2012] Sheng, M., Sabatini, B. L., and Südhof, T. C. (2012). Synapses and alzheimer's disease. *Cold Spring Harbor pers. in biology*, 4(5).

[Shuai and Jung, 2002] Shuai, J.-W. and Jung, P. (2002). Stochastic properties of ca2+ release of inositol 1, 4, 5-trisphosphate receptor clusters. *Biophysical journal*, 83(1):87–97.

[Simon et al., 2015] Simon, D. T., Larsson, K. C., Nilsson, D., Burström, G., Galter, D., Berggren, M., and Richter-Dahlfors, A. (2015). An organic electronic biomimetic neuron enables auto-regulated neuromodulation. *Biosensors and Bioelectronics*, 71:359–364.

[Sperandio et al., 2003] Sperandio, V., Torres, A. G., Jarvis, B., Nataro, J. P., and Kaper, J. B. (2003). Bacteria–host communication: the language of hormones. *Proc. of the National Academy of Sci.*, 100(15):8951–8956.

[Steinman, 1996] Steinman, L. (1996). Multiple sclerosis: a coordinated immunological attack against myelin in the central nervous system. *Cell*, 85(3):299–302.

[Stevens and Wang, 1995] Stevens, C. F. and Wang, Y. (1995). Facilitation and depression at single central synapses. *Neuron*, 14(4):795–802.

[Suzuki et al., 2014] Suzuki, J., Phan, D. H., and Budiman, H. (2014). A non-parametric stochastic optimizer for tdma-based neuronal signaling. *NanoBiosci., IEEE Tran.*, 13(3):244–254.

[Tahayori and Koceja, 2012] Tahayori, B. and Koceja, D. M. (2012). Activity-dependent plasticity of spinal circuits in the developing and mature spinal cord. *Neural plasticity*, 2012.

[Tang et al., 1994] Tang, C.-M., Margulis, M., Shi, Q.-Y., and Fielding, A. (1994). Saturation of postsynaptic glutamate receptors after quantal release of transmitter. *Neuron*, 13(6):1385–1393.

[Tepperman et al., 1968] Tepperman, J. et al. (1968). Metabolic and endocrine physiology. an introductory text. *Metabolic and endocrine physiology. An introductory text.*, (Edn 2).

[Tong and Jahr, 1994] Tong, G. and Jahr, C. E. (1994). Block of glutamate transporters potentiates postsynaptic excitation. *Neuron*, 13(5):1195–1203.

[Unger and Betz, 1998] Unger, J. W. and Betz, M. (1998). Insulin receptors and signal transduction proteins in the hypothalamo-hypophyseal system: a review on morphological findings and functional implications. *Histology and histopathology*, 13(4):1215–1224.

[van Rossum and Turrigiano, 2001] van Rossum, M. C. and Turrigiano, G. G. (2001). Correlation based learning from spike timing dependent plasticity. *Neurocomputing*, 38:409–415.

[Veletić et al., 2016a] Veletić, M., Floor, P. A., Babić, Z., and Balasingham, I. (2016a). Peer-to-peer communication in neuronal nano-network. *IEEE Trans. Commun.*, 64(3):1153–1166.

[Veletić et al., 2016b] Veletić, M., Floor, P. A., Chahibi, Y., and Balasingham, I. (2016b). On the upper bound of the information capacity in neuronal synapses. *IEEE Trans Commun.*, 64(12):5025–5036.

[Ventriglia and Di Maio, 2000] Ventriglia, F. and Di Maio, V. (2000). A brownian simulation model of glutamate synaptic diffusion in the femtosecond time scale. *Biol. Cybern.*, 83(2):93–109.

[Von Neumann, 2012] Von Neumann, J. (2012). *The computer and the brain*. Yale University Press.

[Wei et al., 2013] Wei, G., Bogdan, P., and Marculescu, R. (2013). Efficient modeling and simulation of bacteria-based nanonetworks with bnsim. *Selected Areas in Com., IEEE J.*, 31(12):868–878.

[Weigent et al., 1990] Weigent, D. A., Carr, D. J., and Blalock, J. E. (1990). Bidirectional communication between the neuroendocrine and immune systems common hormones and hormone receptors. *Annals of the New York Academy of Sciences*, 579(1):17–27.

[Wenger et al., 2014] Wenger, N., Moraud, E. M., Raspopovic, S., Bonizzato, M., DiGiovanna, J., Musienko, P., Morari, M., Micera, S., and Courtine, G. (2014). Closed-loop neuromodulation of spinal sensorimotor circuits controls refined locomotion after complete spinal cord injury. *Science translational medicine*, 6(255):255ra133–255ra133.

[Willmann et al., 2007] Willmann, S., Höhn, K., Edginton, A., Sevestre, M., Solodenko, J., Weiss, W., Lippert, J., and Schmitt, W. (2007). Development of a physiology-based whole-body population model for assessing the influence of individual variability on the pharmacokinetics of drugs. *J. of pharmacokinetics and pharmacodynamics*, 34(3):401–431.

[Yoo et al., 2011] Yoo, J.-W., Irvine, D. J., Discher, D. E., and Mitragotri, S. (2011). Bio-inspired, bioengineered and biomimetic drug delivery carriers. *Nature reviews Drug discovery*, 10(7):521–535.

[Zhang et al., 1998] Zhang, L. I., Tao, H. W., Holt, C. E., Harris, W. A., and Poo, M.-m. (1998). A critical window for cooperation and competition among developing retinotectal synapses. *Nature*, 395(6697):37.